

EFFECT OF SPANDREL BEAM ON SEISMIC
RESPONSE OF CONCRETE FRAMES

by

Marco Alfio Di Franco

March 1993



Department of Civil Engineering and Applied Mechanics
McGill University
Montreal, Canada

A thesis submitted to the Faculty of Graduate Studies
and Research in partial fulfilment of the
requirements for the degree of
Master of Engineering.

© Marco A. Di Franco, 1993

ABSTRACT

Full-scale exterior beam-column-slab sub-assemblages were tested under reversed cyclic loading to investigate the role of the spandrel beam in the overall response. Results from specimens having different spandrel beam sizes and different amounts of torsional reinforcement in the spandrel beams provided a better understanding of their behaviour. The test specimens were heavily instrumented to enable detailed strain measurements in the slab bars, the joint region and the spandrel beam. These strains together with the crack pattern provide some insight into the flow of forces from the slab and spandrel beam into the joint region. The tests show that the effective width of the slab contributing to the negative bending of the main beam is affected by the torsional yielding of the spandrel beam. However, after this yielding, a different force mechanism, involving concrete compressive struts, and tension ties in the slab and spandrel beam bars, provides means of transferring additional forces from the slab bars to the joint region. It is important to consider the effect of these forces since they increase the negative moment capacity of the beams, and hence, they may affect the hierarchy of yielding between the columns and the beams. This effect may in turn alter the failure mode of the structure.

Tentative design proposals, accounting for the flow of forces through the spandrel beam, are presented. The application of these proposals are illustrated for a number of different specimens having varying spandrel beam dimensions.

SOMMAIRE

Des spécimens de grandeurs réelles représentant un assemblage de poteau extérieur, poutre et dalle ont été mis à l'essai sous des charges cycliques dans le but de déterminer le rôle de la poutre de rive sur le comportement général de la structure. Les résultats expérimentaux des spécimens avec des poutres de rives de différentes dimensions et une quantité variable d'armature pour reprendre les efforts de torsion ont permis de mieux comprendre leur comportement. Les spécimens ont été bien instrumentés pour obtenir des mesures détaillées des efforts de tension dans les barres de la dalle, la région du joint et dans les poutres de rives. Les tensions et la formation des fissures ont permis de visualiser la transmission des contraintes de cisaillement de la dalle et de la poutre de rive au joint. Les résultats expérimentaux montrent que la largeur effective de la dalle qui participe à la résistance de la poutre principale est influencée par la résistance en torsion de la poutre de rive. Cependant, après l'affaiblissement de la poutre de rive, une autre forme de résistance se manifeste. Celle-ci consiste en un système de bielles de béton en compression et d'efforts de tension dans les barres de la dalle et de la poutre de rive, permettant de transmettre des efforts de tension additionnels des barres de la dalle au joint. Il est important de considérer ces effets, puis qu'ils augmentent la résistance des poutres et peuvent ainsi affecter la hiérarchie de l'affaiblissement entre les poteaux et les poutres. Ces effets peuvent donc changer le mode de rupture de la structure.

Des méthodes de conception qui incluent la transmission des efforts au travers de la poutre de rive sont présentés. Ces méthodes sont illustrées pour plusieurs spécimens ayant des poutres de rives de différentes dimensions.

ACKNOWLEDGEMENTS

The research work reported in this thesis was carried out in the Jamieson Structural Laboratory in the Department of Civil Engineering and Applied Mechanics at McGill University. The financial support of the scholarship and research grant programmes of the Natural Sciences and Engineering Research Council of Canada are gratefully acknowledged.

The author would like to express his deepest gratitude to Professor Denis Mitchell from McGill University and Professor Patrick Paultre from Université de Sherbrooke for their invaluable assistance and excellent guidance throughout this research programme. The author is also grateful to the lab technicians, Ron Sheppard, John Bartczak, Marek Przykorski, and Damon Kiperchuk for their assistance in constructing the specimens. Special thanks are expressed to Rob Katz, Jamie Mitchell, Joanne Crabb, and Phil Zeyl for their help and patience in the testing of the specimens. Furthermore, the helpful suggestions of Dr. William D. Cook and Kent A. Harries along with fellow colleagues are acknowledged. The author would also like to express appreciation to Donello Magni for the use of his dark room facilities for the development of the photographs in this thesis.

Finally, the author would like to thank his family without whom this work would not be possible, for their constant encouragement, support and understanding throughout his studies at McGill University.

TABLE OF CONTENTS

ABSTRACT	1
SOMMAIRE	ii
ACKNOWLEDGEMENTS	iii
LIST OF FIGURES	vii
LIST OF TABLES	x
LIST OF SYMBOLS	xi

CHAPTER

1 INTRODUCTION	1
1.1 Background Information	1
1.2 Design Criteria	2
1.3 Summary of Previous Research	4
1.4 Research Objectives	8
2 EXPERIMENTAL PROGRAMME	10
2.1 Description of Prototype Structures	10
2.1.1 Building Description	10
2.1.2 Loadings and Analysis Assumptions	12
2.2 Details of Test Specimens	13
2.2.1 Specimen Dimensions	13
2.2.2 Design and Details of Column, Beam and Slab Reinforcement ..	14
2.2.3 Details of Spandrel Beam Reinforcement	20
2.3 Material Properties	21
2.3.1 Reinforcing Steel	21
2.3.2 Concrete	21
2.4 Experimental Procedure	24
2.4.1 Test Setup and Loading Apparatus	24
2.4.2 Instrumentation	27
2.4.2.1 Load Measurements	27
2.4.2.2 Deflection Measurements	27
2.4.2.3 Strain Measurements	30
2.4.3 Testing Procedure and Loading Sequence	32

3 REVERSED CYCLIC LOAD TEST RESULTS	33
3.1 Specimen R4S	33
3.1.1 Load Deflection Response	33
3.1.2 Beam Behaviour	36
3.1.3 Slab Behaviour	40
3.1.4 Spandrel beam Behaviour	43
3.1.5 Column Behaviour	45
3.1.6 Joint Behaviour	47
3.2 Specimen R4T	48
3.2.1 Load Deflection Response	48
3.2.2 Beam Behaviour	50
3.2.3 Slab Behaviour	55
3.2.4 Spandrel Beam Behaviour	58
3.2.5 Column Behaviour	62
3.2.6 Joint Behaviour	63
3.3 Specimen R4	65
3.3.1 Load Deflection Response	65
3.3.2 Beam Behaviour	67
3.3.3 Slab Behaviour	72
3.3.4 Spandrel Beam Behaviour	73
3.3.5 Column Behaviour	74
3.3.6 Joint Behaviour	75
4 ANALYSIS AND COMPARISONS OF TESTS RESULTS	76
4.1 Load-Deflection Response	76
4.2 Tip Deflection Components	81
4.3 Hysteretic Loading Behaviour	86
4.3.1 Energy Dissipation	86
4.3.2 Displacement Ductility	87
4.3.3 Damping and Stiffness	88
4.4 Moment-Curvature Response and Predictions	89
4.5 Role of Spandrel Beam and Slab	93
4.5.1 Effect Torsion in Spandrel Beam	93
4.5.2 Strut and Tie Mechanism Transferring Forces from Slab Bars	95
4.5.3 Effective Slab Reinforcement (Effective Width)	98
4.5.4 Measured and Predicted Torsional Response of Spandrel Beams	99
4.5.5 Determination of Effective Slab Reinforcement	101
4.5.6 Simplified Determination of Effective Slab Reinforcement	104
4.5.7 Flexural Strength Ratio	106

5 CONCLUSIONS AND RECOMMENDATIONS	108
5.1 Conclusions	108
5.2 Future Research Recommendations	109
REFERENCES	110
APPENDIX A Calculations for the Design and Detailing of Test Specimens	113
A.1 Beam Design	114
A.2 Column Design	118
A.3 Joint Design	122
APPENDIX B Calculations for the Amount of Effective Slab Reinforcement	124
B.1 Specimen R4 (Rattray, 1986)	125
B.2 Specimen R4S	126
B.3 Specimen R4T	127
B.4 Specimen 1S (Ehsani, 1982)	128
B.5 Specimen J4 (Durrani, 1987)	129
B.6 Specimen 2D-E (Cheung, 1991)	130

LIST OF FIGURES

Chapter 1

- 1.1 : Idealized lateral load versus displacement response of structures having different R values 1
- 1.2 : Exterior sub-assembly subjected to lateral forces. 3
- 1.3 : Different hinge mechanisms for frames 3

Chapter 2

- 2.1 : Plan and elevation view of prototype structure (Paultre 1987) 11
- 2.2 : Location of full scale specimen. 13
- 2.3 : Dimensions of specimen R4S and R4T 14
- 2.4 : Details of reinforcement for $R = 4$ 16
- 2.5 : Photographs of reinforcing steel for specimens R4S 17
- 2.6 : Photographs of reinforcing steel for specimens R4T 18
- 2.7 : Photographs of reinforcing steel for specimens R4 19
- 2.8 : Spandrel reinforcing details for the three specimens 20
- 2.9 : Stress-strain relationship for reinforcing bars 22
- 2.10 : Concrete compressive stress-strain relationships 23
- 2.11 : Test setup for all specimens 25
- 2.12 : Details of column hinge connection 26
- 2.13 : Details of loading mechanism 26
- 2.14 : Instrumentation of test specimens 28
- 2.15 : Details of instrumentation on back face of specimen R4T 29
- 2.16 : Photograph showing locations of targets glued to slab steel 30
- 2.17 : Locations of electrical resistance gauges on reinforcing bars 31
- 2.18 : Loading-history for all specimens 32

Chapter 3

- 3.1 : Load versus tip deflection response for specimen R4S 34
- 3.2 : Photographs of specimen R4S at different stages 37
- 3.3 : Photograph showing buckling of longitudinal bars in specimen R4S 38
- 3.4 : Curvature and shear strain distributions for R4S 39
- 3.5 : Crack patterns in slab of specimen R4S 40
- 3.6 : Photograph showing severe cracking and local crushing around column region of specimen R4S 41
- 3.7 : Strain distributions in slab longitudinal bars 42

3.8 :	Photograph of exterior face of spandrel beam of specimen R4S at general yielding	43
3.9 :	Photograph of exterior face of spandrel beam of specimen R4S	44
3.10 :	Overall view of exterior face of spandrel beam of specimen R4S at end of test	45
3.11 :	Column cross-section before and after separation of concrete cover	46
3.12 :	Photograph of the joint region in the 10th downward cycle of specimen R4S	47
3.13 :	Load-tip deflection response for specimen R4T	48
3.14 :	Photographs of specimen R4T at different stages	51
3.15 :	Buckling of bottom bars at end of test for specimen R4T	53
3.16 :	Curvature and shear strain distribution for R4T	54
3.17 :	Crack pattern in slab of specimen R4T	55
3.18 :	Cracking and crushing of concrete in slab for specimen R4T	56
3.19 :	Strain distribution in slab longitudinal bars for specimen R4T	57
3.20 :	Spandrel beam at general yielding ($\Delta_v = 1.0$) for specimen R4T	58
3.21 :	Photograph of spandrel beam for R4T in the 11th negative loading cycle	59
3.22 :	Exterior view of spandrel beam for specimen R4T at $10.0\Delta_v$	60
3.23 :	Exterior view of spandrel beam for specimen R4T at the end of test	61
3.24 :	Photograph of joint region of specimen R4T	63
3.25 :	Strain distribution in hoop reinforcement in specimen R4T	64
3.26 :	Load versus tip deflection response for specimen R4	65
3.27 :	Photographs of specimen R4 at different stages	68
3.28 :	Photograph of specimen R4 showing damage near the joint	69
3.29 :	Buckling of beam bottom bars at $8\Delta_v$ in specimen R4	70
3.30 :	Curvature and shear strain distributions for R4	71
3.31 :	Strain distribution in slab bars for specimen R4	72
3.32 :	Photograph of spandrel beam of specimen R4 at general yielding	73
3.33 :	Exterior view of specimen R4 in the 10th loading cycle	74
3.34 :	Photograph of joint region of specimen R4 in 10th loading cycle	75

Chapter 4

4.1 :	Load versus tip deflection response for specimen R4	77
4.2 :	Photograph of damage to specimen R4 at the end of test	77
4.3 :	Load versus tip deflection response for specimen R4S	78
4.4 :	Photograph of damage to specimen R4S at the end of test	78
4.5 :	Load versus tip deflection response for specimen R4T	79
4.6 :	Photograph of damage to specimen R4T at the end of test	79
4.7 :	Load versus displacement envelopes for the three specimens	81
4.8 :	Equations for calculating Δ_f	82

4.9 :	Equation for calculating Δ_x	83
4.10 :	Equation for calculating Δ_y	83
4.11 :	Beam tip deflection components for specimen R4	84
4.12 :	Beam tip deflection components for specimen R4S	84
4.12 :	Beam tip deflection components for specimen R4T	85
4.14 :	Definition of damping coefficients α and β	89
4.15 :	Hysteretic damping and stiffness degradation of the test specimen	89
4.16 :	Non-linear strain distributions in the slab bars of the specimens	91
4.17 :	Predicted and experimental moment-curvature responses for specimen R4	92
4.18 :	Predicted and experimental moment-curvature responses for specimen R4S ...	92
4.19 :	Predicted and experimental moment-curvature responses for specimen R4T ...	93
4.20 :	Role of the spandrel beam	94
4.21 :	Measured strain distributions across the slabs at slab-spandrel interfaces ...	95
4.22 :	Disturbed regions of specimen after significant yielding	95
4.23 :	Flow of forces in the "disturbed regions" of the slab	96
4.24 :	Failure surface in specimen R4T	97
4.25 :	Rotations of the column and the spandrel beam in specimen R4T	99
4.26 :	Bending deformations in the spandrel beams	100
4.27 :	Torsional response of spandrel beam in specimen R4T	100
4.28 :	Measured strain distributions across the slab at maximum capacity	102
4.29 :	Loading of spandrel beam in torsion	103
4.30 :	Strut and tie model showing yielding of slab bars	103
4.31 :	Induced torsion in spandrel beam	104
4.32 :	Simplified strut and tie model	105

APPENDIX A

A.1 :	Arrangement of longitudinal reinforcement	115
A.2 :	Details of beam shear reinforcement	117
A.3 :	Trial column reinforcement configuration	118
A.4 :	Determination of design shear force in column	119
A.5 :	Details of column transverse reinforcement	121
A.6 :	Details of joint region reinforcement	123

APPENDIX B

B.1 :	Strut and tie model to determine the effective slab reinforcement	131
-------	---	-----

LIST OF TABLES

Chapter 2

2.1 :	Properties of reinforcing steel	22
2.2 :	Properties of concrete	23

Chapter 3

3.1 :	Applied loads and tip deflections at cycle peaks for specimen R4S	35
3.2 :	Applied loads and tip deflections at cycle peaks for specimen R4T	49
3.3 :	Applied loads and tip deflections at cycle peaks for specimen R4	66

Chapter 4

4.1 :	Comparison of key response parameters for the three specimens	76
4.2 :	Energy dissipation at different ductility levels for specimen R4	86
4.3 :	Energy dissipation at different ductility levels for specimen R4S	87
4.4 :	Energy dissipation at different ductility levels for specimen R4T	88
4.5 :	Comparisons of maximum moments and curvature ductilities	90
4.6 :	Comparison of the "effective slab width" used in current design codes.	98
4.7 :	Comparison of predicted and experimentally determined number of bars yielding	101
4.8 :	Simplified calculation of the number of effective slab bars	106
4.9 :	M_R values for varying effective slab reinforcements	106
4.10 :	Comparison of actual M_R values for the three specimens	107
4.11 :	Maximum recorded negative moments and normalized moments for each specimen	107

LIST OF SYMBOLS

<p>a = depth of equivalent rectangular stress block</p> <p>a_o = depth of uniformly stressed tube in torsion</p> <p>A_c = area of spandrel beam cross section</p> <p>A_{ch} = cross-sectional area of the core of a member</p> <p>A_g = gross area of concrete column</p> <p>A_o = area of concrete enclosed by shear flow path</p> <p>A_{oh} = area enclosed by the centreline of the hoops</p> <p>A_s = area of tension reinforcement</p> <p>A_s^* = area of steel in each set, n_s</p> <p>A_s' = area of compression rein.</p> <p>A_{sl} = area of spandrel beam longitudinal reinforcement</p> <p>A_{st} = area of column reinforcement</p> <p>A_t = area of transverse hoop rein.</p> <p>A_v = area of beam stirrups</p> <p>b = width of concrete member</p> <p>b_o = width between stirrup centrelines</p> <p>b_e = effective width of T-beam in negative bending</p> <p>b_w = width of beam web</p> <p>c = column width.</p> <p>d = distance from extreme fibre to centroid of tension rein.</p> <p>d' = distance from extreme fibre to centroid of compression reinforcement</p> <p>d_b = bar diameter</p> <p>e = eccentricity of slab rein.</p> <p>h = height of main beam</p> <p>h_c = cross-sectional dimension of column core</p> <p>h_f = thickness of slab</p> <p>h_o = height of critical section</p>	<p>f_2 = principal compressive stress</p> <p>$f_{2(max)}$ = limiting compressive stress</p> <p>f_c' = specified compressive strength of concrete</p> <p>f_t = tensile strength of concrete</p> <p>f_y = specified yield strength of steel reinforcement.</p> <p>f_u = ultimate strength of reinforcement</p> <p>F = foundation factor for the structure</p> <p>I = importance factor for the structure</p> <p>j_d = moment lever arm</p> <p>k_y = stiffness at yield</p> <p>k_u = stiffness at ultimate</p> <p>l = distance from loading point to the column face</p> <p>l_{dh} = basic development length</p> <p>l_j = column dimension parallel to beam reinforcing bars</p> <p>l_n = clear span in long direction</p> <p>l_o = length over which transverse reinforcement is provided</p> <p>l_p = length of plastic hinge region</p> <p>M_f = factored moment at a section</p> <p>M_{nb} = nominal resistance of a beam</p> <p>M_{pr} = probable resistance of a beam</p> <p>M_r = beam factored resistance</p> <p>M_{r+} = positive moment resistance</p> <p>M_{r-} = negative moment resistance</p> <p>M_{rc} = column factored resistance</p> <p>M_R = ratio of nominal column strengths to beam strengths</p> <p>M_u = ultimate moment resistance</p> <p>n = number of effective slab bars</p> <p>N = number of slab bars in each set</p> <p>N_f = factored axial load on column</p>
--	---

N_v	=	equivalent factored axial load caused by shear and torsion	w_s	=	distributed load from slab reinforcement
p_c	=	outside perimeter of concrete cross section	W	=	dead load of a structure plus 25% of snow load
p_h	=	perimeter of the centerlines of the closed transverse torsional reinforcement	\bar{x}	=	distance to centroid of area
p_o	=	perimeter of the shear flow path	x	=	effective width of slab reinforcement
P	=	axial load on the column	α	=	stiffness indicator
P_f	=	factored axial load at section	β	=	hysteretic damping coefficient
P_r	=	factored axial load resistance	γ	=	shear strain in a beam
$P_{r(max)}$	=	maximum factored axial load resistance of a column	Δ	=	vertical tip deflection of beam
P_u	=	applied load at ultimate	Δ_f	=	component of beam tip deflection due to flexure
P_y	=	applied load at yield	Δ_j	=	component of beam tip deflection due to bond slip and joint shear distortion
R	=	force modification factor	Δ_{peak}	=	cycle peak tip deflection
S	=	seismic response factor	Δ_s	=	component of beam tip deflection due to shear
s	=	spacing of transverse shear reinforcement	Δ_{tip}	=	beam tip deflection
s_{max}	=	maximum stirrup spacing for shear	Δ_u	=	deflection at ultimate load
s_s	=	spacing of slab reinforcement	Δ_y	=	deflection at general yielding
T	=	fundamental period of vibration of a structure	Δ_{yn}	=	deflection at general yielding in the negative direction
T_{cr}	=	torsional cracking resistance of a beam	Δ_{yp}	=	deflection at general yielding in the positive direction
T_r	=	factored torsional resistance of a beam	e_1	=	principal tensile strain
v	=	velocity ratio for the region	e_s	=	strain in reinforcement
V	=	seismic base shear of the structure	e_y	=	yield strain in slab bars
V_c	=	factored shear resistance provided by the concrete	θ_j	=	rotation of beam at the joint
V_{col}	=	shear in the column	λ	=	factor to account for low density concrete
V_f	=	factored shear force	ρ_{min}	=	minimum reinforcement ratio in a beam
V_j	=	net horizontal joint shear	ρ_{max}	=	maximum reinforcement ratio in a beam
V_r	=	factored shear resistance of a member	ϕ_c	=	resistance factor for concrete
V_s	=	factored shear resistance provided by the steel	ϕ_s	=	resistance factor for reinforcing bars
			ϕ_u	=	ultimate curvature in main beam
			ϕ_y	=	yield curvature in main beam

Chapter 1

INTRODUCTION

1.1 Background Information

The 1990 National Building Code of Canada (NBCC, 1990) contains provisions for the design of structures for earthquakes. A force modification factor, R , is introduced to reflect the overall ductility of the structure and the ability of the structure to dissipate energy through inelastic action. The values of R range from 1.0, for unreinforced masonry construction, to 4.0 for ductile moment-resisting frame structures. The 1984 CSA Standard for the Design of Concrete Structures for Buildings (CSA, 1984) sets out design and detailing requirements corresponding to the different values of R . Figure 1.1 illustrates the idealized lateral load vs displacement responses of four structures all having the same initial stiffness but with different inelastic characteristics (i.e., different R factors). It can be noted that structures designed with a force reduction factor, R , of 4.0, have a lower base shear and a higher level of ductility. Several experimental investigations have been carried out to assess the validity of the current design code and to evaluate the performance of such structures.

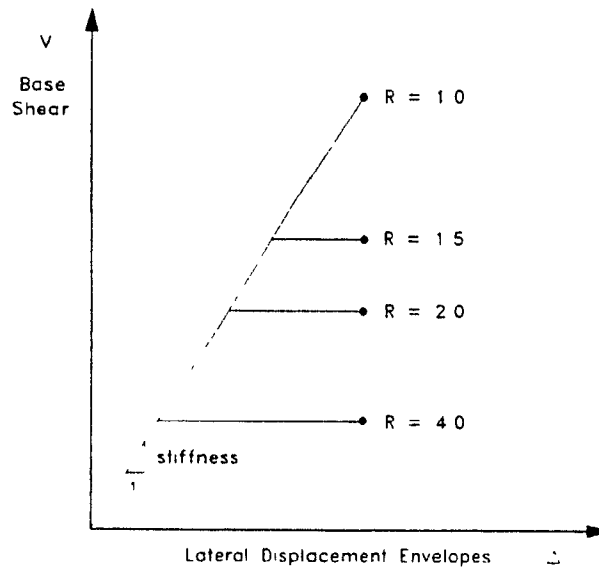


Figure 1.1: Idealized lateral load versus displacement response of structures having different R values

1.2 Design Criteria

The required strength of a ductile moment-resisting reinforced concrete building subjected to seismic actions depends on the structural ductility and the energy dissipating capacity of the structure. A ductile moment-resisting frame structure must have a minimum level of ductility and must be capable of dissipating significant amounts of energy in the inelastic range. In order to achieve these goals the CSA Standard (CSA, 1984) requires that such a structure have the following general characteristics:

- (i) Large displacement capabilities without significant loss of strength
- (ii) A desirable hierarchy of yielding in the members
- (iii) Excellent confinement of regions expected to undergo inelastic action
- (iv) Undesirable, brittle modes of failure in members are avoided
- (v) The reinforcement must be detailed such that it is effective, even after severe distress (e.g., cover spalling).

Figure 1.2 shows an exterior beam-column joint subjected to lateral forces. The shear strength of the beams must be sufficient to develop flexural hinging in the beams before any significant shear distress occurs. At the connections, the beams and columns are designed such that the columns are stronger than the beams. This ensures a "weak-beam, strong-column" response and results in a "beam sidesway mechanism" (see Fig. 1.3c). With this hierarchy of yielding the "column sidesway mechanism" (see Fig. 1.3b), which is associated with small levels of ductility and energy absorption, is avoided. To ensure plastic hinging in the beams, and not in the joints or columns, the CSA Standard requires that the sum of the factored resistances of the columns above and below the joint must be greater than 1.1 times the sum of the nominal flexural resistances of the beams. In the CSA Standard the ratio of nominal strength to factored resistance for a column subjected to a low axial load is 1.2. If the factor, M_R , is defined as the ratio of the nominal column strengths to the nominal beam strengths, then the CSA Standard requires a minimum M_R of $1.1 \times 1.2 = 1.33$. In the 1989 ACI Code (ACI, 1989) the required value of M_R is 1.2. It is interesting to note that the ACI/ASCE Committee 352 (ACI/ASCE, 1985) recommended a value of M_R of 1.40 for beam-column joints subjected to seismic loading. The "weak-beam, strong column" design approach results in the columns remaining elastic, with larger values of M_R , giving not only larger column strengths, but also larger column stiffnesses, hence reducing storey drifts. The nominal strength ratio, M_R , is a key parameter which indicates the hierarchy of yielding. Values of M_R greater than 1.0 force hinging in the beam, while values of M_R less than 1.0 give undesirable yielding in the column.

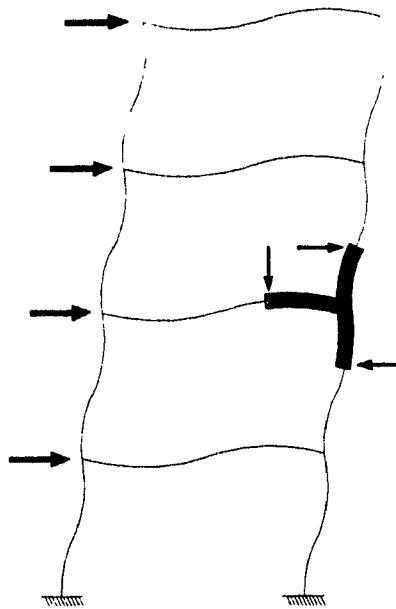


Figure 1.2: Exterior sub-assembly subjected to lateral forces

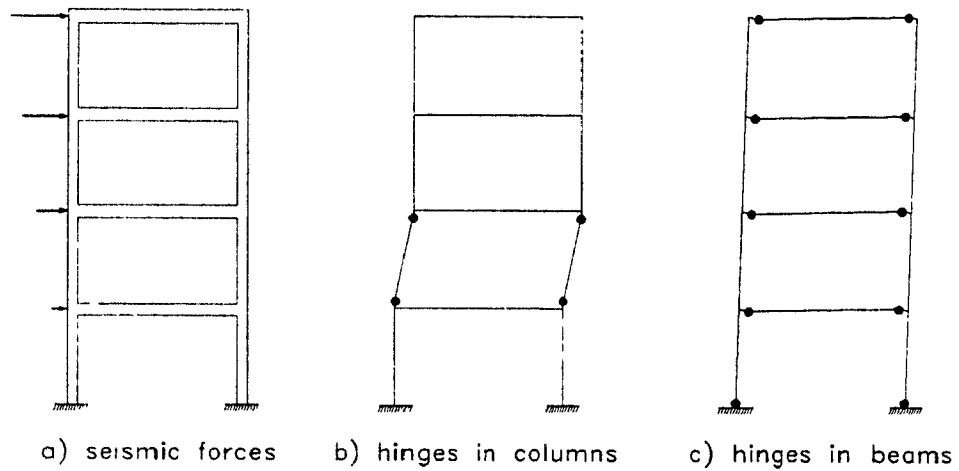


Figure 1.3: Different hinge mechanisms for frames

One of the important issues in ensuring the correct hierarchy of yielding is the determination of the flexural strength of the beams. In determining the nominal flexural resistance of a beam in negative bending, it is necessary to estimate the contribution of the slab reinforcement. In the CSA Standard (CSA, 1984) the effective slab width for this purpose is taken as three times the slab thickness, (i.e., $3h_f$) on both sides of the beam. This criteria does not take into account some of the important parameters affecting the contribution of the slab reinforcement. For example, at exterior joints, the size and strength of the spandrel beam plays an important role in affecting the effective slab width in negative bending.

The design of the joint is also affected by the number of slab bars in the effective slab width since the forces in these bars along with the forces in the beam bars must be transferred to the joint region. In calculating the joint shear, the forces in these bars are computed with a stress of $1.25f_y$, to account for the possibility of yield stresses above the specified yield stress and the effects of strain hardening. For an exterior joint the beam reinforcing bars continue through the joint region and are anchored at the far face of the confined core to ensure proper development of the tensile forces. The transverse reinforcement in the joint must be capable of transmitting the design joint shear and must also provide sufficient confinement of the joint region. The provision of sufficient shear capacity and adequate confinement is essential in order to avoid joint "yielding" and to achieve the "strong-column, weak-beam" hierarchy of yielding.

1.3 Summary of Previous Research

The following section does not attempt to provide a summary of all of the tests on beam-column subassemblages but rather reviews the results of some tests that have had an impact on North American design codes. Special attention will be given to research that has investigated the effects of floor slabs and transverse beams on the response. Of particular importance to this study are tests that have been carried out on exterior joints.

Blume *et al* (1961) carried out some of the first tests on beam-column connections. These tests showed the benefits of joint confinement on the hysteretic behaviour of beams but did not provide a clear understanding of the behaviour of the joint region since these tests did not have any shear transferred through the joint. These tests did not include slabs nor transverse beams.

Hanson and Conner (1967) were the first researchers to publish studies made on beam-column joints. They tested sixteen exterior and interior subassemblages which showed that with properly detailed reinforcement, joints could resist the effects of reversed cyclic loading, without a significant loss of strength. To achieve this desirable behaviour, they suggested the joint region should contain an adequate amount of closed hoops to provide adequate shear strength and good confinement.

Ma *et al* (1976), and Bertero and Popov (1977) tested nine beam-column subassemblages, some of which included slabs. These tests had a major impact on seismic design codes. They observed that the presence of the slabs increased the negative moment capacity of the beam and resulted in an increase in the energy dissipation per cycle of loading. The increased compressive resultant in the beam due to the higher moment capacity was found to cause early buckling of the bottom longitudinal bars in compression and to promote shear degradation. To prevent buckling of the bottom bars, the authors suggested the use of supplementary beam ties. They found that these added ties further increased the energy-dissipating capacity. They also found that the amount of compression reinforcement also affected the energy dissipating capabilities of the beams. They suggested that for improved energy dissipation, that the ratio of bottom to top longitudinal reinforcement in the beams be not less than 0.75. The authors concluded that strength degradation was due to either buckling of the bottom longitudinal bars or due to loss of shear transfer across full-depth cracks in the beam.

Ehsani and Wight (1982, 1985a) tested six exterior concrete beam-column subassemblies having floor slabs and spandrel beams. They also tested six specimens which had columns and main beams only (Ehsani and Wight 1982, and 1985b). The authors observed that pullout of the longitudinal bars was prevented and joint shear cracks were limited by the added confinement provided by the presence of the spandrel beams. They attributed this improved performance to the presence of the spandrel beam bars, passing through the joint region. The slab reinforcement parallel to the main beam was found to contribute significantly to the negative flexural moment capacity of the beam. In the design of the specimens they assumed that only the first set of slab bars adjacent to the beams would contribute. However, they observed that all of the reinforcement across the full width of the slab yielded in tension. This prompted the authors to conclude that the flexural strength ratio, M_R , may be overestimated if the slab reinforcement is neglected in design. They proposed that the slab bars within an effective slab width, at least equal to the width of the beam on each side of the column, be included. They also recommended that the M_R ratio be no less than 1.4. They observed that the avoidance of joint yielding gave more stable hysteretic behaviour. They concluded that the effective width of slabs in tension is not well defined.

A full-scale seven-storey reinforced concrete structure was tested in the U.S.-Japan cooperative research programme on earthquake engineering (Yoshimura and Kurose, 1985). The measured maximum base shear of the building under one-way lateral loading was more than 50% higher than that predicted. The difference was attributed to the contribution of the floor slab reinforcement acting together with the longitudinal beams which was not included in the design. The results from this full-scale test point out the need to properly account for the influence of the floor slabs and their reinforcement.

Durrani and Zerbe (1985) tested six three-quarter scale exterior beam-column-slab subassemblages. The primary objective of this research was to assess the effect of the slab on the behaviour of the connection. The configurations of their test specimens included one with no transverse beams and no slab, one with transverse beams and no slab, and four specimens with transverse beams and slabs of increasing widths. They found that the presence of the slab reinforcement increased the negative flexural capacity of the beam by as much as 70%. For transverse beams that reached their torsional yielding capacity during the test, the effective width of slab contributing to flexure was determined to be equal to the column width plus twice the depth of the transverse spandrel beam (i.e., $b_e = b_c + 2h_s$). The authors also noted that the transverse beams provided confinement to the joint region until their torsional capacities were reached.

A research programme at McGill University (Ratray, 1986, Paultre and Mitchell, 1987 and Paultre *et al.*, 1989) involved the testing of exterior, full-scale, beam-column connections with transverse beams and slabs. This investigation studied the role of the spandrel beams in limiting the effective width of the slab. The spandrel beams are subjected to torsion by the tensions in the slab bars which have a torsional eccentricity from the centroid of the spandrel beam. The torsional resistance of the spandrel beam was found to limit the amount of yielding of the slab longitudinal bars parallel to the beam. The CSA Standard (CSA, 1984) simply suggests a flange width of three times the slab thickness on each side of the main beam. For these tests the effective flange width was significantly greater than that of the CSA Standard.

They concluded that the slab contribution increases the beam strength and therefore reduces the flexural strength ratio and the negative moment ductility. The decrease in M_R , in some cases, could result in "weak columns" and "strong beams" which could alter the failure mode and reduce the overall ductility of the structure.

French and Boroojerdi (1987) tested three one-half scale interior beam-column subassemblages with transverse beams and slabs at the University of Michigan. These tests were

conducted to determine the influence of the torsional stiffness of the transverse beams on the effective slab width participating in tension at interior joints. One specimen had no transverse beams while another specimen had transverse beams identical to the main beam. A third specimen had intermediate sized transverse beams. They found that the specimens with increased torsional stiffness had a greater effective slab participation. The authors noted, however, that this difference between specimens decreased with increased deformations. The effective slab width from the test results was found to be greater than that determined from the ACI Committee 318 Section 8.10.2 (ACI, 1989). They also observed that the negative moment ductility was decreased for specimens with increased slab widths. They pointed out that this slab participation may decrease in frames subjected to skew earthquakes which would cause loading of the transverse beams and hence additional damage to these beams.

Cheung, Paulay, and Park (1991) tested three full-scale beam-column-slab assemblies, one of which was an exterior joint. They simulated loads that would result from earthquake actions along a line skewed from the frame line. For the exterior assembly tested, this resulted in the application of loads directly to the main beam as well as the spandrel beams at various stages. An investigation was carried out to determine the contributions of the floor slabs in the enhancement of the flexural strength of the beams. They found that the slab contribution was greatly decreased due to earlier yielding and stiffness loss of the loaded transverse beams as compared to uni-directional loading where the transverse beams were not loaded directly. They noted that even with this reduction in the effective width, the effective flange width was still larger than $b_e = b_c + 2h_f$ (twice the flange thickness on each side of the column) suggested by the New Zealand Standard 3101 (NZS, 1982). After considering the influence of many parameters, such as slab membrane action and effective anchorage of slab bars, they concluded that a high degree of accuracy in determining the effective width is not warranted, unless the amount of reinforcement in the slab relative to the beam is large and the level of protection assigned to columns is significant. They recommended that the effective width of slabs at exterior joints with transverse beams be taken as the lesser of: one quarter of the span of the transverse edge beam on each side of the column centreline, or one quarter of the span of the main beam taken on each side of the column centreline.

Gentry and Wight (1992), at the University of Michigan, carried out a study on the use of wide beam-column connections in reinforced concrete frame structures. These connections represent two way slabs on shallow beams where the beams are wider than the columns. The use of wide beams resulted in some of the longitudinal reinforcement of the main beam being anchored in the spandrel

beams, that is, outside the column region. The effective use of this part of the reinforcement in the calculation of the negative moment capacity is controlled by the torsional resistance of the spandrel beams. Hence, if the spandrel beam cannot resist the torsion induced by the tensions in these bars, the flexural capacity of the main beam may not reach the calculated design value. The cracking torque was found to be a reasonable upper bound in the torsional demand expected by the spandrel beams. The authors concluded that limiting the amount of longitudinal steel anchored in the spandrel beams and limiting the ratio of beam-width to column-width, would result in good performance of these structures.

1.4 Research Objectives

The overall objective of this research programme was to investigate the behaviour of beam-column-slab subassemblies in ductile moment-resisting concrete frames subjected to earthquake-type loading. In particular, the goal was to study the effect of the spandrel beams in limiting the contribution of the longitudinal slab bars (i.e., parallel to the main beam) to the flexural negative moment capacity of beams. One of the objectives is to develop a simple expression that would give the effective slab width, in which the slab bars are contributing. This effective slab width influences a number of key parameters in the design including:

- 1) The flexural strength ratio M_R between beams and columns may be overestimated if the effective slab width is underestimated in design.
- 2) The hierarchy of yielding between beams and columns to ensure "weak-beams" and "strong-columns" may be jeopardized if the slab contribution is not properly assessed.
- 3) The ductility and energy dissipating capacities of the beams may be significantly reduced by the increase in negative moment capacity due to the contribution of the slab bars.
- 4) A larger effective slab width would result in larger shears and moments entering the joint region and hence could result in premature joint yielding.

This study will also attempt to investigate the overall behaviour of the specimens designed with a force modification factor, R , of 4.0 and designed and detailed using the requirements of the CSA Standard (CSA, 1984). The extensive instrumentation of the test specimens will enable the

measurements of strains, displacements and loads during the loading sequence. The behavioral aspects of the specimens will be illustrated by: (1) the load versus deflection response; (2) the moment versus curvature response; (3) strain distributions across the slab width; (4) experimentally determined curvatures and shear strains along the main beam; (5) the tip deflection components and (6) the energy dissipating capacities of the specimens

Three full-scale exterior beam-column-slab assemblies with spandrel beams were constructed and tested to assess the above factors. One of the specimens was tested earlier by Rattray (1986) and Paultre (1987) under a similar programme. These specimens were subjected to uni-directional reversed cyclic loading.

Chapter 2

EXPERIMENTAL PROGRAMME

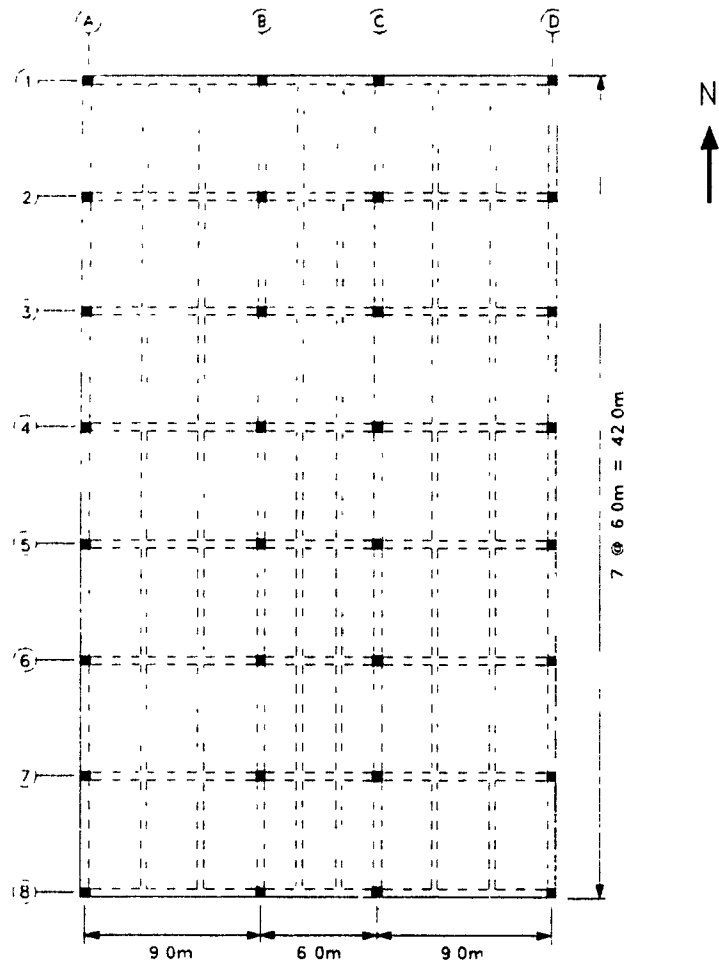
2.1 Description of Prototype Structure

The prototype structure is a six-storey reinforced concrete frame building located in Montreal. It has been designed using the 1990 National Building Code of Canada (NBCC, 1990) and the 1984 CSA Standard (CSA, 1984) with a force reduction factor, R of 4.0. This structure was previously used as part of a research program carried out by Paultre (1987) to assess the influence of design and detailing on the seismic performance of concrete structures in Canada. It was also used to study the influence of slabs in contributing to the negative moment capacity of beams located at exterior joints. This research was performed by Rattray (1986) as well as Castele (1988).

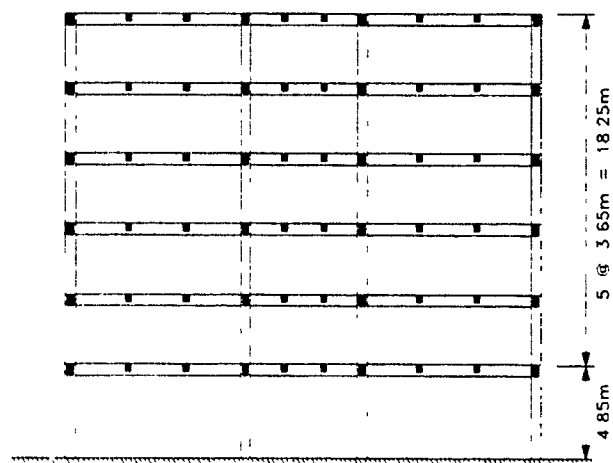
2.1.1 Building Description

The six-storey reinforced concrete frame building consists of 7 identical bays in the N-S direction spanning 6.0 m and 3 bays in the E-W direction where 2 - 9 m office bays are separated by a central 6 m wide corridor bay. The first storey height is 4.85 m and the remaining storeys are 3.65 m high. A plan and elevation view is shown in Fig. 2.1.

The interior columns have cross-sectional dimensions of 500 x 500 mm and the exterior columns are all 450 x 450 mm in cross-section. The main beams in both the N-S and E-W directions are 400 x 600 mm for the first 3 storeys and 400 x 550 mm in the top 3 storeys. The floor system consists of a one-way slab 110 mm thick supported on secondary beams spanning in the N-S direction. These beams are all 300 mm wide and 350 mm deep including the slab thickness. The exterior spandrel beams in the prototype structure are 400 mm wide and 600 mm deep.



PLAN



ELEVATION

Figure 2.1: Plan and elevation view of prototype structure (Paultre 1987)

2.1.2 Loading and Analysis Assumptions

The loadings for the original prototype structure designed by Paultre (1987) were determined using the 1985 NBCC Code (NBCC, 1985). However, the loadings from the 1990 NBCC gave factored base shears which were almost identical. Therefore, the design of the structure did not need to be modified. The design parameters using the 1990 NBC Code are given below

Floor live load.	2.4	kN/m ² on typical floors
	4.8	kN/m ² on 6 m corridor bay
Roof load:	2.2	kN/m ² full snow load
	1.6	kN/m ² mechanical services loading on 6 m wide strip over corridor bay
Dead loads:	24.0	kN/m ³ self-weight of concrete members
	1.0	kN/m ² partition loading
	0.5	kN/m ² mechanical services
	0.5	kN/m ² roof insulation
Wind loading:	1.24	kN/m ² net lateral pressure for top 4 storeys.
	1.18	kN/m ² net lateral pressure for bottom 2 storeys.
Seismic loading:	$v = 0.1$	seismic velocity for Montreal area
	$T = \text{estimated period} = \# \text{ of storeys} / 10 = 0.6$	
	$S = \text{seismic response factor} = 1.5 / \sqrt{T} = 1.94$	
	$I = \text{importance factor, taken as } 1.0$	
	$F = \text{foundation factor, taken as } 1.0$	
	$V = 0.03W$	where W is weight of structure plus 25% of snow load

An analysis of the building was carried out by Paultre (1987) using a linear elastic plane frame program in both directions. In the N-S direction, the analysis was simplified by reducing the structural model to a single frame subjected to one-eighth of the lateral load since the floor slab system was assumed to act as a rigid diaphragm. To obtain more realistic results due to cracking of concrete, the gross stiffnesses EI were reduced by 50% in the beam members and by 20% in the columns. The forces obtained from this analysis were then superimposed with those from the gravity load analysis.

2.2 Details of Test Specimens

2.2.1 Specimen Dimensions

The test specimens consist of three full scale, 2nd storey exterior joint subassemblages located as shown in Fig. 2.2. These specimens represent beam-column-slab connections with transverse spandrel beams. The test specimens are labelled R4, R4S, R4T. R4 was tested by Rattray (1988) and was designed using the 1985 Code with a K factor of 0.7. This corresponds to a force modification factor, R , of 4.0 in the 1990 NBCC. R4S and R4T were designed using the 1990 Code with R equal to 4.0. The only varying parameters in the three specimens are the dimensions and reinforcing details of the spandrel beams. R4S represents a specimen with a reduced Spandrel dimension and R4T has the same dimensions as specimen R4S but has less Torsional reinforcement. The objective of these different spandrel details is to achieve three different torsional resistances, which enables a study of the role of the spandrel beam in limiting the contribution of the slab bars in negative bending.

The cross-sectional dimensions of the specimens were dictated by the design of the prototype structure, while the overall dimensions were chosen to simulate the points of contraflexure in the beams and columns and to maximize the slab width which can be accommodated in the testing machine.

All three specimens consisted of 450 x 450 mm square columns having a total height of 3 m, which includes sections 1.2 m in length above and below the beam. This was the maximum height allowed under the loading mechanism. The main beam had a 400 x 600 mm cross section and extended 2 m from the face of the column. The slab was 110 mm thick and 1900 mm wide. The spandrel beam cross-section for R4 is 400 mm wide, 600 mm deep and extends 750 mm from the column face, while the dimensions for R4S and R4T are 250 mm wide and 600 mm deep. The 250 mm width dimension is the smallest allowed by the 1984 CSA Standard Clause 21.3.1(d) in order for it to be considered as part of a ductile space frame with a ductility of R equal to 4.0. A summary of these dimensions is illustrated in Fig. 2.3.

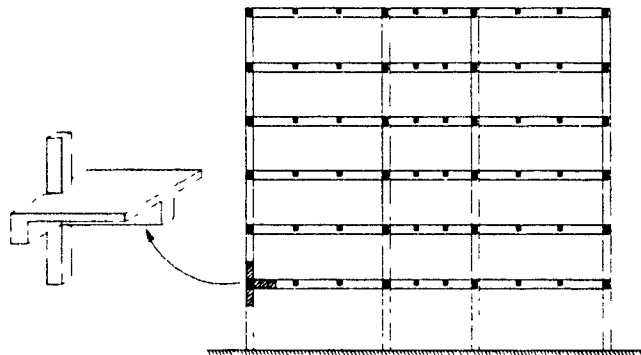


Figure 2.2: Location of full scale specimen

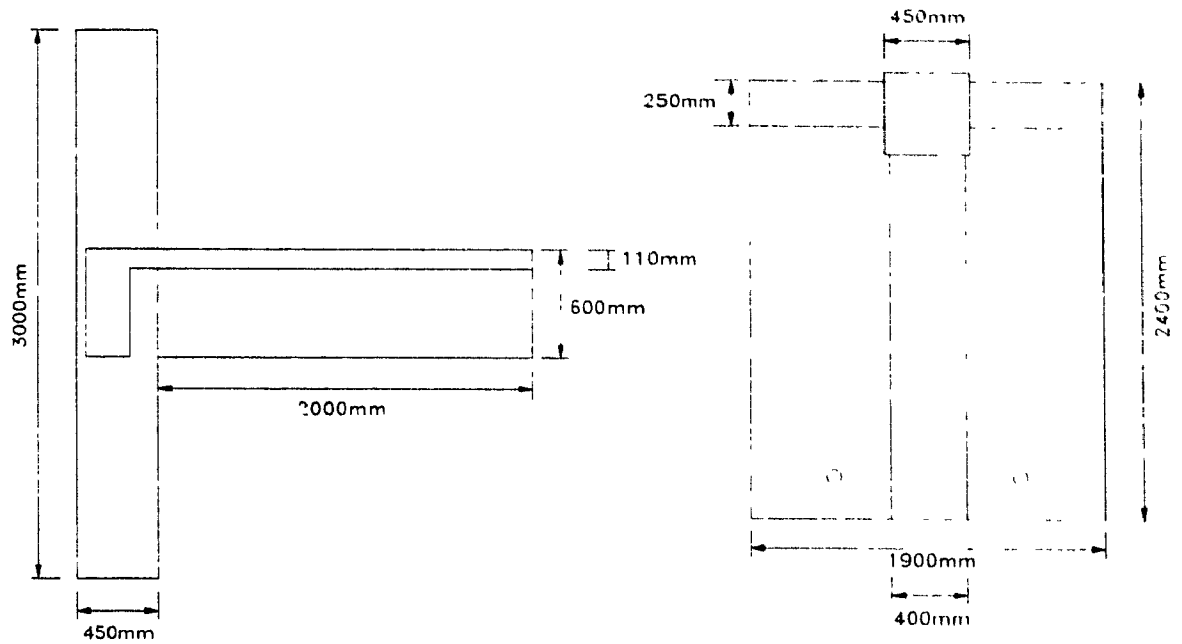


Figure 2.3: Dimensions of specimen R4S and R4T

2.2.2 Design and Details of Column, Beam and Slab Reinforcement

The design of all three specimens was carried out using a specified yield stress in all reinforcement, f_y , of 400 MPa and a concrete compressive strength, f_c' , of 30 MPa. The reinforcing design details for the main beam, the column and slab for each specimen were identical. The complete design calculations for the specimens are given in Appendix A. A brief discussion of the designs for the beams, the columns and the slabs for R equal to 4.0 are given below.

The requirements of Clause 21, "Special Provisions for Seismic Design" in the 1984 CSA Standard (CSA, 1984) governed the design of the beam, column and joint region. Design moments were obtained from the governing loading case assuming a moment redistribution of 20% in the beams.

The beam longitudinal reinforcement bars at the column face are limited by Clause 21.6.5.6, to a diameter, d_b , of $l_j / 24$, where l_j is the width of the joint region parallel to the main beam. For the joint dimension of 450 mm, the beam bars must be less than or equal to 19 mm. Hence, No.20 bars were used. The number of bars required to satisfy the factored negative moment was 4 - No.20 bars, considering that slab bars within a distance of $3h_f$ given by Clause 21.4.2.2 are effective. Since the positive moment at the column face must be at least half that of the negative moment stated by

Clause 21.3.2.2, 4 - No.20 bars were used for the bottom reinforcement in the beam. See the reinforcement details given in Fig. 2.4. Figures 2.5 to 2.7 show photographs of the test specimens.

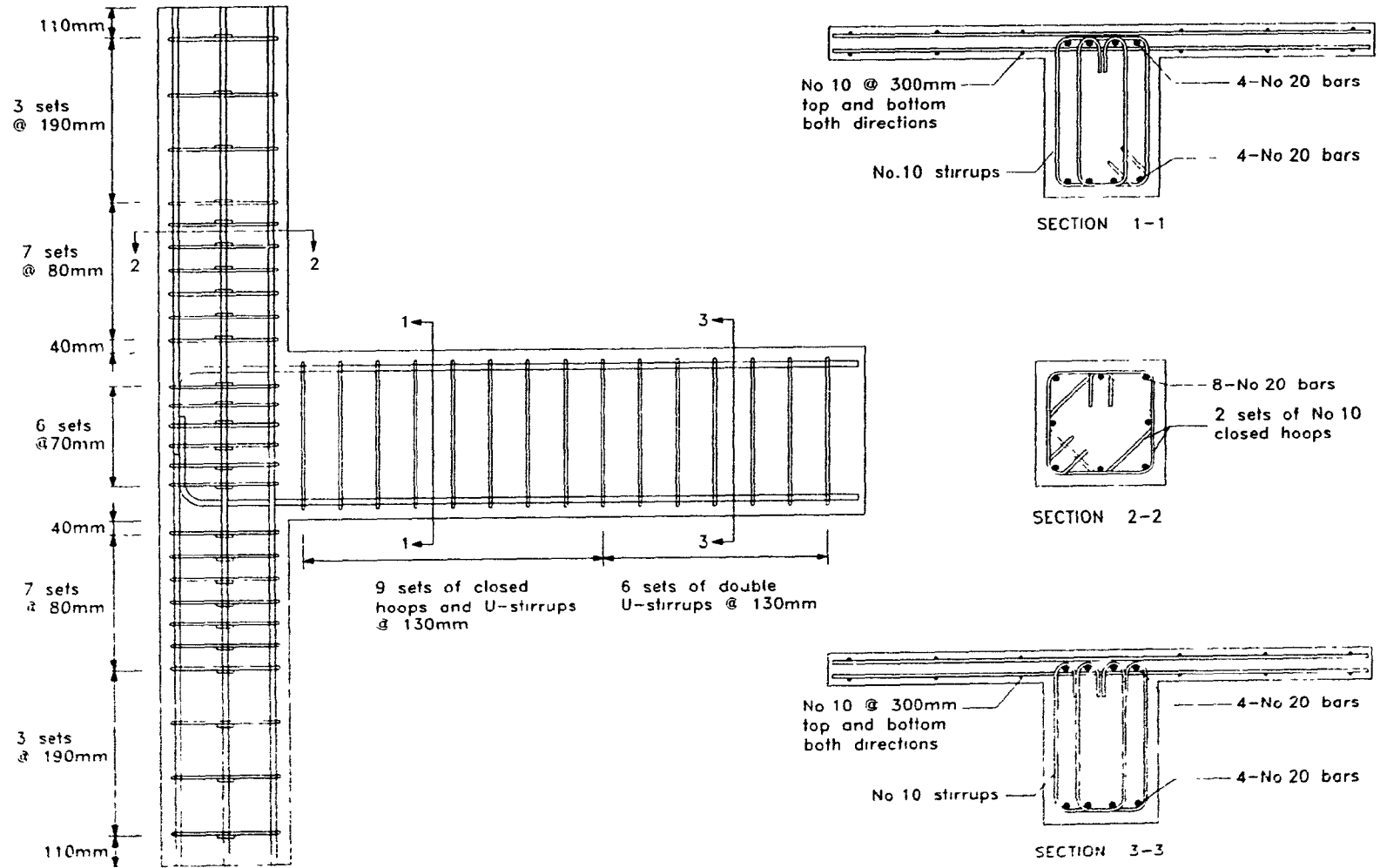
The shear reinforcement in the beam was determined considering the development of flexural hinging at the ends of the beam. Hoops, to prevent buckling of longitudinal bars, are required over a length of $2d$ from the column face (Clause 21.3.3.2). The spacing of these hoops shall not exceed that stated in Clause 21.3.3.3. Therefore hoops were provided at a spacing of 130 mm limited by a maximum spacing of $d/4$, over a distance of $2d$ or 1052 mm. In order to satisfy Clause 21.3.3.4 closed hoops providing 4 stirrup legs are necessary within this distance of $2d$. The first set of hoops were placed 50 mm from the column face and had 135 degree bends along with bar end extensions of $10d_b$, conforming with Clause 21.3.3.6. In the remaining section of the beam, the closed hoops were replaced by U-stirrups at 130 mm as shown in Fig 2.4

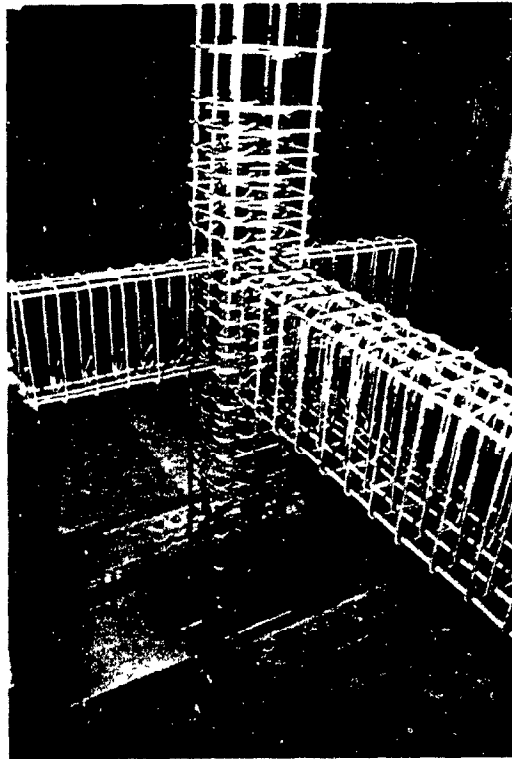
The diameter of the column longitudinal bars were also limited to $l_j / 24 = 600 / 24 = 25$ mm. To satisfy axial load and moment strength requirements, 8 - No.20 bars were adequate and provided a good confining configuration (see Fig. 2.4). This arrangement also resulted in a factored moment resistance which satisfied Clause 21.4.2.2, that the sum of the factored resistances of the columns be greater than 1.1 times the sum of the nominal flexural strengths of the beams ($\Sigma M_{rc} > 1.1 \Sigma M_{nb}$). The transverse reinforcement in the column was governed by Clause 21.4.4.2 which required closed perimeter hoops as well as diamond shaped hoops to provide the necessary confinement. The spacing of these hoops was 80 mm (Clause 21.4.4.3) and the hoops were required over a distance one-sixth the height of the column, (i.e., 508 mm). These hoops also had 135 degree bends along with $10d_b$ free end extensions. The first set was placed 50 mm from the slab face and 50 mm from the bottom of the beam. Outside this region hoops were spaced at 190 mm which corresponds to half the effective depth of the column (Clause 11.3.8)

Transverse reinforcement in the joint was used to provide confinement and sufficient shear resistance to the joint region. The design shear forces resulting from a stress of $1.25f_y$ in the beam longitudinal bars and contributing slab bars resulted in the use of 6 sets of hoops for this exterior joint region (see Fig. 2.4). These hoops were spaced at 70 mm (Clause 21.4.4).

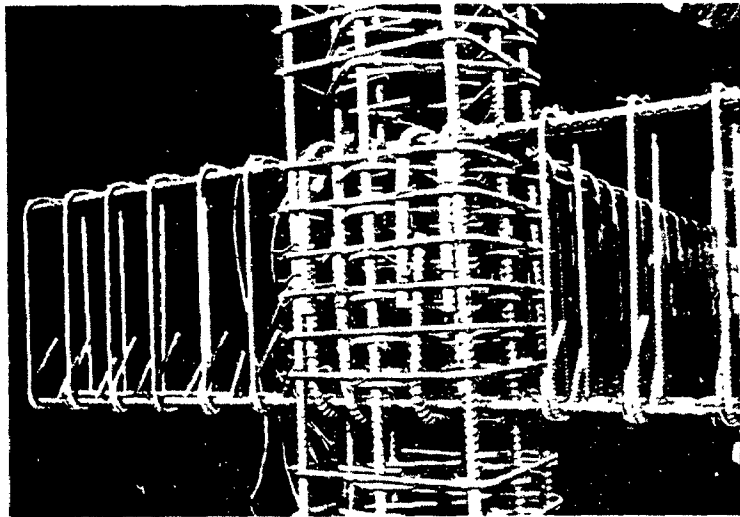
The slab reinforcement consisted of No 10 bars top and bottom spaced on 300 mm centres in both directions. The first set of bars around the column in both directions were placed at 50 mm from the column face. The bars anchored in the spandrel had 90 degree hooks with free end extensions of $12d_b$ confined within the core of the spandrel reinforcement. The clear cover for the slab bars was 20 mm.

Figure 2.4: Details of reinforcement for R = 4



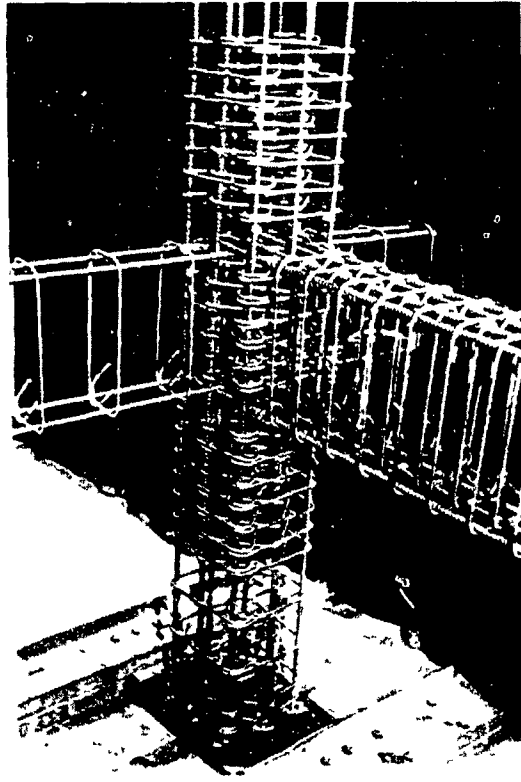


a) View of reinforcing cage and base connection

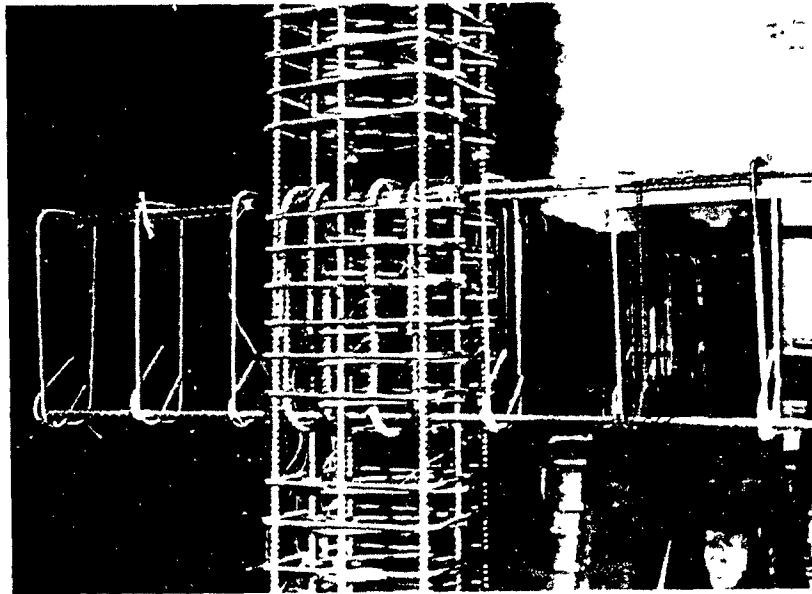


b) Back view of cage showing spandrel and joint details

Figure 2.5. Photographs of reinforcing steel for specimens R4S

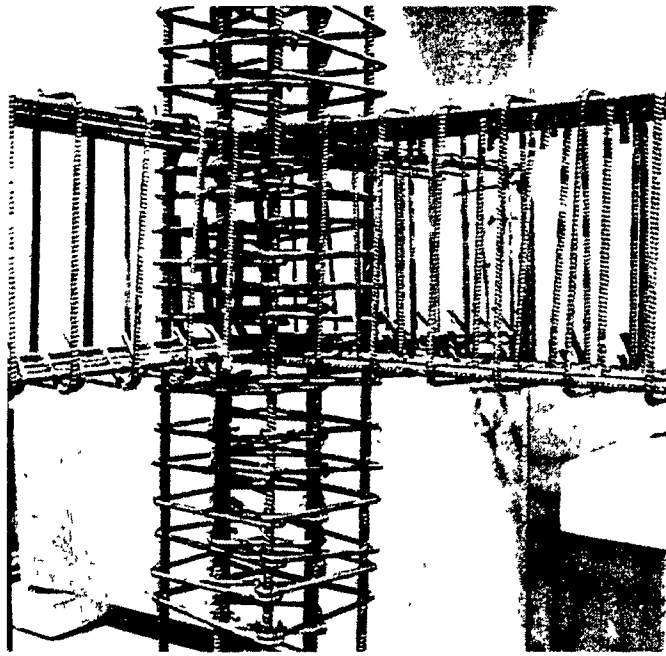


a) View of reinforcing cage and base connection

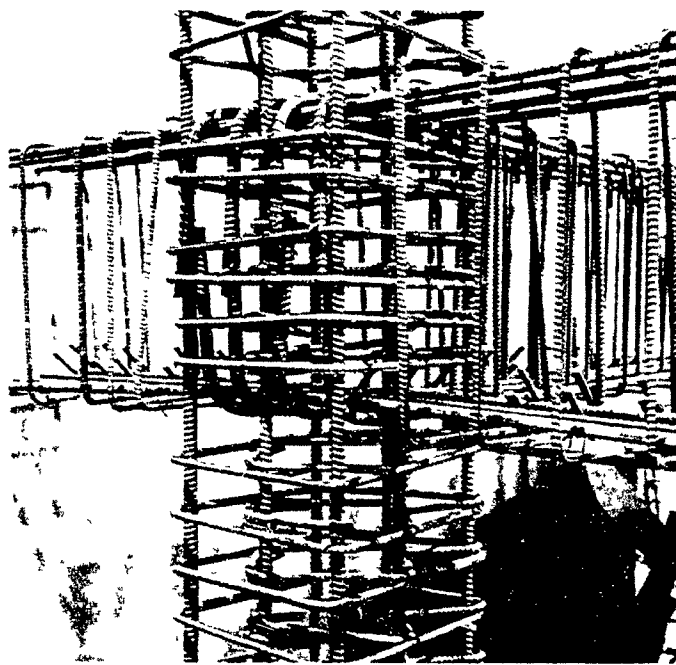


b) Back view of cage showing spandrel and joint details

Figure 2.6: Photographs of reinforcing steel for specimens R4T



a) View of reinforcing cage



b) Back view of cage showing spandrel and joint details

Figure 2.7: Photographs of reinforcing steel for specimens R4

2.2.3 Design and details of spandrel beam reinforcement

The details of the spandrel beam have been varied for the three specimens to investigate the influence of different spandrel beams on the overall seismic response of the specimen. The first specimen R4, had a 400 mm wide by 600 mm deep spandrel beam. The longitudinal reinforcement consisted of 4-No.15 bars on the top and 4-No.15 bars on the bottom, confined with closed hoops at a spacing of 125 mm. This spacing is governed by Clause 21.3.3.3.

Specimen R4S had a 250 mm wide by 600 mm deep spandrel. It was reinforced with 3-No.15 longitudinal top bars and 3-No.15 longitudinal bottom bars, confined with the same hoop spacing of 125 mm as in specimen R4.

Specimen R4T had same dimensions as R4S. The reinforcement, however, has been detailed in order to reduce the torsional capacity to about one half that of R4S. It consisted of 2-No.15 longitudinal bars on the top and 2-No.15 longitudinal bottom bars, confined with closed hoops spaced at 250 mm. Figure 2.8 shows the reinforcing details for each of the three specimens.

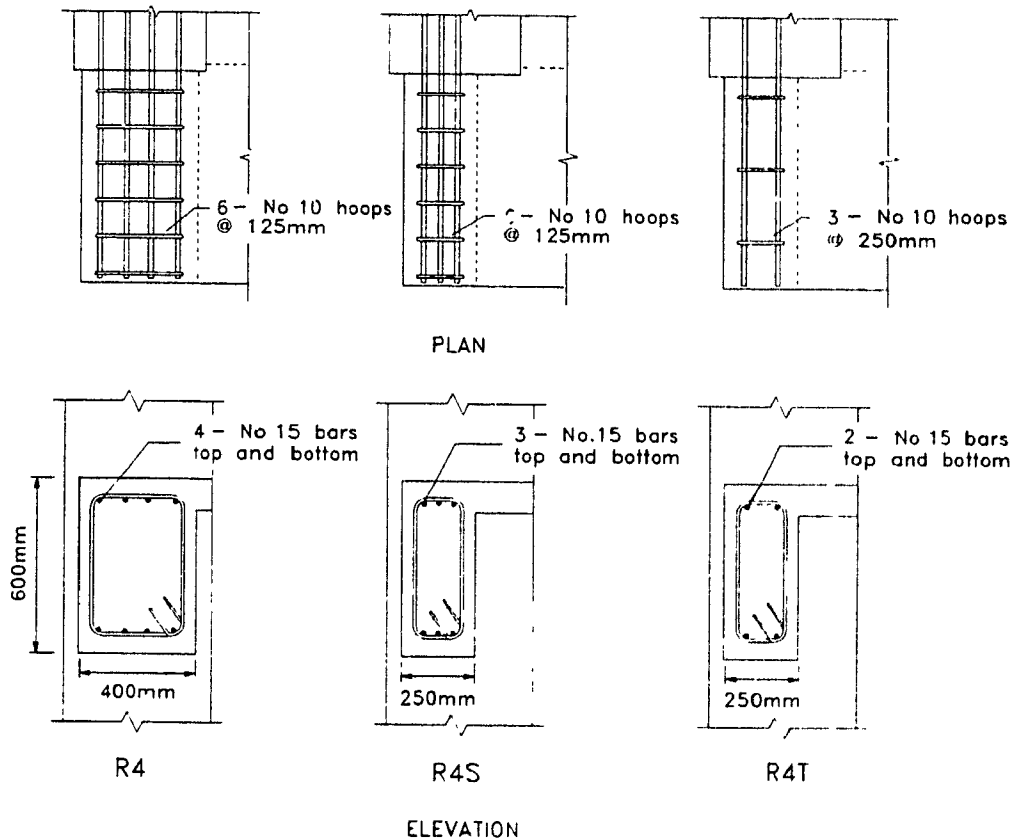


Figure 2.8: Spandrel reinforcing details for the three specimens

2.3 Material Properties

2.3.1 Reinforcing Steel

All reinforcement conformed to the CSA G30.16-M standard. In order to obtain stress-strain relationships for the bars, tension tests were performed on several samples taken from each bar size. Figure 2.9 shows the tensile stress-strain relationship obtained for the different bar sizes. It must be noted that strain readings were limited by the range of the 50 mm gauge length extensometer. Results of these tests are summarized in Table 2.1. The reinforcing steel properties for specimen R4 were those reported by Rattray (1986).

2.3.2 Concrete

Ready-mix concrete was used with a minimum specified 28 day compressive strength of 30 MPa. The maximum aggregate size was 20 mm and the slump was 100 mm. To simulate the actual construction sequence, two casts were required. The first batch was used for the lower column, the main beam with the slab and the spandrel beam. The second batch was used for the top half of the column. A total of 6 - 150 x 300 mm cylinder specimens were taken from each cast in order to determine the average concrete compressive strength and splitting tensile strength. These tests were done on each of the 4 batches from specimens R4S and R4T. Similarly, 6 - 150 x 150 x 600 mm flexural beam tests were performed to determine the modulus of rupture. Figure 2.10 shows the concrete compressive stress-strain relationship for these specimens.

The testing of specimen R4S was performed 97 days after casting of the first batch and had a compressive strength of 34.3 MPa while specimen R4T was tested 67 days after casting of the first batch and had a higher compressive strength of $f'_c = 46.6$ MPa. The results of the compressive and flexural strength tests are tabulated in Table 2.2.

Table 2.1: Properties of reinforcing steel

Specimen	Bar Size	f_y	e_y	f_{ub}
R4S & R4T	No. 10	486.9	0.0024	667.9
	No. 15	460.3	0.0026	731.6
	No. 20	463.6	0.0028	745.9
R4	No. 10	480.4	0.0024	520.9
	No. 15	471.5	0.0025	774.0
	No. 20	478.3	0.0026	763.3

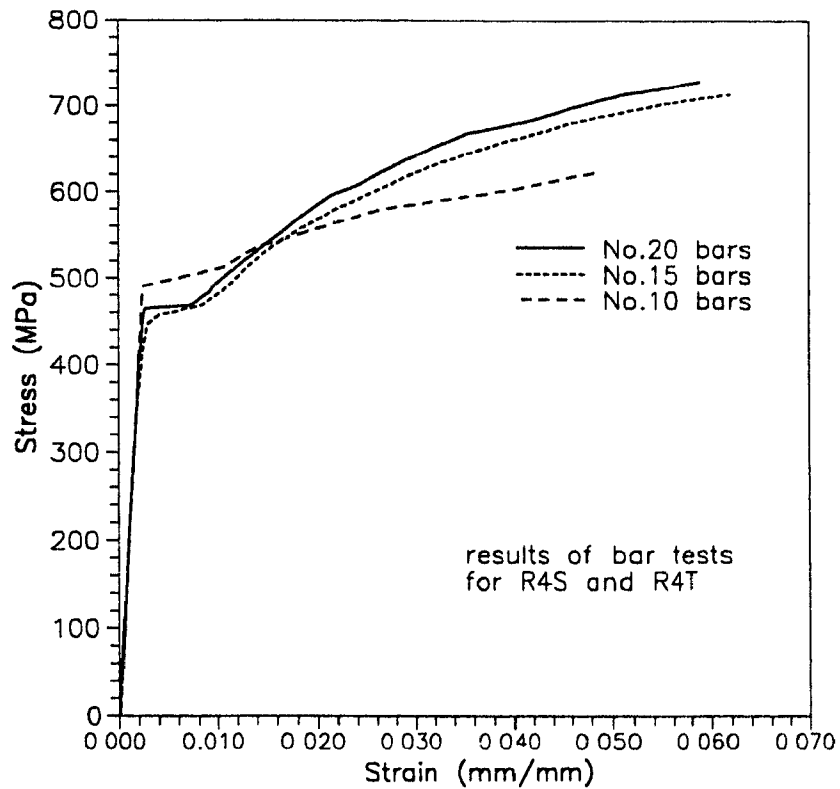


Figure 2.9: Stress-strain relationship for reinforcing bars

Table 2.2: Properties of concrete

Specimen	Batch	f_c'	f_t
R4S	1st	34.3	3.19
	2nd	25.0	3.04
R4T	1st	46.6	4.00
	2nd	30.5	3.65
R4	1st	40.4	2.60
	2nd	36.2	2.60

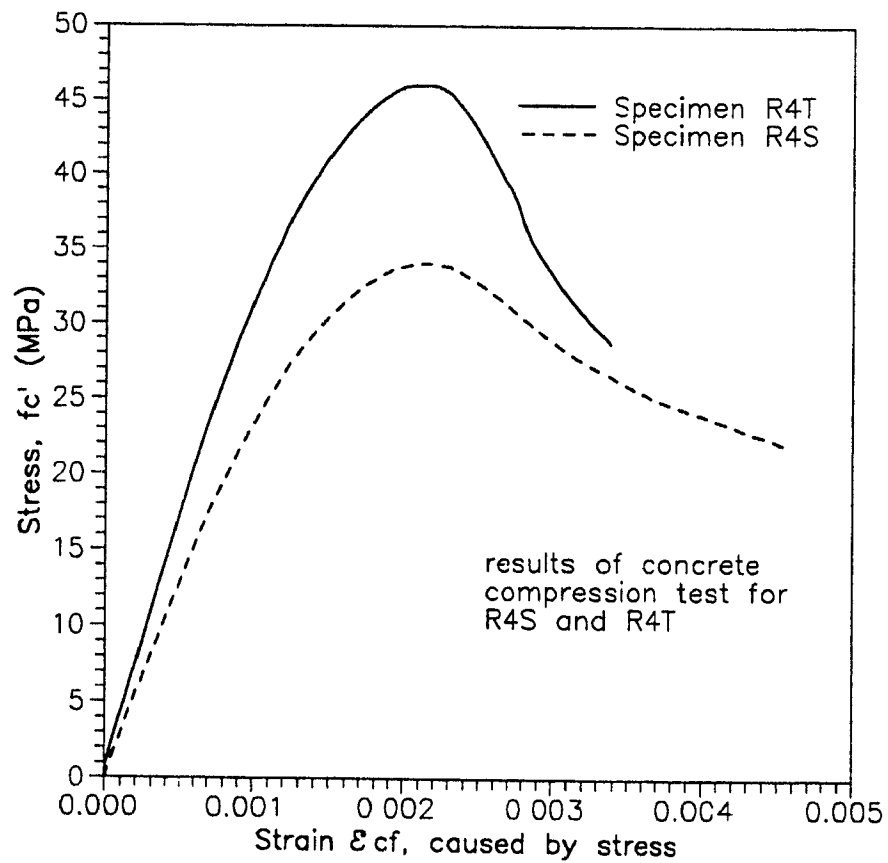


Figure 2.10: Concrete compressive stress-strain relationships

2.4 Experimental Procedure

2.4.1 Test Setup and Loading Apparatus

The full scale tests were performed in the Jamieson Structures Laboratory at McGill University which is equipped with a universal testing machine and a reaction strong floor. Figure 2.11 shows the overall test setup. The specimens were centred under the testing machine and subjected to an axial load representing the gravity loading in the real structure at the second storey level. As discussed in Section 2.2.1, the column length was chosen so that the ends would coincide with the points of contraflexure in the column. To simulate a hinge at the column ends the axial load was applied through a 76 mm diameter roller bearing against thick distribution plates. To provide lateral restraint at the ends of the columns, a 6 mm steel plate was bolted to two channel cross beams reacting against the testing machine and bolted to a plate which was welded to the longitudinal column bars. See details in Fig 2.12. The flexible plates allowed rotation without generating significant moments.

The lateral loads acting on the prototype structure were simulated in the laboratory by applying vertical loads to the main beam at a distance of 2000 mm from the column centreline. The loading producing negative moments in the beam was applied by pulling down on two 32 mm threaded rods. These rods loaded the main beam of the specimen through a steel loading beam bearing on a concrete surface area of 400 x 200 mm. This loading was provided by two 250 mm stroke hydraulic rams under the strong floor. Similarly, two 150 mm stroke hydraulic rams provided upward loading, producing positive bending in the main beam. These rams reacted against the bottom of the beam through a 50 mm diameter roller and a 400 x 100 mm plate. See the loading details in Fig 2.13.

The ends of both the column and the beam were heavily reinforced to prevent vertical splitting of the columns and premature shear failure of the beam loading end. To ensure proper development of the longitudinal bars in the spandrel beam reinforcement, 50 x 50 x 6 mm steel plates were welded to the ends.

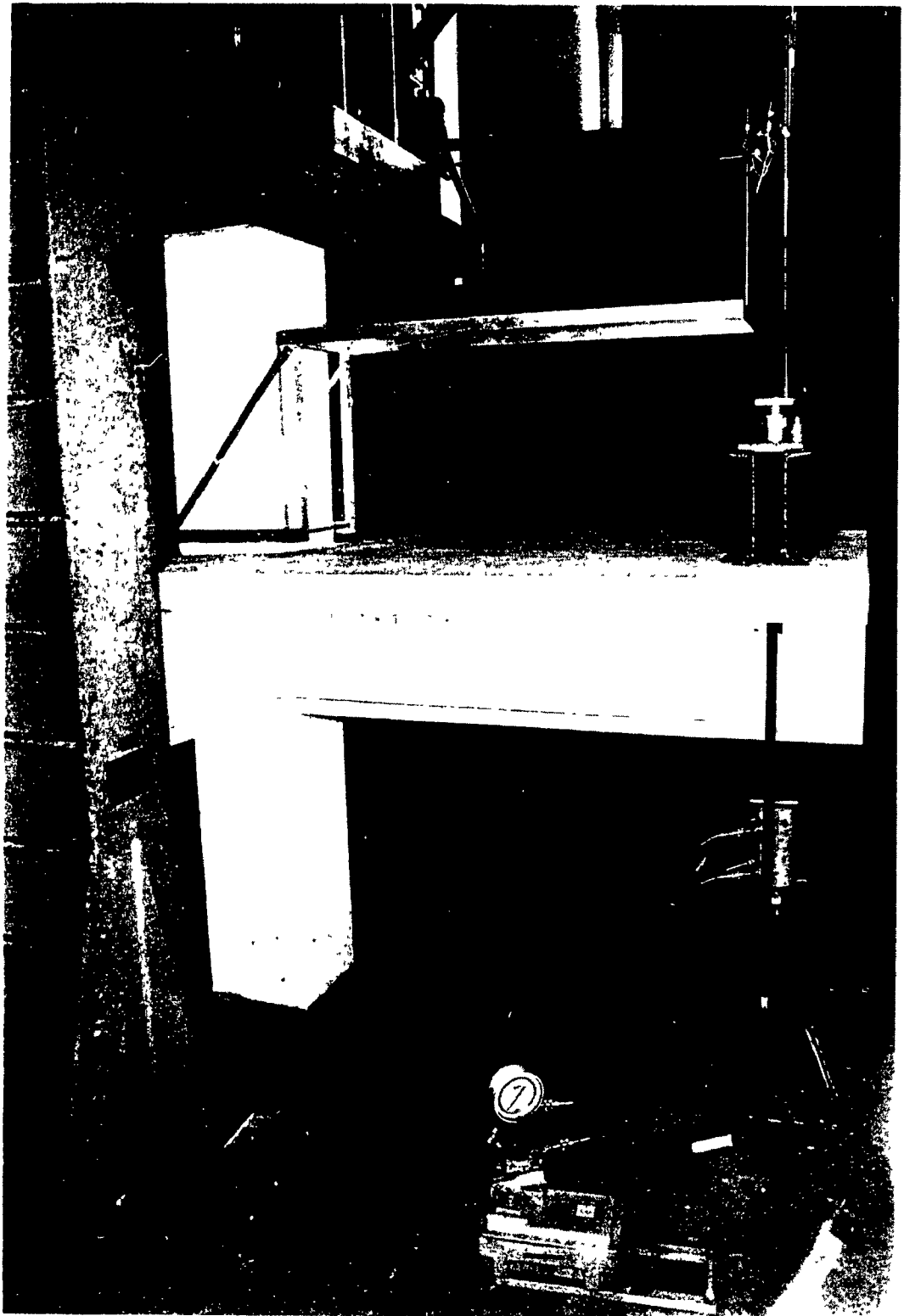


Figure 2.11 Test setup for all specimens

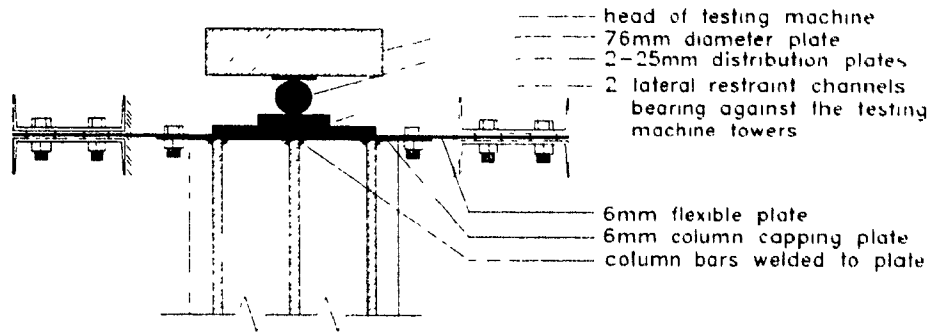


Figure 2.12: Details of column hinge connection

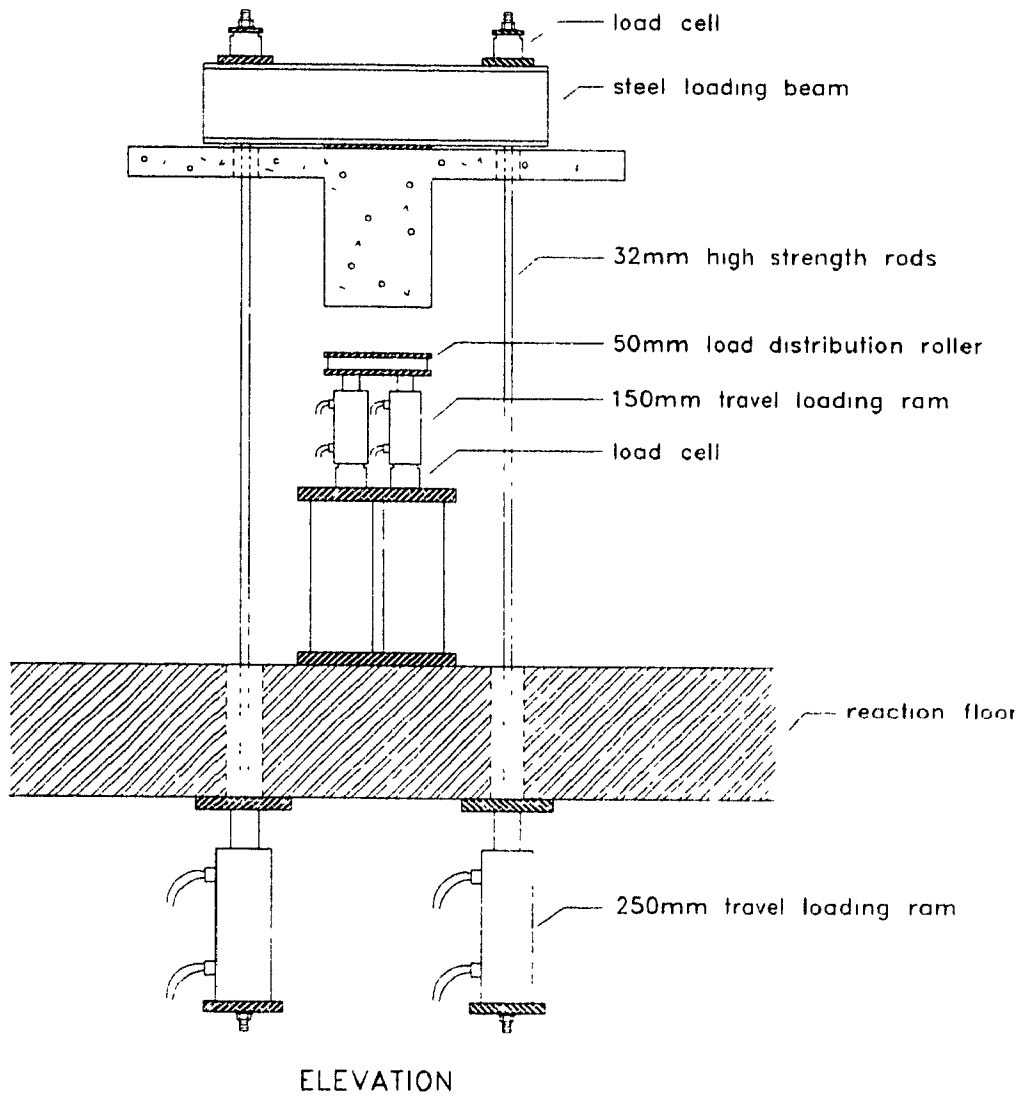


Figure 2.13: Details of loading mechanism

2.4.2 Instrumentation

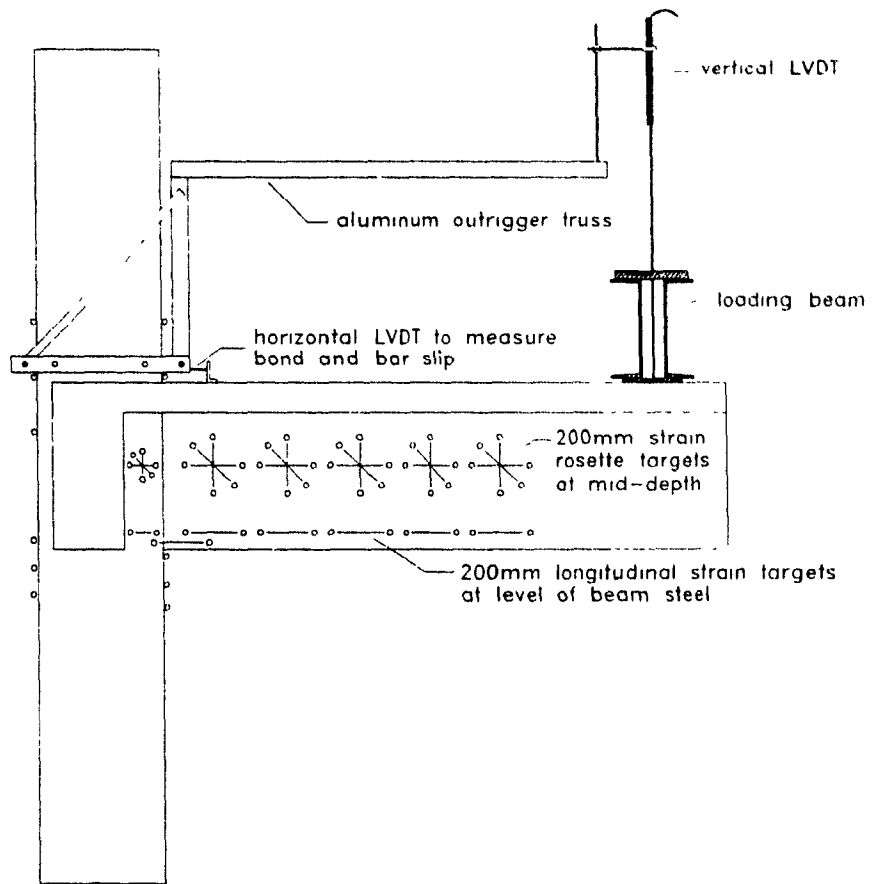
The instrumentation for the three specimens included load cells to measure forces, electrical resistance and mechanical strain gauges to measure strains and linear voltage differential transducers, LVDT's, to measure displacements. Load cells, electrical resistance strain gauges and LVDT readings were continually recorded by a data acquisition system. Mechanical strain readings were entered manually into a computer program during testing to provide calculated strains as testing progressed.

2.4.2.1 Load Measurements

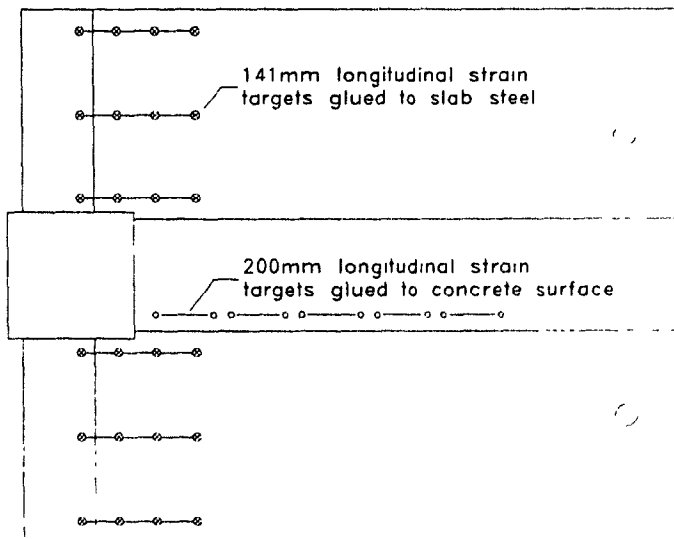
Two 445 kN and two 350 kN load cells were used to record the downwards and upwards loads respectively, applied to the main beam. The location of the load cells are shown in Fig. 2.13. The constant axial load on the column was measured by the 440 kip (2000 kN) capacity load cell of the universal testing machine.

2.4.2.2 Deflection Measurements

Two 250 mm travel LVDT's permitted measurements of vertical displacements of up to 225 mm in the downwards direction and up to 150 mm in the upwards direction. These LVDT's were mounted on a special frame as shown in Fig 2.14. This frame was fixed to the upper column just above the slab to permit the measurement of the beam displacement relative to the column. This displacement along with the measured beam end loads were used to monitor the overall response of the specimen. Two LVDT's attached to the slab and to the column below the main beam were used to estimate the bond slip and joint shear distortion at the top and the bottom of the joint. Two additional LVDT's were used to measure the movement across the cold joint between the upper column and the slab and to measure the relative deformations between the lower column and the bottom of the main beam. Figure 2.15 shows two of these four LVDT's visible from the top. The other two LVDT's are arranged similarly below the joint. For specimen R4T, four extra LVDT's were installed on the back face of the specimen to estimate the shear deformation in the joint, the twist of the spandrel relative to the joint, as well as the weak-axis bending deformations of the spandrel beam (see Fig 2.15)



ELEVATION



PLAN

Figure 2.14. Instrumentation of test specimens

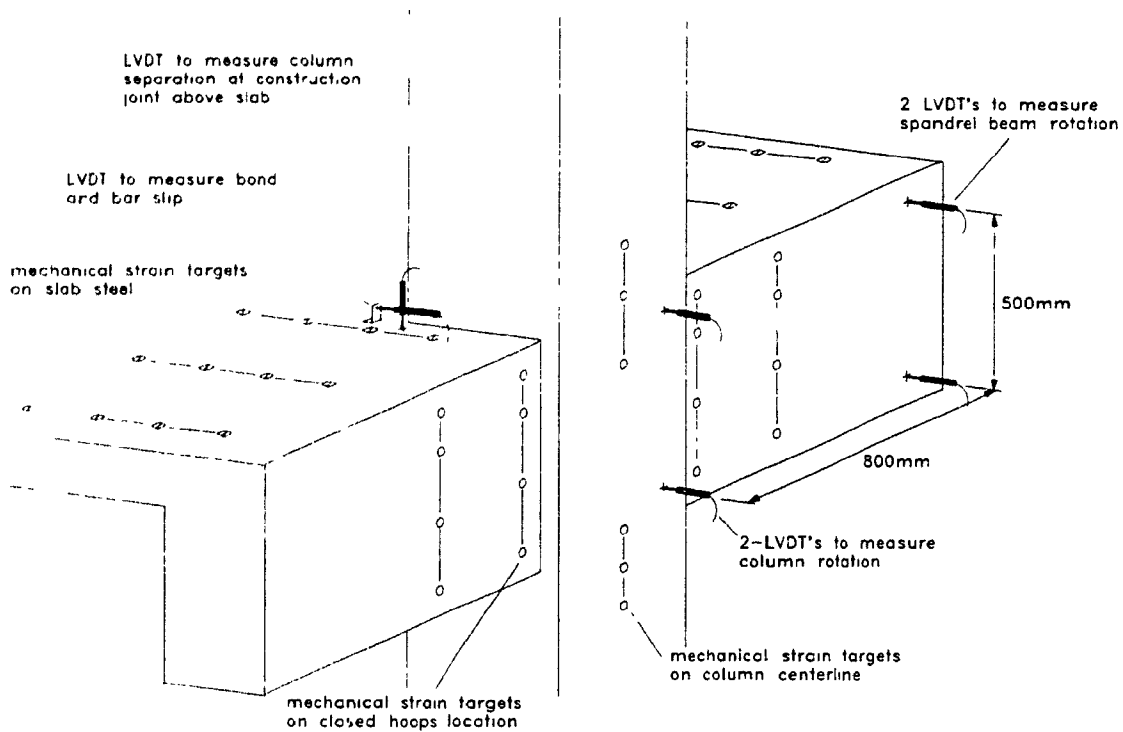


Figure 2.15: Details of instrumentation on back face of specimen R4T

2.4.2.3 Strain Measurements

Longitudinal strains were obtained along the beam at five different locations. These strain readings were taken on the top of the slab and at the level of the reinforcing bars at the bottom of the beam. The strain measurements were taken with a 200 mm gauge length, mechanical extensometer which reads the displacements between two targets on the concrete surface. The strains determined from these readings were used to calculate the curvatures along the beam. From these curvatures it was possible to estimate the component of tip deflection of the main beam due to flexure.

Five strain rosettes were formed by gluing strain targets to the surface of the web at mid-depth of the beam as shown in Fig 2.14. The strain readings obtained from these rosettes enabled the calculation of shear strains as well as the principal strains and their directions. The integration of these strains along the length of the beam enabled the estimation of the contribution of the shear

deformations to the tip deflection of the beam. For specimen R4S and R4T, a sixth rosette was placed on the side faces of the joint, exposed due to the smaller spandrel beam dimension. The spandrel beam was instrumented with strain targets having a 100 mm and 200 mm gauge length. These readings were used to obtain the strain in the hoop reinforcement on the exterior and interior faces of the spandrel beam on both east and west sides. Column strains were measured on all four faces near the joint region. The strains in the slab bars were measured by placing 10 mm high brass targets glued directly to the slab steel and accessible through small holes in the concrete cover formed by removable styrofoam plugs as shown in Fig. 2.16. As shown in Fig. 2.14, the strain targets were arranged to enable the determination of average strains in the slab bars across the slab width. These strain targets were located in rows along the slab-spandrel beam interface, along the beam-column interface, and along a row just in front of the column face. These readings would provide an estimate of the effective width of the slab.

In addition to the mechanical strain readings, electrical resistance strain gauges were used to monitor local strains at several key locations. Four gauges were placed on the four corners bars in the beam reinforcement at the face of the column to determine first yielding of the beam in positive and negative bending (see Fig. 2.17a). One gauge was placed on the spandrel beam longitudinal bar near the exterior face on both the east and west sides of the column-spandrel beam interface.

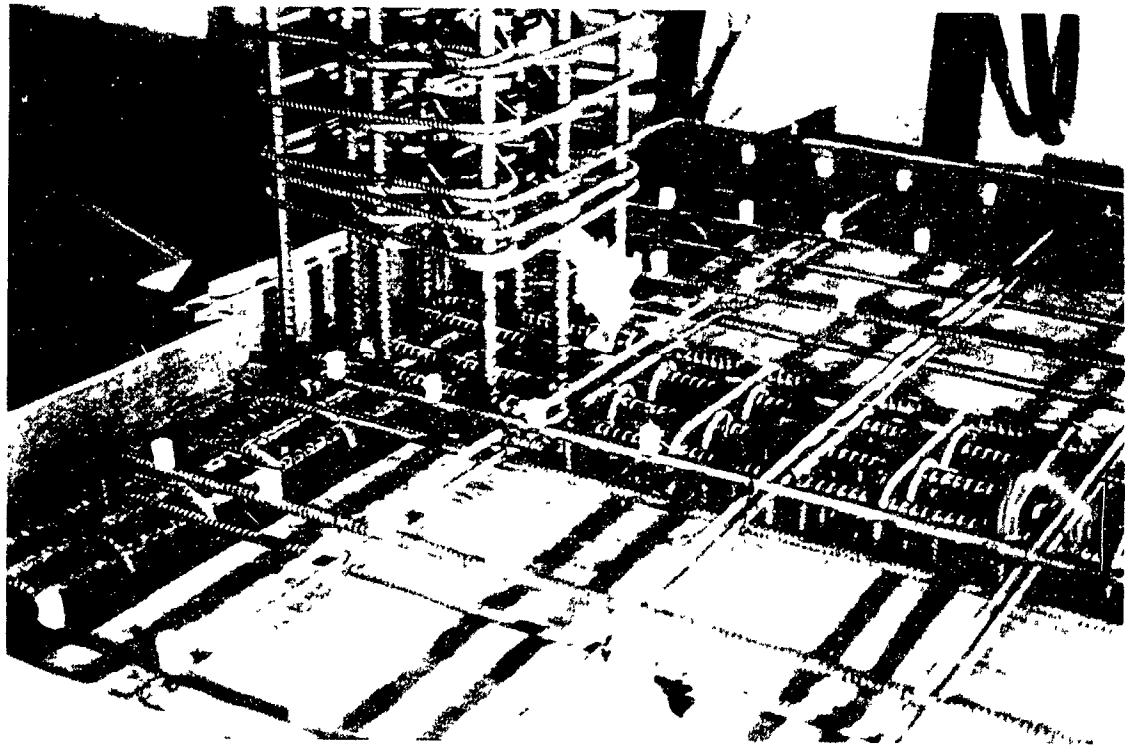


Figure 2.16 Photograph showing locations of targets glued to slab steel

Two gauges were also placed on the interior corner column bars at the slab interface. To study the behaviour of the joint region, four of the six square hoops were instrumented. The location of these gauges are shown in Fig 2.17.

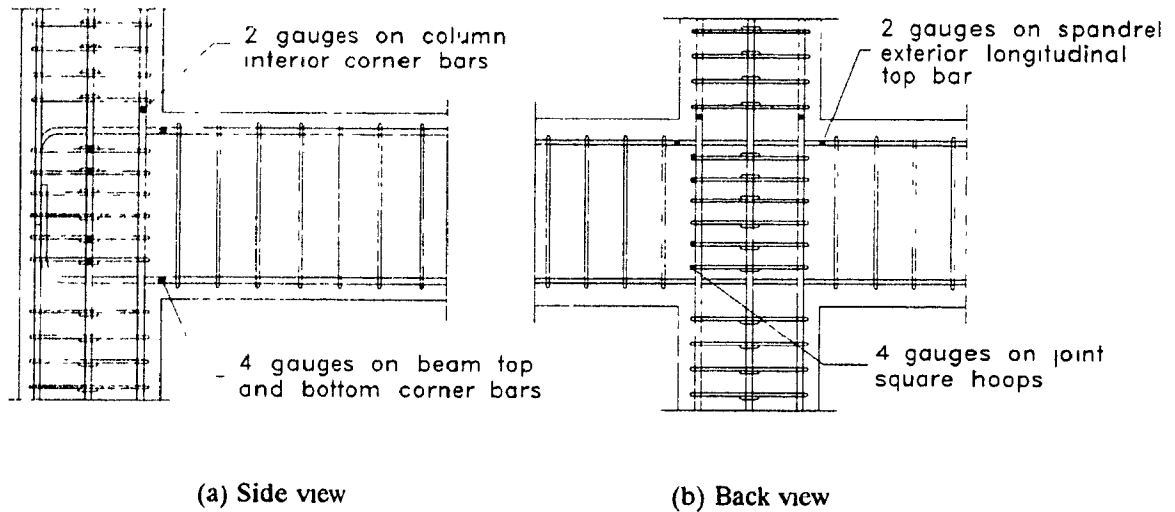


Figure 2.17: Locations of electrical resistance gauges on reinforcing bars

2.4.3 Testing Procedure and Loading Sequence

The specimens were subjected to a constant axial load on the column of 1076 kN, which is equivalent to 90% of the dead load on the prototype structure. This axial load corresponds to about 20% of the column capacity. The reversed cyclic loading procedure followed the loading history shown in Fig 2.18.

Downward deflections and loads on the main beam are taken as positive quantities while upwards deflections and loads are taken as negative quantities. Therefore downward loading produces negative moments in the beam. In the first cycle, load was applied until the full service moment in the beam was obtained. This corresponds to a moment 20% greater than the cracking moment ($1.2 M_{cr}$). In the second cycle, the beam was loaded until first yielding was obtained in the beam top longitudinal reinforcement. This was monitored by the top two strain gauges in the beam along with the longitudinal mechanical strain readings on top of the slab. In the third cycle, load was applied until general yielding of the beam occurred, that is, when the load-deflection response becomes non-

linear. The corresponding displacement was termed the general yielding deflection, Δ_y . Subsequent cycles were deflection controlled to peak deflections which were multiples of Δ_y .

During testing full sets of readings were taken at zero load, the peak load obtained in the previous cycle, the new peak load, and upon unloading at half the new peak load. The measurements included 70 mechanical strain readings and 20 electrical resistance strain readings. At the peak load of each cycle, several photographs of different elements of the specimen were taken. The loads, deflections and the electrical resistance strain gauges were sampled every 7 seconds during loading by the computerized data acquisition system to obtain complete response information.

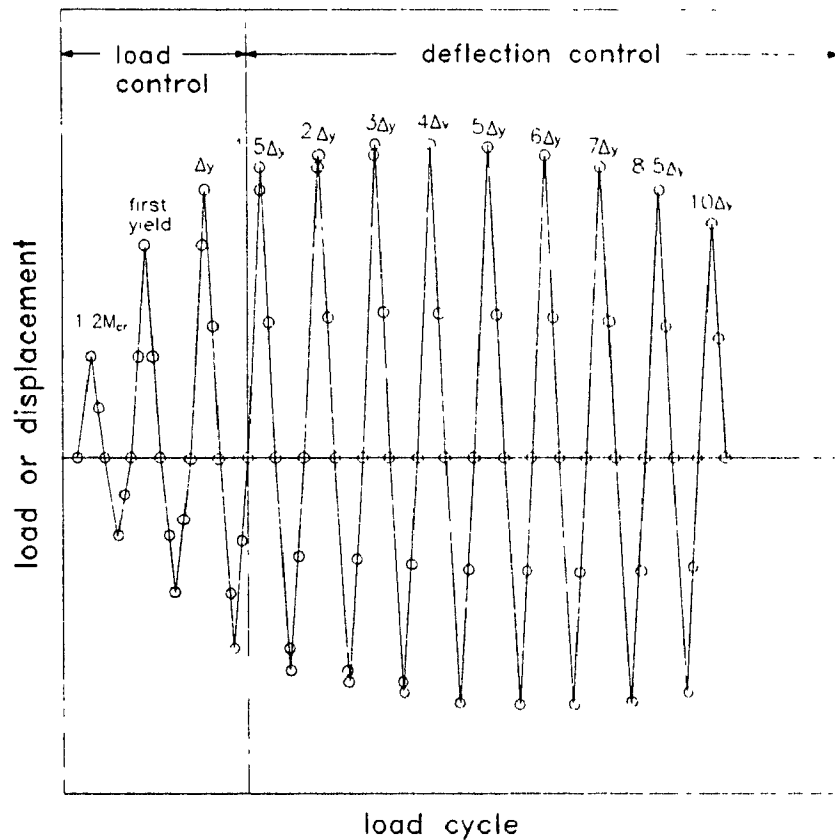


Figure 2.18: Loading-history for all specimens

Chapter 3

EXPERIMENTAL RESULTS

The overall responses of the test specimens are illustrated by means of load versus tip deflection responses. For these responses the loads and displacements plotted were those measured near the end of the beam, 2000 mm from the centre of the column (1775 mm from the face of the column). The moments in the beam at the column face were calculated from the applied load multiplied by a lever arm of 1.775 m and added algebraically to the beam and loading mechanism dead load moment of 23.6 kNm.

3.1 Specimen R4S

3.1.1 Load deflection response

The applied load vs tip deflection response for specimen R4S is shown in Fig. 3.1. The peak loads in each cycle and corresponding beam tip deflections are summarized in Table 3.1. In the initial loading stage, first cracking of the main beam in the positive loading direction (i.e., a downwards load) occurred at a load of +74.4 kN resulting in a cracking moment M_{cr} of 155.7 kNm. In the negative loading direction first cracking occurred at a load of -65 kN corresponding to a positive moment in the beam of 91.8 kNm. The value of the cracking moments for the beam were predicted to be 158.1 kNm for negative bending and 107.8 kNm for positive bending. These cracking moments were calculated assuming a modulus of rupture, determined from flexural specimens.

In the first cycle, the "service load" moment, assumed to be $1.2 M_{cr}$, in the positive loading direction occurred at an applied load of +89.4 kN and a deflection of 2.0 mm, resulting in a moment of 180 kNm. In the negative loading direction, the "service load" moment occurred at a peak load of -76 kN with a -0.8 mm deflection and moment of 115 kNm.

In the second cycle, first yielding of the beam longitudinal reinforcement in the positive loading direction occurred at a load of +199 kN at a deflection of 12.3 mm. This was confirmed by

frequent monitoring of the electrical resistance strain gauges and mechanical strain readings. In the negative loading direction, first yielding occurred at -123.2 kN with a deflection of -3.0 mm

At a positive load of +242.0 kN and a corresponding deflection, Δ_{yp} , of 19.4 mm, general yielding was judged to occur. In the negative half cycle, general yielding occurred at a deflection Δ_{yn} of 10.0 mm with a peak load of -193.2 kN

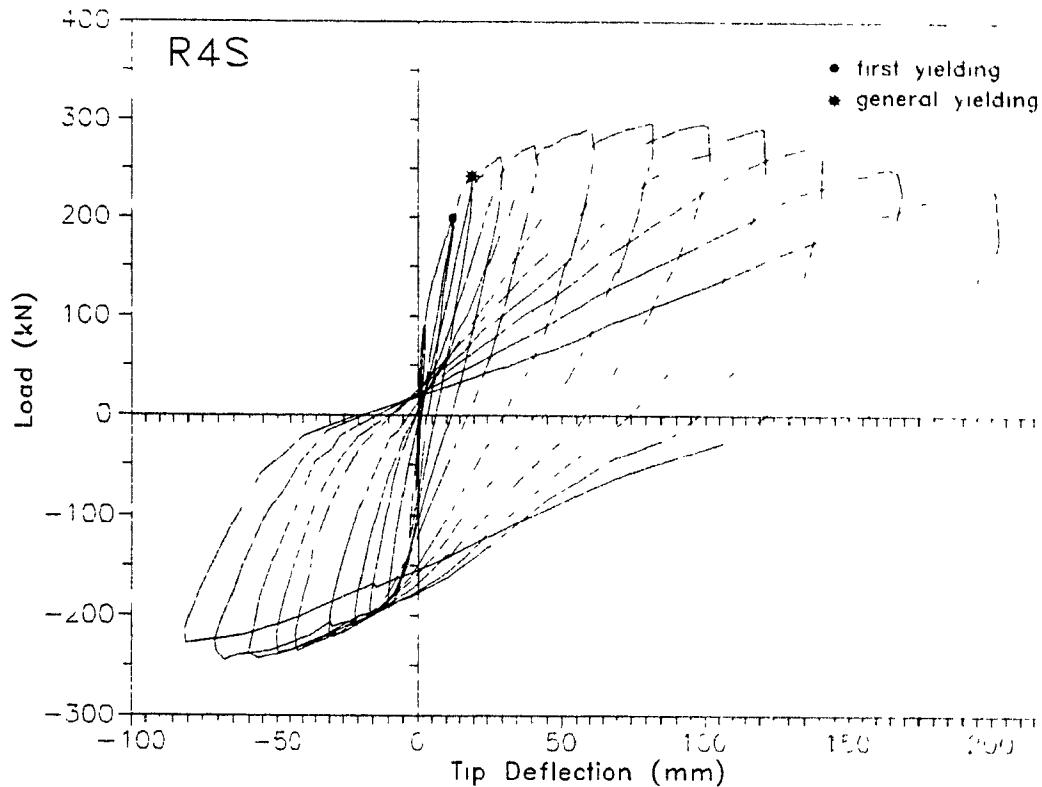


Figure 3.1: Load versus tip deflection response for specimen R4S

In subsequent cycles, the test was controlled by displacements in multiples of Δ_y in both loading directions. The maximum load sustained by the specimen in the positive direction came in the 7th cycle at a displacement ductility of $\Delta/\Delta_{yp} = 4$. The peak load was +296.8 kN with a corresponding maximum moment of 548.8 kNm in the beam and a corresponding deflection of 82.0 mm. The peak negative load was -245.5 kN with a positive moment of 415.7 kNm in the beam and a deflection of -70.1 mm. Upon further loading the specimen continued to maintain peak loads higher than the general yielding load and displayed increasingly larger hysteresis loops in both directions of loading. This continued until the beam bottom longitudinal bars buckled at a ductility of $8.5\Delta_{yp}$. All four bottom bars buckled between the first set of hoops spaced at 130 mm where

considerable spalling had occurred. The specimen was loaded one cycle further, after the bars buckled, to a displacement ductility of $10\Delta_{yp}$ in the positive loading direction. The recorded beam tip deflection at this point was 200.7 mm and testing was discontinued at this stage.

In general, the specimen showed excellent energy dissipating capabilities throughout the test. No significant signs of "pinching" were observed in the hysteresis loops. Stiffness degradation of the specimen increased at a uniform rate during the test.

Table 3.1 Applied loads and tip deflections at cycle peaks for specimen R4S

Cycle	Event at peak loads	Stage	Load (kN)	Deflection (mm)
1A	1.2Mcr	1	89.4	2.0
1B		5	-76.0	-0.8
2A	1st yield	9	199.0	12.3
2B		13	-123.2	-3.0
3A	gen. yield Δ_y	17	242.0	19.4
3B		21	-193.2	-10.0
4A	1.5 Δ_y	25	262.1	29.4
4B		29	-200.9	-15.8
5A	2 Δ_y	33	273.8	40.6
5B		37	-208.7	-20.7
6A	3 Δ_y	41	290.3	59.8
6B		45	-220.5	-29.6
7A	4 Δ_y	49	296.8	82.0
7B		53	-235.1	-42.0
8A	5 Δ_y	56	295.5	99.0
8B		59	-236.7	-49.6
9A	6 Δ_y	62	290.3	121.6
9B		65	-242.6	-56.9
10A	7 Δ_y	68	276.1	140.5
10B		71	-245.5	-70.1
11A	8.5 Δ_y	74	250.4	167.1
11B		77	-227.0	-80.6
12A	10 Δ_y	79	228.6	200.7

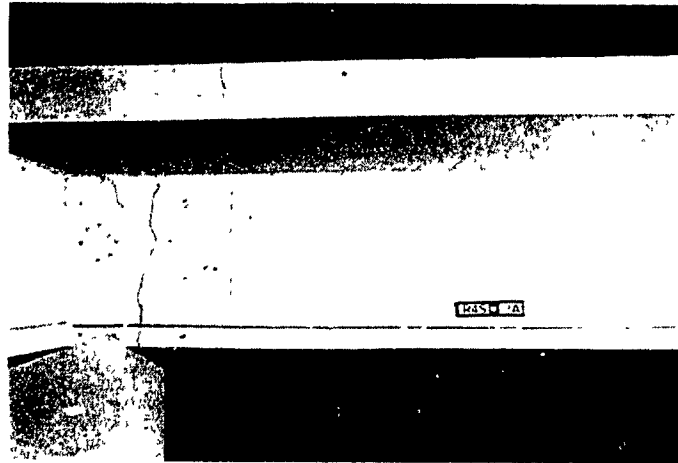
3.1.2 Beam behaviour

The first hairline crack in the first downward cycle of loading occurred at a distance of 90 mm from the column face and extended vertically through the slab to mid-height of the beam. A second crack appeared in the slab but did not propagate into the web of the beam. In the first negative loading cycle, two hairline cracks occurred on the bottom face of the beam at a location 50 mm from the column face and it joined with the first crack in the positive loading direction at mid-height. A second crack occurred 280 mm from the column face.

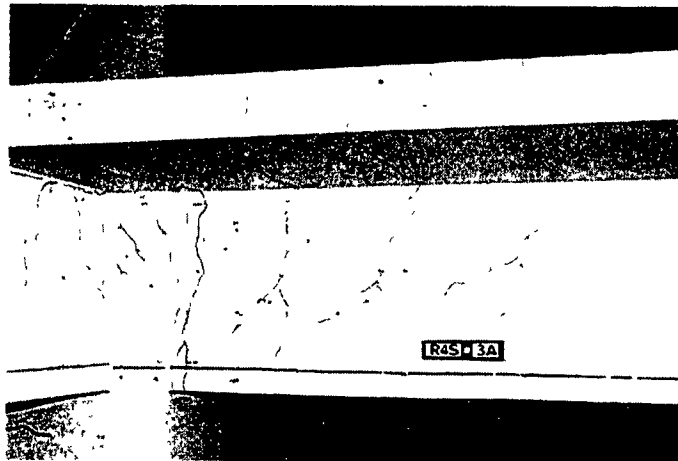
In the second positive loading cycle, a crack appeared on the exposed faces of the joint region at a load of +120 kN followed by three new flexural cracks at equal spacings along the beam (see Fig. 3.2a). The flexural crack spacing was 300 mm and corresponded with the spacing of the slab transverse reinforcement. These slab bars, with only 20 mm clear cover act as crack "initiators". These three new cracks occurred at loads of +125 kN, +140 kN, and +190 kN, respectively and became more inclined with increasing distance from the column, due to shear. The maximum crack width at this stage was 0.1 mm. In the second negative half cycle, more cracks appeared and joined with the previous cracks at mid-height.

At general yielding in the positive cycle, two 45 degree shear cracks appeared in the exposed region of the joint (see Fig. 3.2b). The cracks in the main beam opened up to widths of 1.0 mm in downward loading direction and 0.6 mm in upward loadings. In subsequent cycles, cracks continued to open and did not close fully upon load reversal.

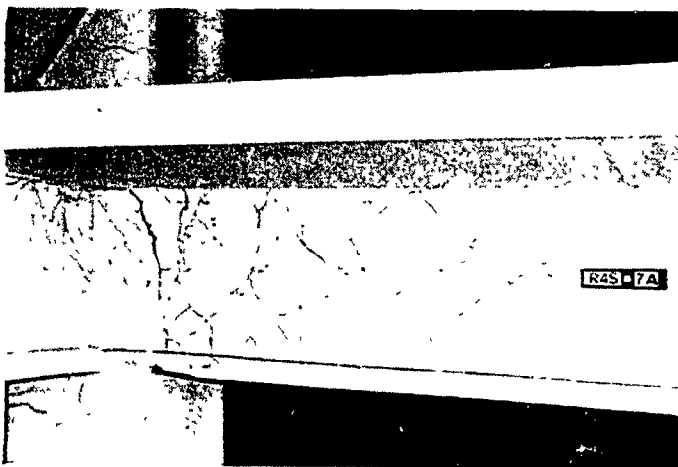
Crushing of the concrete in the beam occurred at the bottom face of the beam near the column in the 5th positive loading cycle. Cracks at this point opened up to 3.0 mm at the face of the column. Figure 3.2c shows the beam crack pattern in the 7th cycle where the maximum applied load was recorded. Cracks at this point were 7.0 mm in width. Flexural shear cracking was very evident especially on upwards loading. The flexural hinge region in the beam was estimated from curvature readings to be about 400 mm from the column face. In the 8th downwards loading cycle, the beam top bars near the column showed no increase in strain even though progressively larger cracks and displacements were taking place. This is evidence of some loss of bond of these bars and it was noted that the cover concrete showed signs of both crushing and spalling from the previous cycle. Splitting cracks, aligned with the bottom beam bars, appeared in the 10th cycle within a region 500 mm from the face of the column. Spalling of the concrete underneath the main beam occurred in the 10th cycle of positive loading and extended from the face of the column to the second set of hoops exposing the beam bottom longitudinal bars. Following the spalling of the concrete, at the peak downwards load in the 11th cycle, significant buckling of the 4-No 20 bars occurred between the first two sets of transverse hoops.



a) First yielding, $P = +199.0$ kN



b) General yielding, $P = +242.0$ kN



c) Maximum applied load, $P = +296.8$ kN

Figure 3.2: Photographs of specimen R4S at different stages

Figure 3.3 shows the buckled bars as well as the spalling of the concrete at a load of +250.4 kN, that is slightly greater than the general yielding load of +242.0 kN. In the 12th cycle, the peak load dropped below the general yielding load for the first time but the hysteresis loops showed that the energy dissipating capacity still increased. Figure 3.4 shows the curvature and shear strain distribution in the beam at different stages during the test. The curvature at general yielding was 12.5×10^{-3} rad/m while the maximum measured curvature was obtained in the 10th cycle with a value of 90×10^{-3} rad/m. The maximum shear strain at general yielding was 142.5×10^{-5} rad and the maximum value in the test was found in the 9th cycle to be 255×10^{-5} rad. In assessing these experimentally determined curvatures and shear strains it is important to recognize that there would be a considerable scatter of these values due to the discrete nature of the cracks. For situations where the cracks pass between the strain targets, larger curvatures and shear strains will be obtained.



Figure 3.3: Photograph showing buckling of longitudinal bars in specimen R4S

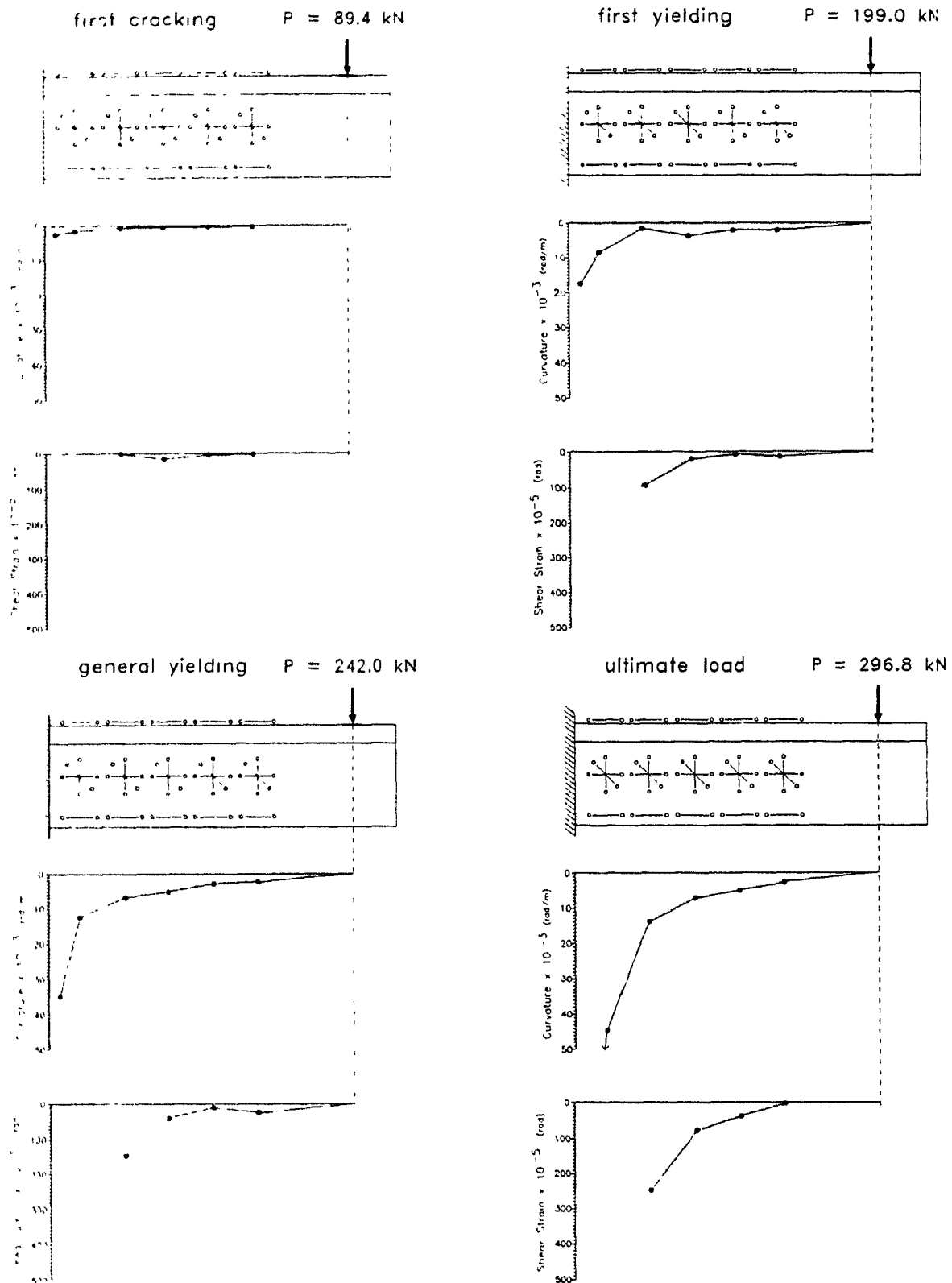


Figure 3.4: Curvature and shear strain distributions for R4S

3.1.3 Slab behaviour

In the first downwards loading cycle, two flexural cracks formed, crossing the first two sets of longitudinal slab bars, located closest to the column. In addition to these cracks, one small crack radiated out, at about 45 degrees, from each side of the column towards the spandrel beam. This was the first sign of torsional cracking. In the second downwards loading cycle, a second set of inclined torsional cracks appeared in this region as shown in Fig. 3.5a. Two new flexural cracks appeared in the slab at the 3rd and 4th transverse slab bars and extended across the entire width of the slab.

In the 5th downwards loading cycle, significant distress was noted around the column. The slab displayed longitudinal splitting cracks directly above some of the longitudinal slab and beam bars close to the column. Flexural cracks in the slab at this stage reached widths of up to 2.5 mm. At the peak load in the beam in the 7th positive loading cycle, there were four torsional cracks on the slab surface due to torsion in the spandrel beam, with a maximum crack width of 4.0 mm. Significant crushing of the concrete in the diagonal compressive struts occurred on the side faces of the column.

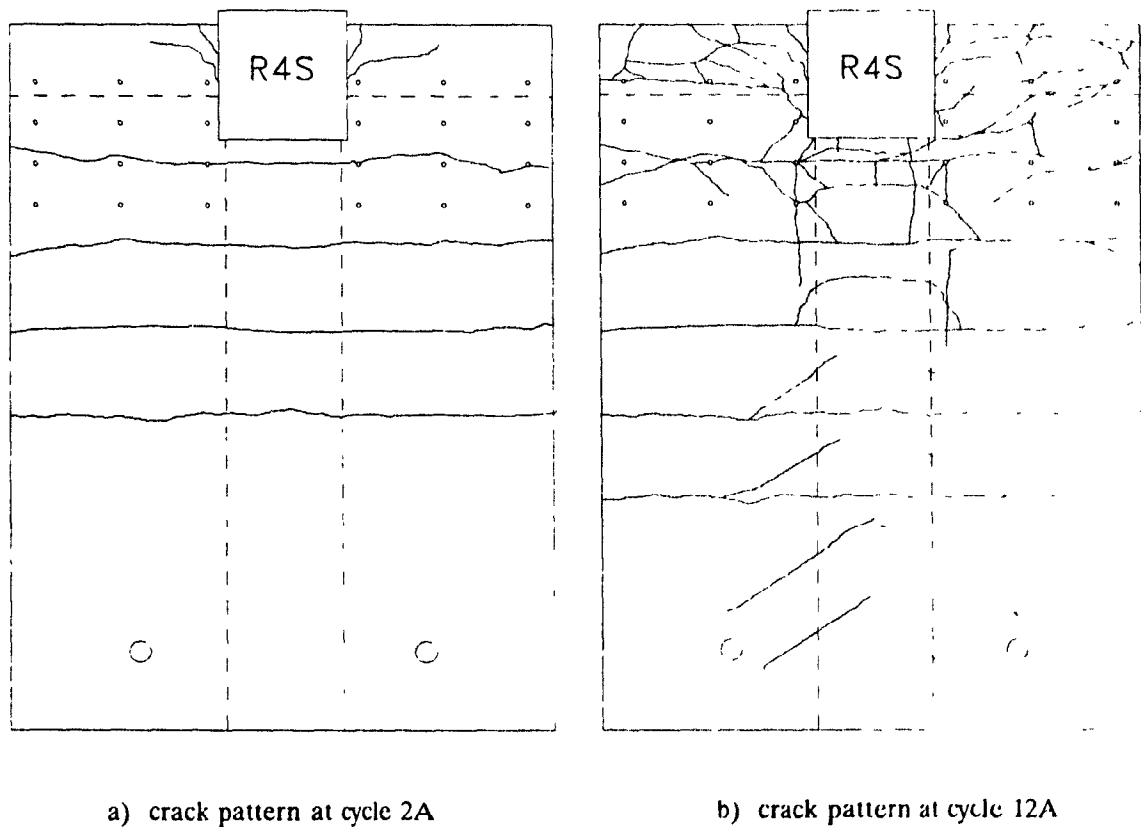


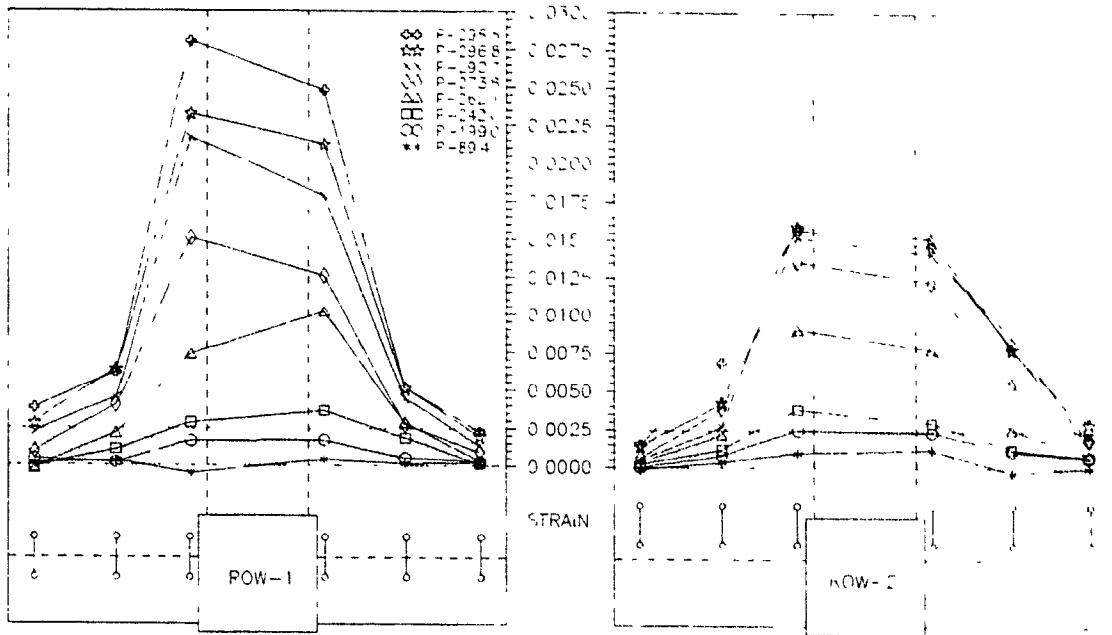
Figure 3.5: Crack patterns in slab of specimen R4S

In the 8th positive loading cycle, four sets of inclined cracks formed over the main beam. These cracks radiated out from the main beam and extended towards the loading point at an angle of about 45 degrees (see Fig 3.5b). Figure 3.6 shows that by the 11th downward loading cycle the large flexural crack at the column face had joined with the largest 45 degree torsional crack on the top surface of the slab, directly over the spandrel beam. This torsional crack spiralled around the spandrel beam (see Section 3.1.4)

Figure 3.7 shows the strain distribution in the longitudinal slab bars for specimen R4S. Each figure is a plan view of the specimen with strains plotted at the peak load in each positive loading cycle. These graphs show the strains determined over a gauge length of 141 mm at the locations indicated. The shaded region on the figure indicates strain values less than the yield strain, ϵ_y . The yield strain for these No 10 bars is 0.0024. As can be seen, at general yielding ($P = +242$ kN), two slab bars had yielded. Higher strains were measured in the slab bars along the slab-spandrel beam interface than along the line of the beam-column interface. The strains in ROW-3, some distance out from the column face are lower than at the column face, as expected.



Figure 3.6: Photograph showing severe cracking and local crushing around column region of specimen R4S



R4S

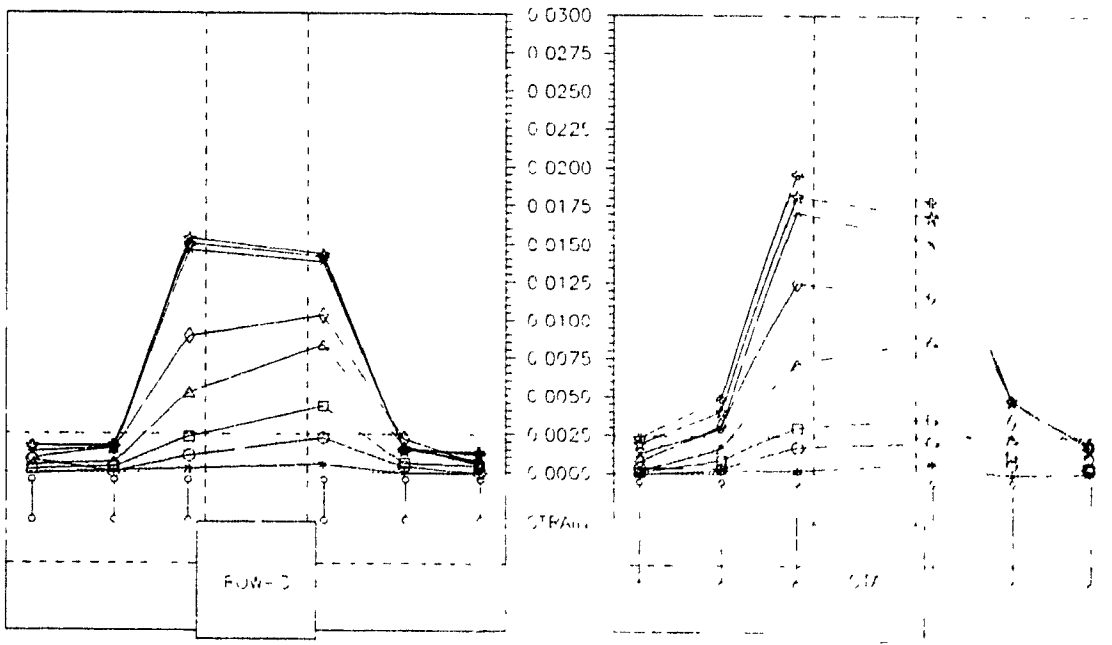


Figure 3.7: Strain distributions in slab longitudinal bars for specimen R4S

3.1.4 Spandrel beam behaviour

Cracks in the spandrel beam appeared in the very 1st downward loading cycle. The first crack occurred along the two spandrel beam-column interfaces extending over two-thirds of the depth of the beam. At the peak load of +89 kN in that cycle, a crack appeared in the spandrel beam on each side of the column at about 100 mm from the joint face between the first two sets of closed hoops spaced at 125 mm. These cracks were only 70 mm long and were signs of the start of torsional cracking in the spandrel beam.

In the second downward loading cycle, at a load of +199 kN, the interfacial shear crack reached the bottom of the interface and the torsional crack extended to mid-height of the beam inclined at approximately 45 degrees. The maximum crack width at this stage was 0.4 mm indicating yielding of the spandrel beam. On the interior face of the spandrel, the slab cracked right along the spandrel beam-slab interface and the torsional crack that occurred on the exterior face had spiralled around to the interior face of the beam. In the subsequent upwards loading cycle, these cracks closed completely.

At general yielding, the 45 degree torsional cracks in the spandrel beam extended all the way to the bottom face with a maximum measured crack width of 0.9 mm (see Fig 3.8).

Onset of new torsional cracks occurred at a downwards load of +274 kN starting at the top of the spandrel beam, at a distance of 400 mm from the column face



Figure 3.8 Photograph of exterior face of spandrel beam of specimen R4S at general yielding

At this stage significant twisting of the spandrel beam had occurred and maximum crack widths of 4.0 and 3.5 mm were recorded on the exterior face of each spandrel beam. The interior face of the spandrel beam also displayed significant cracking and concrete crushing started along the spandrel beam-slab interface. At a downwards load of +297 kN, significant diagonal crushing of the concrete occurred on the top surface of the beam close to the column. In subsequent cycles, the torsional cracks continued to open and reached a width of 10 mm by the 9th downward loading cycle. Figure 3.9 shows the twisting of the spandrel beam, with concentrated rotations occurring at the beam-column interface and at the main torsional crack locations. In addition there was lateral bending of the spandrel beam giving deflections towards the interior of the specimen. The final state of the spandrel beam near the column region can be seen from Fig. 3.3. Some crushing of the concrete was evident at the bottom of the interior face near the joint region due to diagonal compressive stresses caused by the torsion. After testing the slab had completely separated from the spandrel beam close to the column. The exterior view of the specimen, shown in Fig. 3.10, clearly shows the torsional cracking of the spandrel beam at the end of the test.

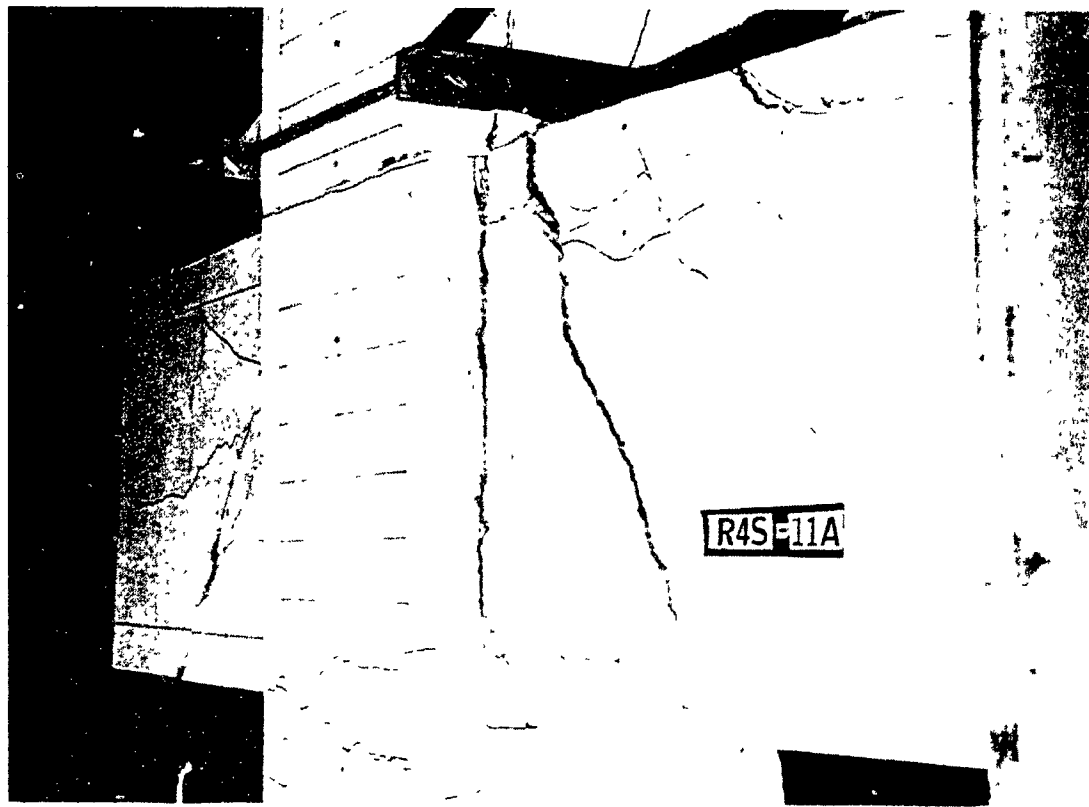


Figure 3.9: Photograph of exterior face of spandrel beam of specimen R4S

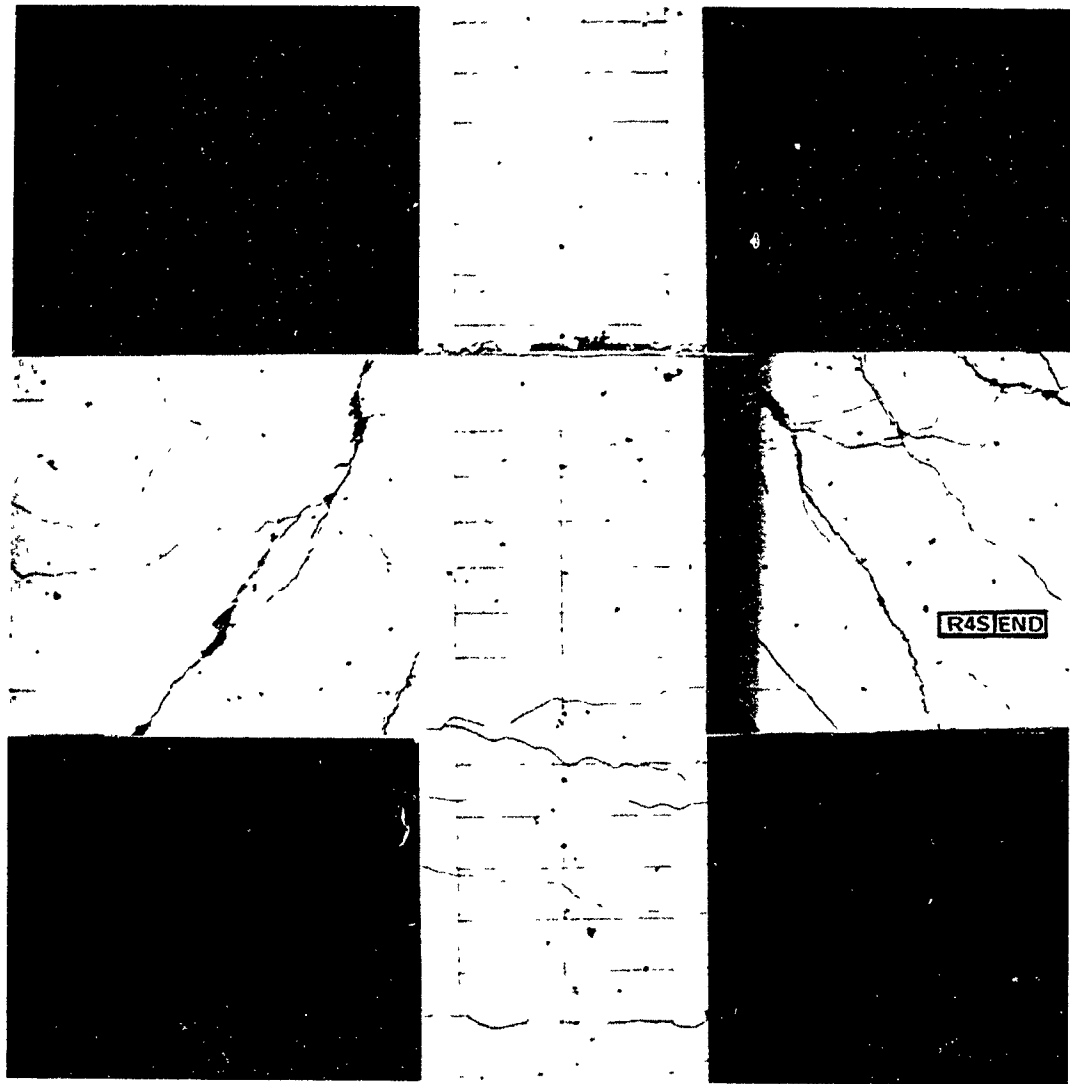


Figure 3.10 Overall view of exterior face of spandrel beam of specimen R4S at end of test

3.1.5 Column behaviour

Throughout the testing the column remained elastic with yielding taking place only near the end of testing in the longitudinal bars at the location of the construction joint. First cracking in the column did not occur until the 3rd (general yielding) downward loading cycle at a load of +175 kN on the exterior face of the column just below the joint region. First cracking on the interior face of

the column occurred above the slab at a load of +200 kN. By the peak load of +242 kN, two more hairline cracks appeared on the interior face of the upper column with the uppermost crack at a height of 500 mm above the slab. In the negative loading direction, cracks from the previous half cycle closed completely and a new crack formed on the back face of the column right at the construction joint between the slab and the upper column. After this cycle, no new significant flexural cracks formed in the column.

The 8-No.20 bar configuration, having two bars located at the neutral axis (see Fig. 3.11a), provided excellent confinement to the concrete core, and at the same time provided sufficient flexural and axial load capacities. The maximum moment carried by the column was 275 kNm above and below the joint with an applied axial load of 1076 kN. The axial load was noted to fluctuate in the order of $\pm 5\%$ between positive and negative beam peak loads.

In the 5th loading cycle, the column longitudinal bars reached the yield strain at the slab construction joint, both in the positive and negative loading directions. In the 6th downward loading cycle, a vertical splitting crack near the exterior face extended 200 mm above the slab (see Fig. 3.9). This cracking indicates that the back 40 mm of concrete cover had detached itself from the column core (see Fig. 3.11b). In the following cycle, this vertical crack propagated to the bottom of the spandrel beam and by the 11th cycle had extended 250 mm below the joint region. Although the concrete cover did not spall off, it is evident that the cover was not effective in contributing to the column resistance. A similar vertical splitting crack occurred on the interior face of the column below the beam in the 7th loading cycle (see Fig. 3.2c).



a) Column longitudinal bar arrangement

b) Exterior cover separation

Figure 3.11: Column cross-section before and after separation of concrete cover

Spalling of the concrete occurred on the interior face of the column just under the main beam in the 9th downward loading cycle (see Fig. 3.12). In the 10th upward loading cycle, spalling of the cover occurred on the interior face of the column to a height of 200 mm above the slab (see Fig. 3.6).

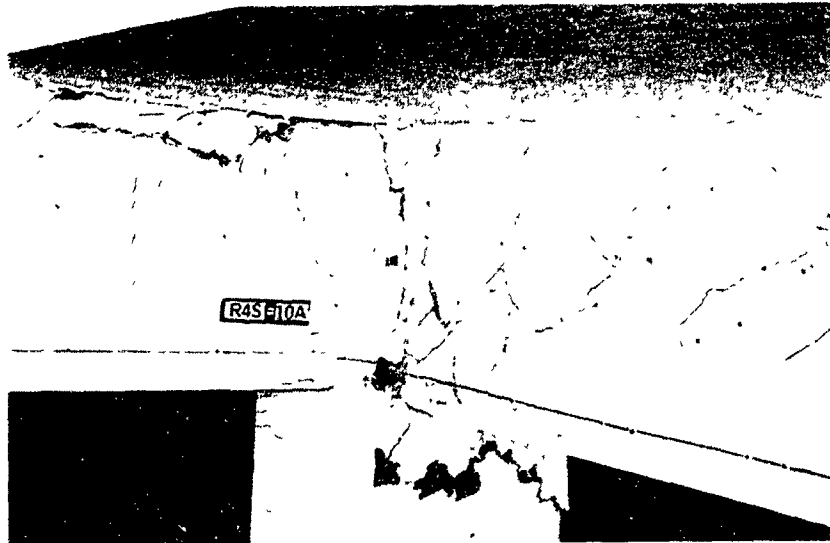


Figure 3.12 Photograph of the joint region in the 10th downward cycle of specimen R4S

3.1.6 Joint behaviour

The behaviour of the joint during the test could be observed because part of the joint region was exposed due to the relatively narrow spandrel beam. Shear cracking was well controlled by the six sets of closed hoop reinforcement provided. In the second downward loading cycle, a shear crack passed through the joint at approximately 45 degrees. In the 3rd downward loading cycle, two more shear hairline cracks appeared in the joint region (see Fig. 3.2b). In the 6th loading cycle, a shear crack due to upward loading appeared at the bottom of the joint region crossing the previously formed shear cracks. By the 7th cycle, a total of six shear cracks formed indicating the flow of compressive stresses in the joint (see Fig. 3.2c). At a load of +270 kN, first yielding occurred in the uppermost joint just under the slab. Although one closed hoop yielded in the joint region the amount of shear reinforcement was sufficient to limit the spread of yielding in the joint region.

3.2 Specimen R4T

3.2.1 Load deflection response

The applied load vs tip deflection response for specimen R4T is shown in Fig. 3.13. The peak loads in each cycle and corresponding beam tip deflections are summarized in Table 3.2. First flexural cracking of the beam in the positive loading direction occurred at a load of +75.7 kN resulting in a negative moment at cracking of 156.8 kNm. In the negative loading direction, first cracking occurred at a load of -74.6 kN corresponding to a positive moment of 110.0 kNm at the column face. Using the experimentally determined moduli of rupture, the predicted values of the cracking moments were 184.7 kNm for negative bending and 125.9 kNm for positive bending. These values are higher than those calculated for specimen R4S since the concrete compressive strength of specimen R4T was 46.6 MPa, as compared to 34.3 MPa for specimen R4S.

In the first positive loading cycle, the "service load" moment in the beam, assumed to be $1.2 M_{cr}$ was reached at a peak load of +93.7 kN resulting in a moment of 188.7 kNm. The corresponding downward beam tip deflection was 1.8 mm. In the negative loading cycle, the "service load" moment was reached at a load of -90.3 kN and moment of -137.9 kNm with a corresponding deflection of -1.3 mm.

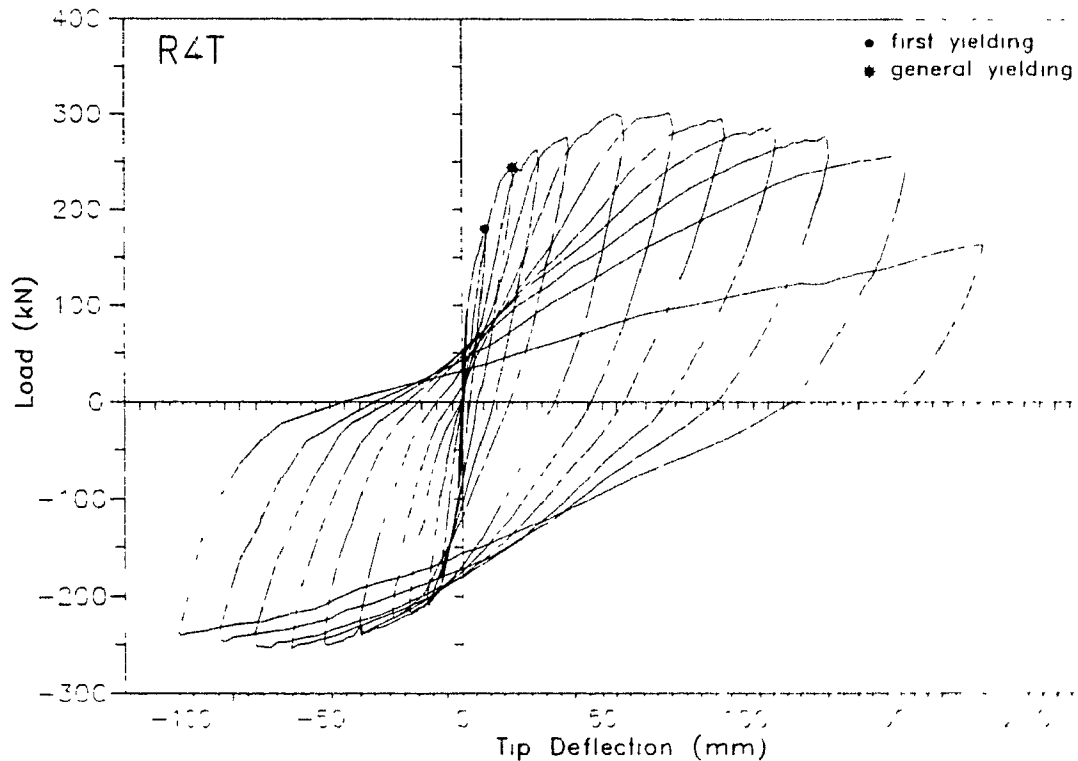


Figure 3.13: Load versus tip deflection response for specimen R4T

In the second positive loading cycle, first yielding of the beam top longitudinal reinforcing bars was reached at a load of +180.2 kN at deflection of 8.4 mm. In the negative loading direction, first yielding occurred at a load of -180.9 kN with a deflection of -7.0 mm.

General yielding of the specimen was judged to occur in the third cycle at a positive downwards load of +243.8 kN with a deflection Δ_{yp} , equal to 18.4 mm. In the negative loading direction, general yielding occurred at a tip deflection Δ_{yn} of -11.9 mm at a load of -209.9 kN.

Table 3.2 Applied loads and tip deflections at cycle peaks for specimen R4T

Cycle	Event at peak load	Stage	Load (kN)	Deflection (mm)
1A	1.2Mcr	1	93.7	1.8
1B		4	-90.3	-1.3
2A	1st yield	8	180.2	8.4
2B		12	-180.9	-7.0
3A	Gen yield Δ_y	16	243.8	18.4
3B		20	-209.9	-11.9
4A	1.5 Δ_y	24	263.2	27.5
4B		28	-216.9	-17.8
5A	2 Δ_y	32	276.0	37.6
5B		36	-223.0	-23.8
6A	3 Δ_y	40	300.5	54.8
6B		44	-237.8	-34.1
7A	4 Δ_y	48	301.2	74.7
7B		52	-249.9	-45.6
8A	5 Δ_y	55	295.8	92.3
8B		58	-253.4	-60.2
9A	6 Δ_y	61	288.0	111.2
9B		64	-252.8	-67.4
10A	7 Δ_y	67	277.9	129.4
10B		70	-247.2	-83.3
11A	8.5 Δ_y	73	258.8	155.9
11B		76	-240.0	-100.0
12A	10 Δ_y	79	163.8	183.8

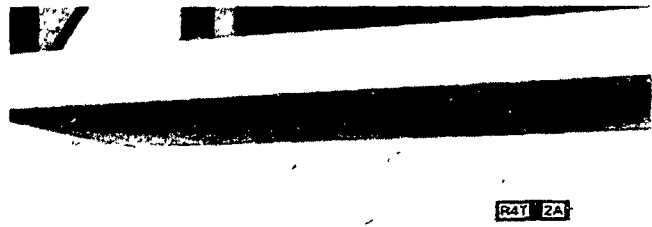
The maximum applied load sustained by the specimen in the positive loading direction was reached in the 7th cycle at a load of +301.2 kN with a moment of 557.0 kNm including the dead load moments. The downwards displacement at this point was 74.7 mm corresponding to a ductility of $\Delta/\Delta_{yp} = 4$. In the negative loading direction, the maximum load was -253.4 kN with a positive moment of 427.4 kNm and a displacement of -60.2 mm. Similar to specimen R4S, specimen R4T continued to maintain loads higher than that of general yielding until the 11th positive loading cycle when the beam bottom longitudinal bars started to buckle. The positive displacement ductility at this point was 8.5Δ , at a deflection of 155.9 mm. The test was continued for one final cycle until a displacement ductility of 10Δ , was reached. At this stage, a load of +163.8 kN was applied and a downwards deflection of 183.8 mm was attained. The slab had separated from the main beam over a distance of about 1000 mm. This will be discussed further in Section 3.2.2. The energy dissipating capacity was excellent throughout the test. No sign of "pinching" in the hysteresis loops was observed for the duration of the test.

3.2.2 Beam behaviour

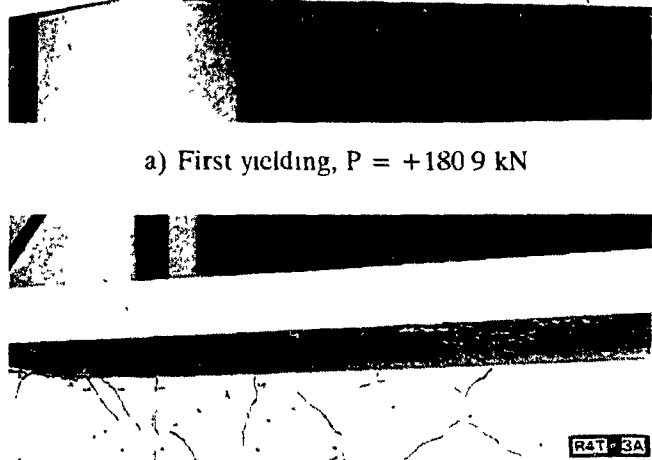
In the first downward loading cycle, the first flexural crack, having a width of 0.1 mm, occurred in the beam, 60 mm from the column face and extended to mid-height of the beam web. In the upwards loading cycle, four hairline cracks occurred on the bottom face of the beam with one crack appearing at the column face. These cracks did not join with the previous, negative moment flexural cracks at this stage.

In the second positive loading cycle, two new cracks appeared in the main beam at 340 mm and at 660 mm at loads of +110 kN and +160 kN, respectively. These two cracks extended through the slab thickness, and across the entire the slab width. The cracks were spaced at 300 mm and corresponded to the slab transverse bar spacing. The maximum recorded crack width at this stage was 0.25 mm (see Fig. 3.14a). In the negative loading cycle, five new flexural cracks appeared three of which extended upwards, as shear cracks, at about 45 degrees toward the column face. The largest flexural crack width was 0.4 mm at the column face.

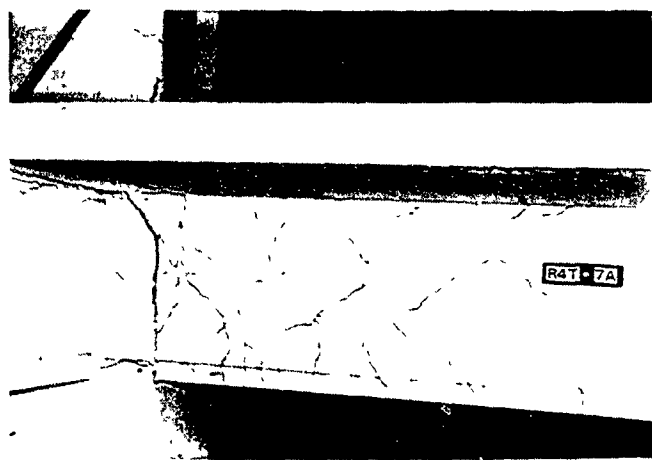
At general yielding in the positive loading direction, a fourth flexure-shear crack started at a location 950 mm from the column face, at a load of +210 kN. This crack was inclined towards the column (see Fig. 3.14b). The flexural crack closest to the column measured 0.6 mm in width. In the negative loading cycle, a new crack occurred 1300 mm from the face of the column and previous cracks reached mid-height of the main beam.



a) First yielding, $P = +180.9 \text{ kN}$



b) General yielding, $P = +243.8 \text{ kN}$



c) Maximum applied load, $P = +301.2 \text{ kN}$

Figure 3.14 Photographs of specimen R4T at different stages

In the 4th positive loading cycle, strain readings on the beam surface near the face of the column gave inconsistent results due to the loosening of the concrete cover in this region. In subsequent cycles, the cracks did not close completely upon load reversal. Figure 3.14c shows the crack pattern in the beam in the 7th positive loading cycle where the ultimate peak load was obtained. The maximum crack width at this stage was 10 mm measured at the column face where considerable separation between the beam and the joint face was observed. A splitting crack formed at the level of the beam bottom longitudinal bars close to the column face (see Fig. 3.14c).

Spalling of the concrete cover on the bottom and sides of the main beam occurred in the 11th negative loading cycle over a distance of 200 mm from the joint face. This spalling probably was initiated in the previous positive loading cycle when significant splitting was evident along the bottom longitudinal bars. In the 12th downward loading cycle, the buckling of the bottom bars was observed between the first two sets of hoops. Figure 3.15 shows the final state of the specimen with the buckled beam bars and the significant spalling.

At a load of about +120 kN, in this cycle, a large separation crack between the slab and the beam web was noted. This separation, due to loss of shear transfer over the plastic hinge region, had propagated 1000 mm from the face of the joint by the peak load in that cycle of +164 kN (see Fig. 3.15). A loss of load carrying capacity and a significant loss of stiffness was observed in the last positive loading cycle (see Fig. 3.13).



Figure 3.15: Buckling of bottom bars at end of test for specimen R4T

Figure 3 16 shows the curvature and shear strain distributions at different stages during the test. The maximum curvature at general yielding was 4.12×10^{-3} rad/m while the maximum recorded curvature was 142.2×10^{-3} rad/m in the 9th positive cycle. The maximum shear strain recorded at general yielding was 106.5×10^{-5} rad and the maximum value during the test was 402.5×10^{-5} rad in the 7th cycle.

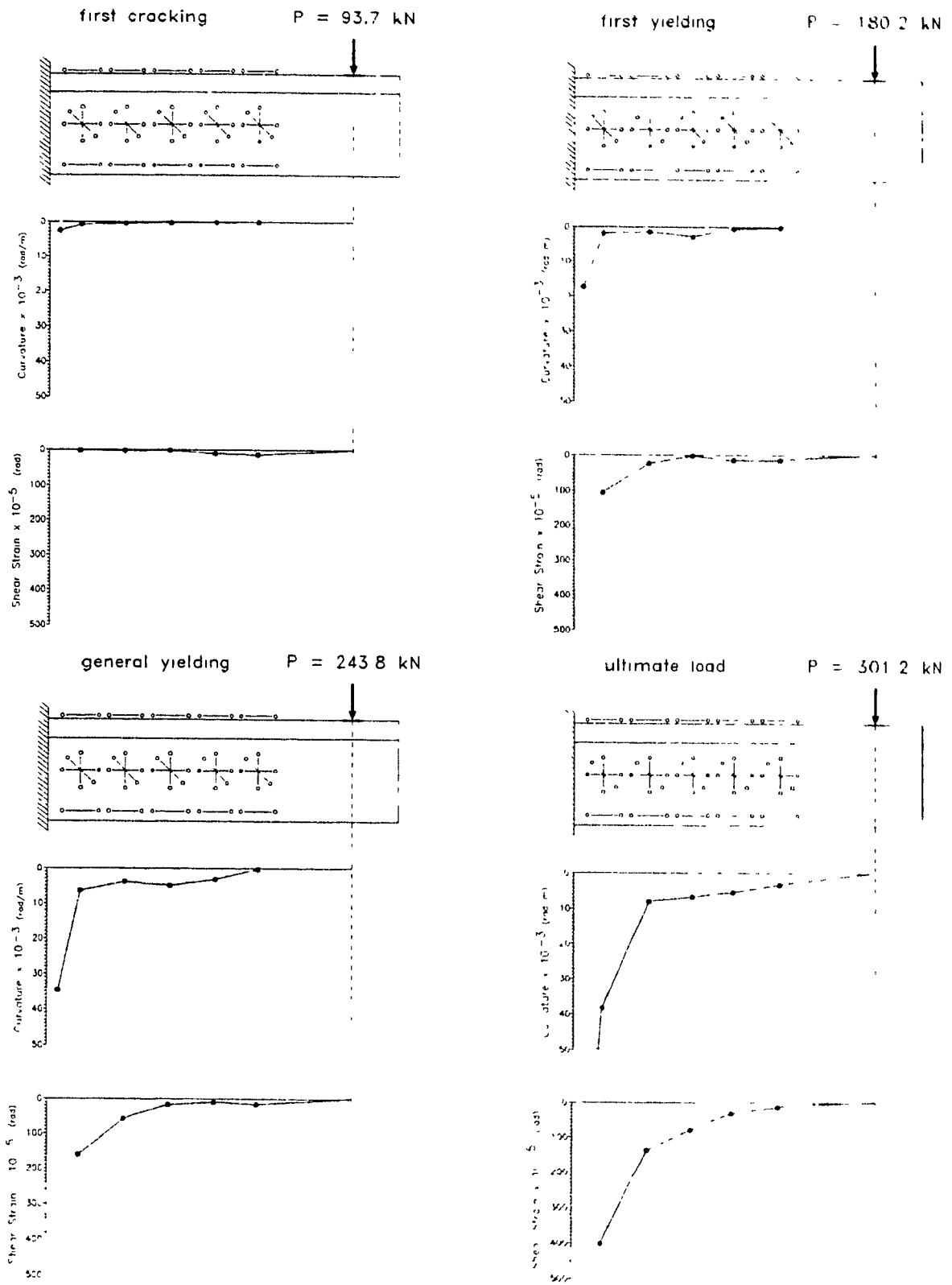
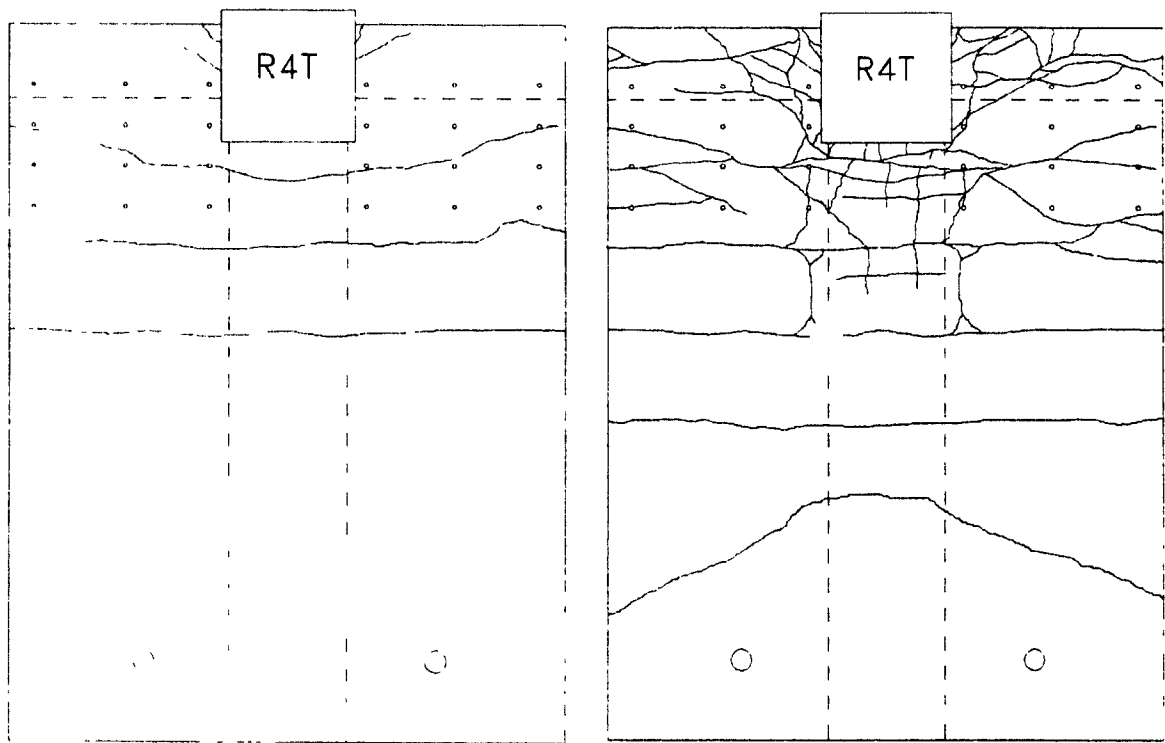


Figure 3.16: Curvature and shear strain distributions for R4T

3.2.3 Slab behaviour

In the first downwards loading cycle, one flexural crack appeared on the slab surface directly above the first transverse slab bar and crossed the first two sets of longitudinal slab bars on each side of the beam. Directly above the spandrel beam, a crack appeared on the top surface of the slab on the east side of the column radiating out, at about 45 degrees, from the centre of the column face toward the exterior face of the specimen. This hairline crack was the first torsional crack in the spandrel beam.

In the second positive loading cycle, two new flexural cracks formed at a spacing of 300 mm from the first crack, along with three new torsional cracks over the spandrel beam. One of these torsional cracks formed on the west side at a load of +110 kN and matched the previously formed crack. The other two cracks formed, at a load of +180 kN, producing a second set of torsional cracks on each side of the column for a total of four torsional cracks (see Fig. 3.17a). In the joint region an inclined shear crack formed directly below the main torsional crack in the slab. The maximum torsional crack width at this stage was 0.3 mm.



a) crack pattern at cycle 2A

b) crack pattern at cycle 12A

Figure 3.17: Crack pattern in slab of specimen R4T

At general yielding in the positive loading cycle, the main torsional cracks on the slab measured 1.0 mm and a new flexural crack formed at the 4th transverse slab bar at a load of +210 kN. In the 6th positive loading cycle, diagonal crushing of the concrete in the slab above the spandrel, next to the side faces of the column, was observed. The portion of the slab on the interior face of the column displayed 100 mm long splitting cracks directly above the main beam longitudinal bars. Similar splitting cracks formed directly above the first set of slab longitudinal bars on both sides of the beam as in specimen R4S. Furthermore, at the peak load of +300.5 kN, a fifth flexural crack occurred at the fifth transverse slab bars above the beam and crossed the entire slab width and were inclined at about 45 degrees towards the loading mechanism (see Fig. 3.17b). In the 9th positive loading cycle, torsional cracks spiralled around the spandrel beam and had maximum crack width of 8 mm. Figure 3.18 shows a close-up view of the slab surface in the 12th positive loading cycle.



Figure 3.18: Cracking and crushing of concrete in slab for specimen R4T

A diagonal compressive strut due to torsion is evident on the slab surface next to the column side face. Figure 3.19 shows the strain distribution in the longitudinal slab bars for specimen R4T. The strains are much reduced as compared with those of specimen R4S. From the strains at the slab

spandrel beam interface, one can conclude that only the first set of slab bars achieved strains higher than the yield value. The strains at the beam-column interface, however, are significantly higher. This behaviour in the slab will be discussed in detail in Chapter 4. At later stages of loading, there were

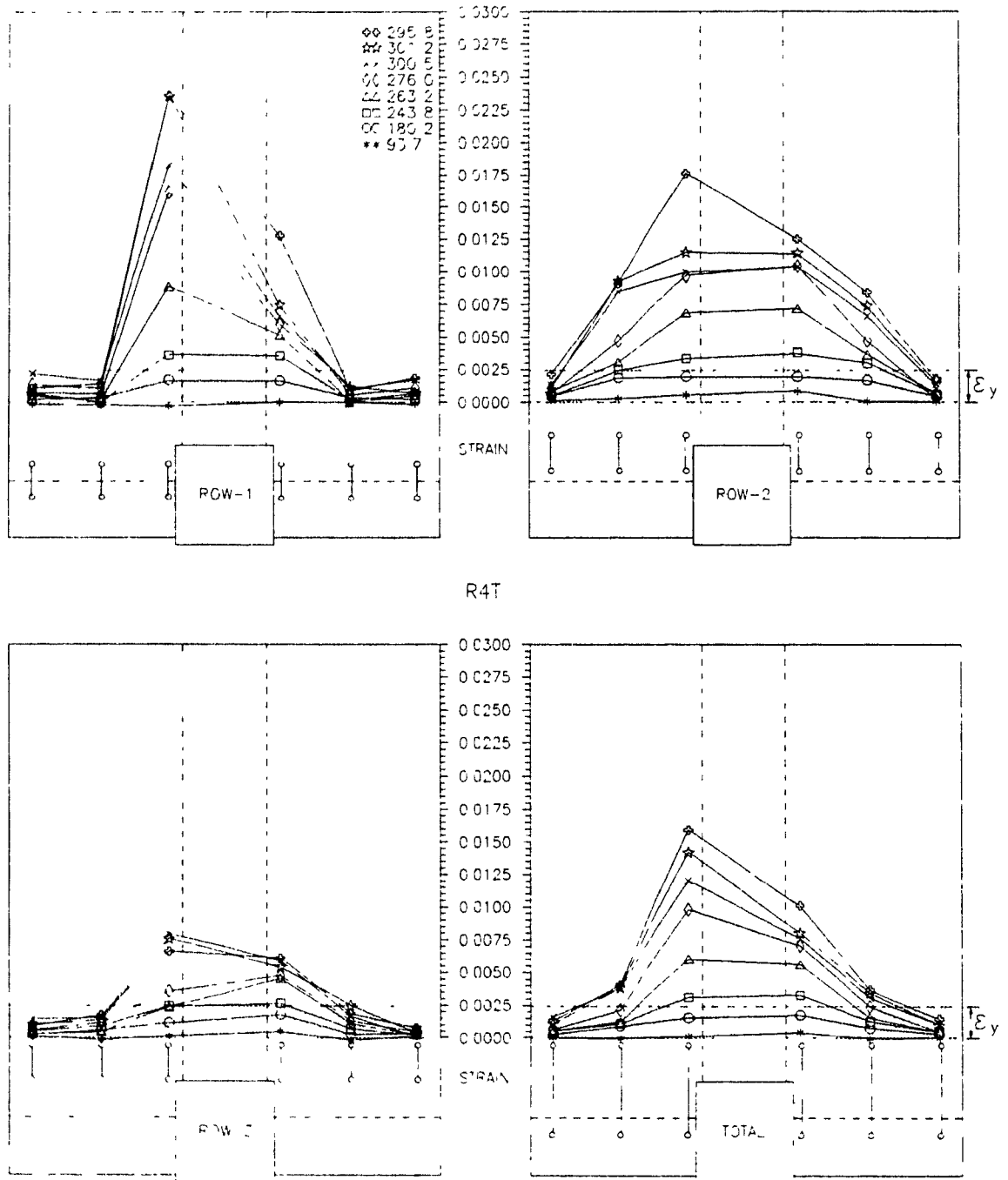


Figure 3.19. Strain distribution in slab longitudinal bars for specimen R4T

noticeably smaller strains in one slab bar adjacent to the column, at the slab-spandrel beam interface. This was due to the fact that the main torsional crack just missed the gauge length on this bar.

3.2.4 Spandrel behaviour

In the first positive loading cycle, due to the torsion induced by the tensions in the slab longitudinal bars, two cracks formed on both spandrel beam-column interfaces extending to approximately mid-height of the beam. On the east spandrel, an additional hairline torsional crack appeared between the first set of stirrups about 120 mm from the column face and extended downwards over a distance of 150 mm. In the second positive loading cycle, a similar torsional crack formed in the west spandrel beam, at a load of +100 kN and extended to mid-depth of the beam by a load of +150 kN. The crack on the east spandrel beam also extended to mid-depth of the beam. The widths of these torsional cracks were 0.35 mm and 0.2 mm on the west and east sides, respectively. The interfacial vertical cracks at the column faces extended down to the bottom of the spandrel and were 0.10 mm in width.

On the interior face of the spandrel a crack formed at the slab-spandrel beam interface on both sides of the column extending horizontally about 150 mm from the joint region. Figure 3.20 shows the torsional cracks at general yielding in the third cycle. A second set of torsional cracks appeared at the bottom of both spandrel beams at a load of +210 kN.

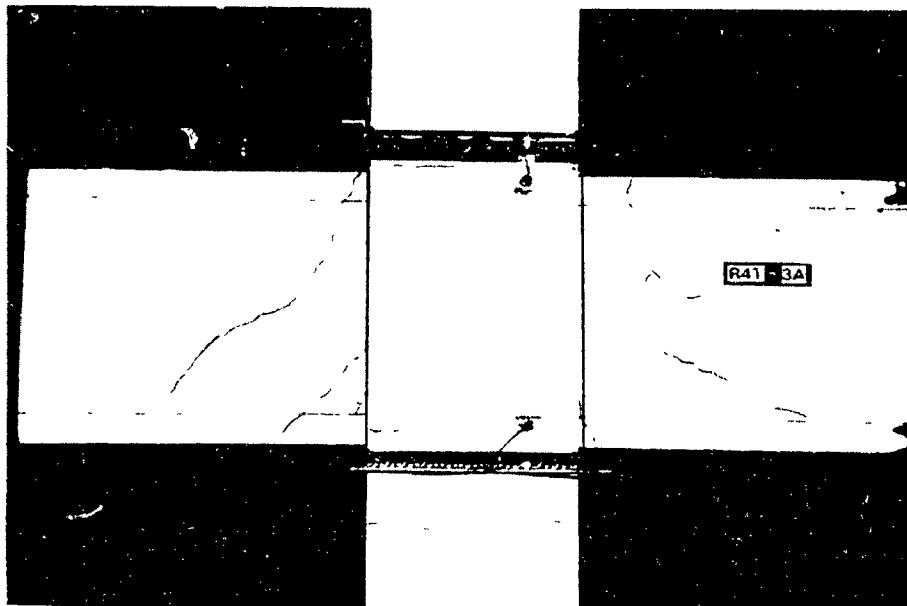


Figure 3.20 Spandrel beam at general yielding ($\Delta_e = 1.0$) for specimen R41

Crack widths at the top of both spandrel beams at the level of the longitudinal bars were 1.0 mm. The near 45 degree cracks on the exterior face of the spandrel beam spiralled around the top of the beam and over part of the depth of the interior face of the spandrel. Yielding of the exterior corner longitudinal No 15 bar in the spandrel occurred due to combined bending and torsion in the 3rd positive loading cycle. In the 4th positive loading cycle the large torsional cracks together with the hoop strains indicated that yielding of the spandrel beam hoops had occurred. In the 5th negative loading cycle, upward displacements caused the separation crack between the slab and the spandrel beam on the interior face to extended to the full length of the spandrel. By the 6th positive loading cycle, a second set of torsional cracks appeared between the second and third hoops in the spandrel beam. On the exterior faces the maximum torsional crack widths were 4.0 mm and 3.0 mm on the west and east sides, respectively. In the same cycle, onset of crushing of the concrete on the interior face of the spandrel beam was noted at the top and at the bottom corner near the joint face.



Figure 3.21. Photograph of spandrel beam for R4T in the 11th negative loading cycle

In subsequent cycles, more torsional cracks formed on the exterior face. In the 9th positive loading cycle, the main torsional cracks were 140 mm and 150 mm wide on the west and east exterior faces, respectively. Extensive twisting of the spandrel beam, concentrated at the main torsional crack locations, had occurred at this stage. Figure 3.21 shows the state of the spandrel beam in the 11th negative loading cycle, with the large torsional cracks and the separation of the spandrel from the slab. The torsional cracks on the interior face showed signs of reversed torsional loading and the major cracks had propagated through the thickness of the cross section. Due to the significant separation between the slab and the spandrel beam, on upwards loading, the slab was rotating about the 90 degree bend anchorages in the slab bars framing into the spandrel core. The slab-spandrel beam separation crack extended to the exterior faces of the spandrel beams at about one third the depth of the spandrel beam from the top of the slab. Figure 3.22 shows this horizontal crack as well as the large torsional crack at the final stages of the test. First yielding of the No.10 hoops occurred in the 4th positive loading with strains reaching 10 times their yield value by the 12th positive loading cycle.



Figure 3.22. Exterior view of spandrel beam for specimen R4T at 100 Δ ,

By the end of the testing, the top No.15 corner bar had reached 10 times the yield strain and the severe cracking of the beam was evidence that the No.15 bottom corner bar had yielded.

Figure 3.22 and 3.23 show the twisting and severe torsional cracking of the spandrel beam caused by the tension in the slab bars anchored at the top of the beam

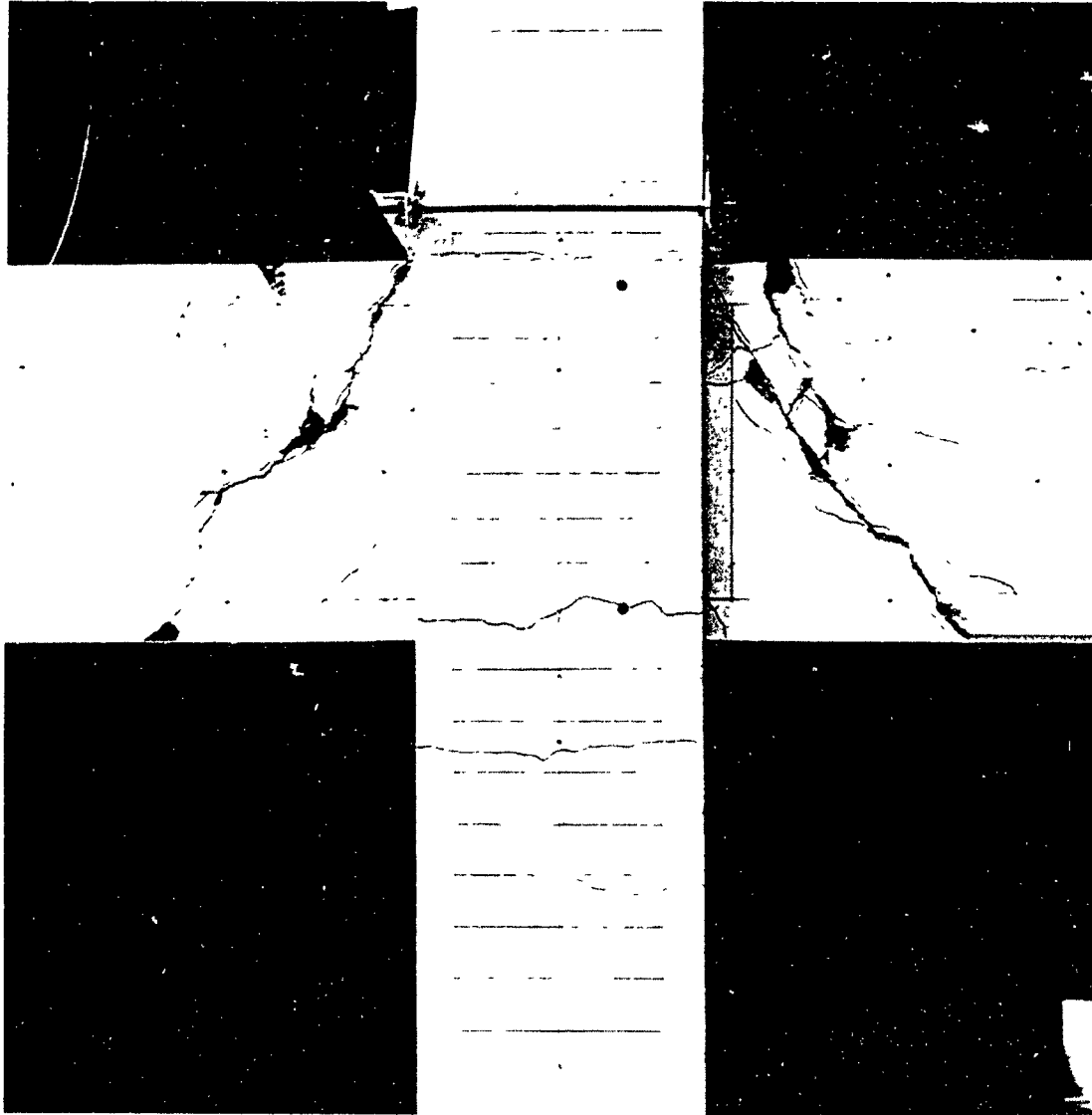


Figure 3.23: Exterior view of spandrel beam for specimen R4T at the end of test

3.2.5 Column behaviour

The first visible crack in the column occurred at the construction joint at the top of the slab in the second positive loading cycle. In the negative loading cycle, a crack formed on the exterior face of the column at the slab interface and had a width of 0.05 mm. At general yielding in the positive loading direction, the crack at the interior face of the column had a width of 1.0 mm and a new crack formed on the exterior face below the spandrel beam at a load of +210 kN.

The column longitudinal bars, near the interior face, yielded at the peak load in the 4th cycle at the slab interface. Strains at this location reached a maximum of 2.7 times the yield strain by the 8th positive loading cycle. First yielding of the column bars near the exterior face occurred in the 6th negative loading cycle at the construction joint and reached twice the yield value by the 11th cycle. The maximum moment in the column transferred by flexure in the main beam and by torsion in the two spandrel beams was 280 kNm. This was well below the capacity of the column.

The exterior face of the column at the joint region was instrumented by two LVDTs spaced at 500 mm as described in Section 2.4.2.2 to obtain a measure of the column rotation. At the peak load in the first cycle, the column rotation was 0.0006 rad and at general yielding it had reached 0.0026 rad. The highest value occurred in the 6th positive cycle, with a rotation of 0.0048 rad, when the beam was close to reaching its maximum capacity. From this point on, due to flexural hinging in the beam, the rotations took place in the beam rather than in the column.

By the 6th positive loading cycle, two new hairline flexural cracks appeared on the interior face as high as 600 mm above the slab and a new crack formed on the exterior face well below the spandrel beam. On the side faces of the column just above the slab, two vertical splitting cracks about 100 mm in length were noted at the level of the front and middle longitudinal bars. The front crack was the onset of concrete cover spalling in the column, with noticeable spalling occurring in the 8th positive loading cycle. In the 7th positive loading cycle, another vertical separation crack was noted at the exterior face over the longitudinal column bars. Like specimen R4S this indicated that the exterior cover on the column had begun to separate from the column core. The crack extended 200 mm above the slab and along the column-spandrel beam interface. This crack extended 500 mm above the slab by the 8th positive loading cycle and extended down to 200 mm below the spandrel beam by the 10th positive loading cycle (see Fig. 3.22). Vertical splitting also occurred near the interior face of the column and led to spalling of the concrete below the level of the main beam in the 8th positive loading cycle (see Fig. 3.24).

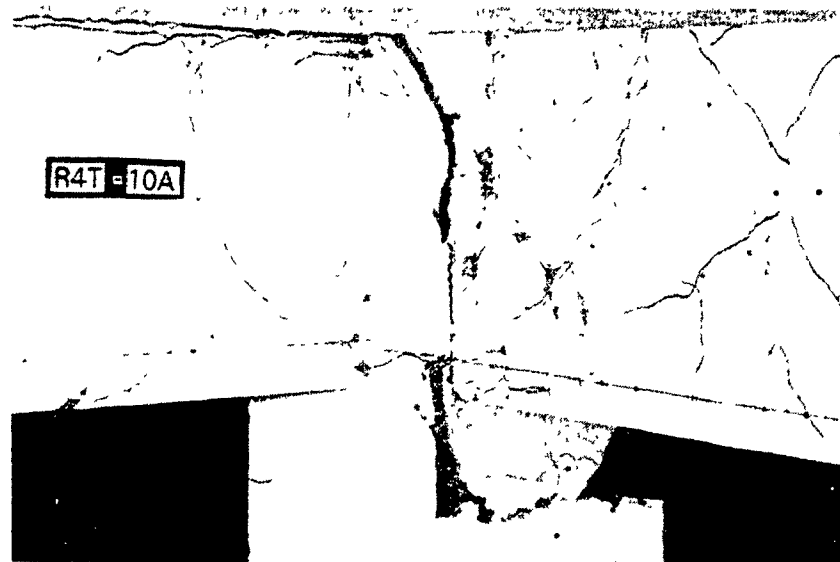


Figure 3.24: Photograph of joint region of specimen R4T

3.2.6 Joint behaviour

The joint region which contained six sets of closed square and diamond-shaped hoops showed excellent behaviour. First shear cracks occurred on the exposed side faces of the joint as early as the 2nd positive loading cycle. These cracks were hairline in thickness and were inclined at an angle of about 45 degrees. These two cracks originated from underneath the slab and radiated parallel to each other over a distance of 100 mm (see Fig. 3.14a). In the 4th positive loading cycle, at a peak load of +263.2 kN, two new hairline shear cracks formed in the middle of the joint region. Upon upward loading in the 5th negative cycle, a shear crack which crossed previously formed shear cracks was observed. In the same cycle, a vertical splitting crack appeared at the level of the column longitudinal bars near the interior face. This crack extended from 100 mm below the joint up to about mid-height of the joint region (see Fig. 3.14c). The uppermost shear crack had formed into a flexural crack at the beam-column interface. As can be seen from Fig. 3.14c, this crack opened up considerably since it curved around the outside of the joint hoops and extended vertically along the beam-column interface. By the 6th loading cycle, a total of six shear cracks had formed in the positive loading direction and two shear cracks had formed in the negative loading direction.

First yielding of the hoop reinforcement confining the joint was occurred in the 6th positive loading cycle in the uppermost joint hoop at a shear load of +280 kN. Figure 3.25 shows the strain in four of the six joint hoops at the peak loads in each positive loading cycle. It can be seen that yielding had occurred in only the uppermost hoop. Crack widths on the exposed side faces of the joint were controlled by the closely spaced hoops to within 0.2 mm.

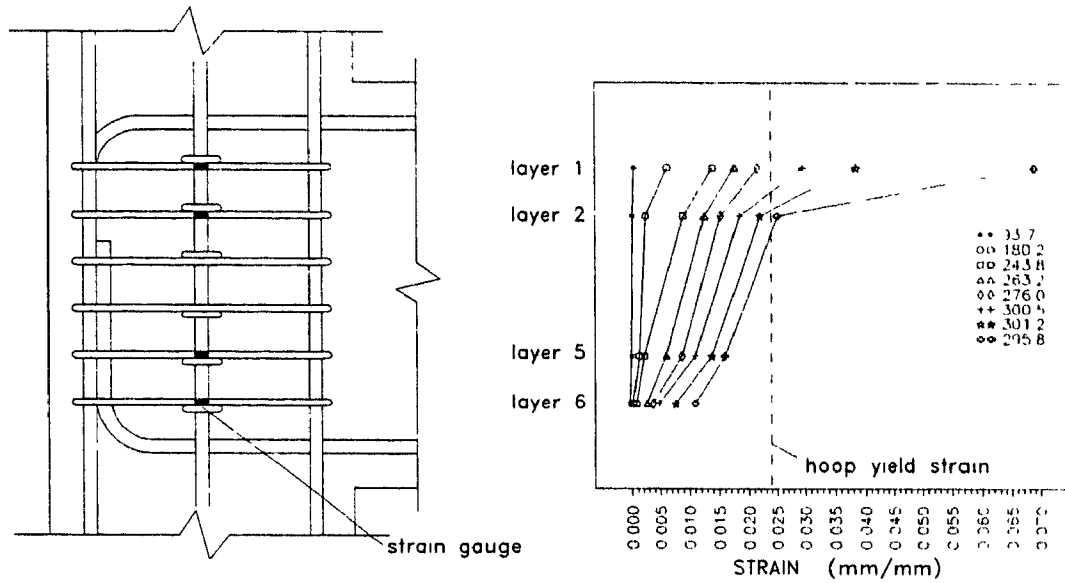


Figure 3.25: Strain distribution in hoop reinforcement in specimen R4T

3.3 Specimen R4

Specimen R4 was tested by S. Rattray (1986) and forms part of the larger testing programme at McGill University. This specimen with its 400 by 600 mm spandrel beam can be compared directly with specimens R4S and R4T to study the influence of the spandrel beam.

3.3.1 Load deflection response

The applied load vs tip deflection response for specimen R4 is shown in Fig. 3.26. The peak loads in each cycle and corresponding beam tip deflections are summarized in Table 3.3. In the first positive loading cycle, the "service load" moment in the beam was obtained at a load of +101.7 kN and a deflection of 2.9 mm corresponding to a negative moment of 203 kNm at the column face. For this specimen the dead load moment was 22.4 kNm. In the negative loading direction, the "service load" moment was reached at a load of -79.9 kN corresponding to a moment of 119 kNm and a tip deflection of -1.5 mm.

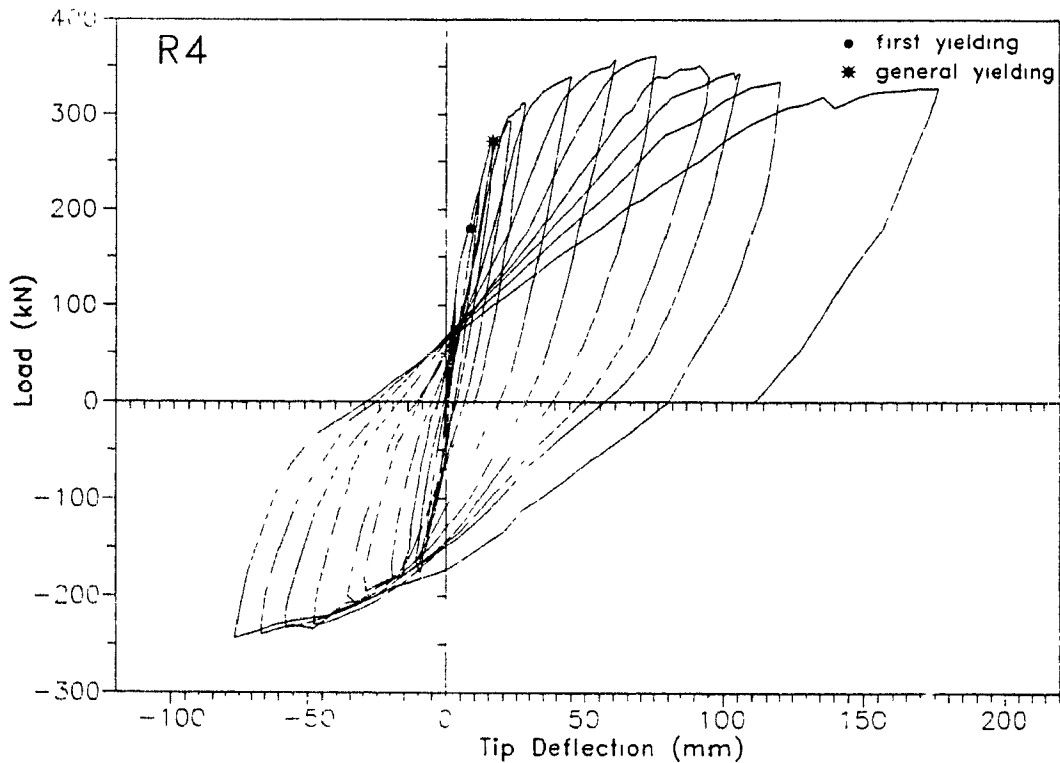


Figure 3.26. Load versus tip deflection response for specimen R4

In the second positive loading cycle, first yielding of the beam longitudinal reinforcement was obtained at a load of +218.6 kN and a deflection of 11.4 mm. In the negative loading cycle, first

yielding occurred at a load of -140.5 kN and a corresponding tip deflection of -6.6 mm.

In the third positive loading cycle, general yielding was observed at a positive deflection Δ_{yp} , equal to 16.6 mm at an applied load of +271.6 kN. In the negative loading direction, the general yield deflection Δ_{yn} , was judged to occur at a displacement of -9.4 mm and at a load of -175.9 kN.

Table 3.3: Applied loads and tip deflections at cycle peaks for specimen R4

Cycle	Event at peak load	Stage	Load (kN)	Deflection (mm)
1A	1.2Mcr	5	101.7	2.9
1B		18	-79.9	-1.5
2A	1st yield	34	218.6	11.4
2B		62	-140.5	-6.6
3A	gen. yield Δ_y	101	271.6	16.6
3B		135	-175.9	-9.4
4A	1.5 Δ_y	167	292.8	22.2
4B		190	-178.6	-15.2
5A	2 Δ_y	219	312.1	28.1
5B		241	-180.4	-19.3
6A	3 Δ_y	273	339.0	45.2
6B		296	-195.1	-29.2
7A	4 Δ_y	326	357.5	60.8
7B		349	-207.2	-32.7
8A	5 Δ_y	381	360.5	75.8
8B		415	-229.0	-48.1
9A	6 Δ_y	447	351.1	91.7
9B			-232.3	-57.4
10A	7 Δ_y		343.9	103.4
10B			-238.9	-66.5
11A	8 Δ_y		333.7	120.2
11B			-242.9	-76.7
12A	9 Δ_y		327.1	176.4

In subsequent cycles, load increased steadily up to a maximum positive peak load of +360.5 kN in the 8th positive loading cycle resulting in a maximum moment of 662.0 kNm at the

column face. The tip deflection at this point was 75.8 mm corresponding to a displacement ductility of Δ/Δ_{yp} equal to 5. In the negative loading direction, the load continued to increase for the duration of the test. The load at the 11th and final upward loading cycle was -242.9 kN at a negative deflection of -76.7 mm corresponding maximum positive moment of 409 kNm.

The specimen maintained loads greater than that of general yielding in the positive loading directions for the remainder of the test. In the 11th positive loading cycle, the four bottom longitudinal bars in the main beam buckled between the second and third sets of hoops. The load at this point was +333.7 kN at a tip deflection of 120.2 mm corresponding to a positive displacement ductility of 8. The test was continued for one more positive loading cycle until lack of travel was reached in the loading rams. The maximum tip deflection recorded at this stage was 176.4 mm corresponding to a displacement ductility of 10.4. The energy dissipating capacity was excellent with no observed sign of "pinching" in the hysteresis loops throughout the test.

3.3.2 Beam behaviour

Upon loading in the first positive cycle, two flexural cracks formed at distances of 80 mm and 360 mm from the column face. These two cracks extended down through the slab and into the beam web having maximum crack widths of 0.10 mm in the beam below the slab. In the negative loading cycle, the previous cracks closed completely with new cracks forming on the bottom face of the beam at the column face and at a distance of 140 mm from the column face.

In the second positive loading cycle, three new flexural cracks formed in the beam extending to mid-depth of the beam while the previous two cracks lengthened. These cracks are flexural shear cracks and had maximum crack widths of 0.5 mm at this stage (see Fig. 3.27a). In the negative loading cycle, six new flexural cracks formed at approximately 130 mm intervals corresponding to the beam hoop spacing. These cracks extended vertically about 200 mm and then inclined at 45 degrees intersecting with previously formed shear cracks at mid-depth (see Fig. 3.27b).

At general yielding, two new flexural cracks formed for a total of seven with the maximum recorded crack width of 0.70 mm. In the negative loading cycle, the cracks forming from downwards loading were noted to have remained open upon load reversal indicating permanent deformations in the main beam.

Local crushing of the concrete at the bottom of the beam was observed at the peak load of +339.0 kN in the 6th positive loading cycle, along with onset of spalling at the joint interface. Splitting cracks were noted at this stage at the level of the bottom longitudinal reinforcement near the joint. Figure 3.27c shows the crack pattern in the 8th positive loading cycle at the maximum applied load of +360.5 kN with crushing and spalling of the concrete outside the joint region.



a) First yielding, $P = +218.6 \text{ kN}$



b) General yielding, $P = +271.6 \text{ kN}$



c) Maximum applied load, $P = +360.5 \text{ kN}$

Figure 3.27. Photographs of specimen R4 at different stages

In the 8th negative loading cycle, the bottom 40 mm cover over a distance of 180 mm was lost exposing the longitudinal steel and beam hoop reinforcement. In the following cycles, more spalling occurred near the joint region where flexural hinging in the beam had become evident. Figure 3.28 shows the joint region of the specimen in the 11th positive loading cycle at a displacement ductility of $8\Delta_u$, corresponding to a load of +333.7 kN and a displacement of 120.2 mm. At this stage buckling of the 4-No 20 bottom bars had occurred. Figure 3.29 shows the buckling of the beam bars along with the extensive spalling and large flexural crack within the hinge region. It was noted that in the last four loading cycles the cracks widened in a region within a distance of 300 mm from the joint face, with maximum crack widths of several millimetres.



Figure 3.28: Photograph of specimen R4 showing damage near the joint

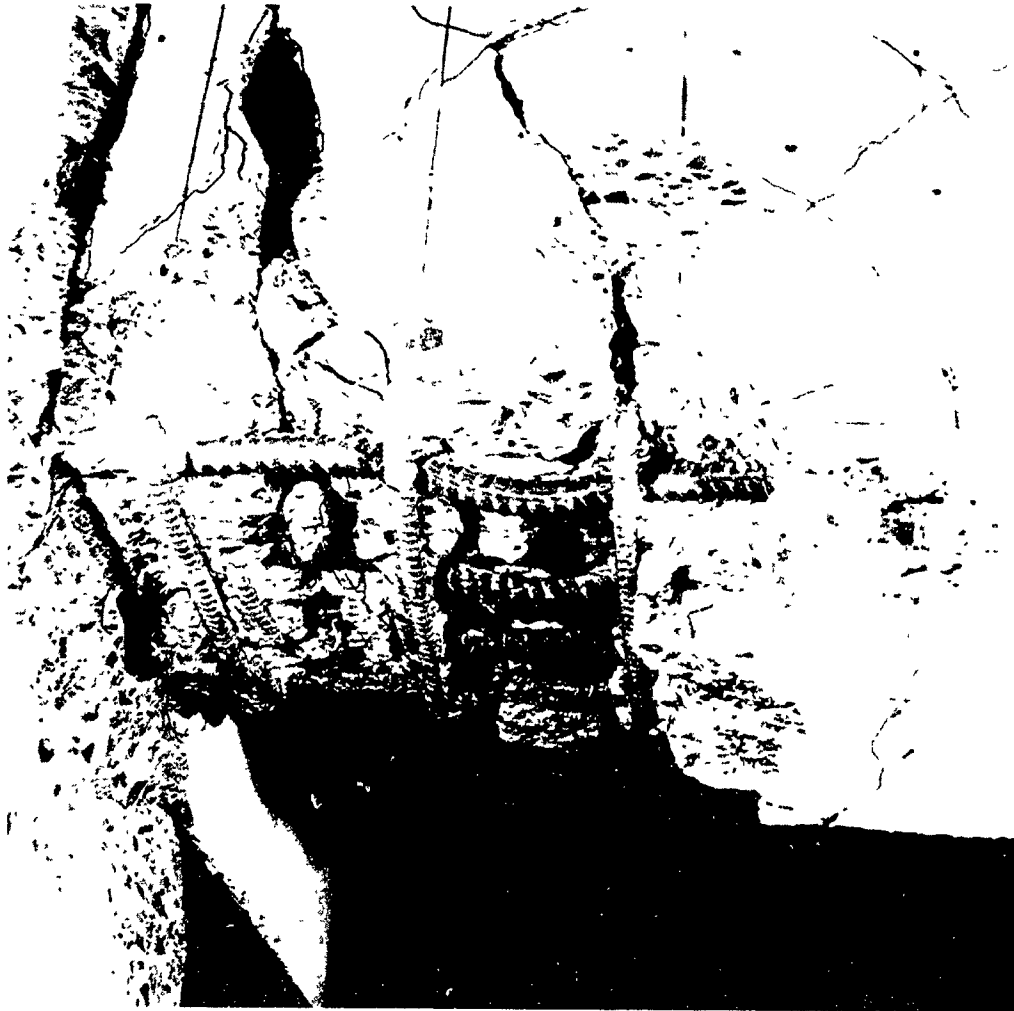


Figure 3.29 Buckling of beam bottom bars at $8\Delta_y$ in specimen R4

Figure 3.30 shows the distribution of measured curvatures and shear strains along the beam at different load stages. The yield curvature at the column face was 8.9×10^{-3} rad/m, in the positive loading direction while a maximum recorded curvature of 50.8×10^{-3} rad/m was obtained at a ductility of $6\Delta_y$. From the measured curvatures, the plastic hinge region was estimated to be within 400 mm from the column interface. The maximum measured shear strain in the beam occurred in the 5th positive cycle with a value of 1.159×10^{-2} radians at 180 mm from the beam face. Discontinuities in the distribution plots are due to the discrete nature of the crack patterns.

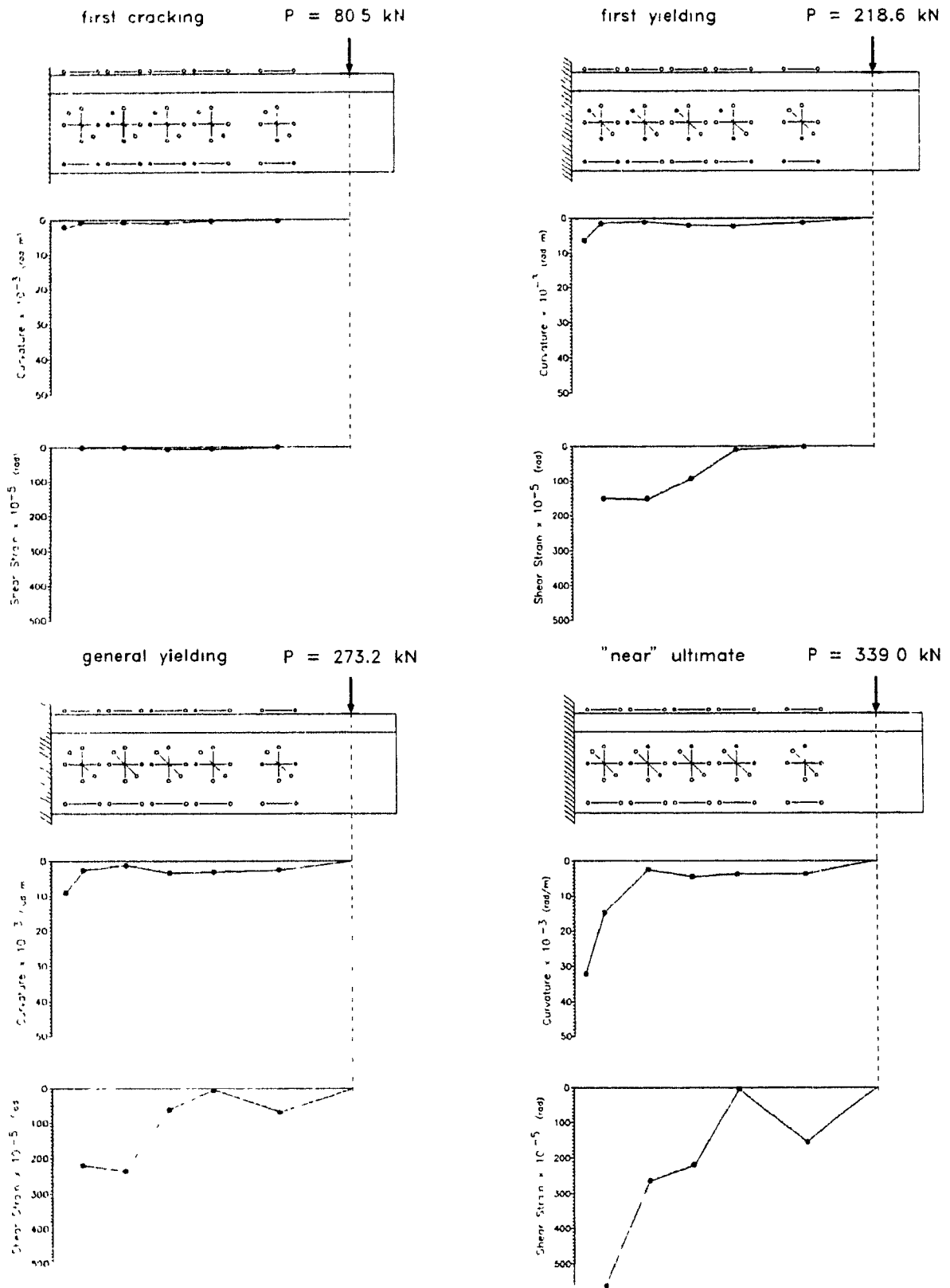


Figure 3.30 Curvature and shear strain distributions for R4

3.3.3 Slab behaviour

In the first positive loading cycle, two flexural cracks appeared on the slab surface at the location of the transverse slab bars. These cracks crossed the entire width of the slab surface. In the negative loading direction these cracks closed completely. In the second positive loading cycle, there were six transverse cracks on the slab with maximum crack widths of 0.3 mm and by general yielding, these cracks opened up to widths of 0.5 mm. By the peak load in this cycle a torsional crack had formed on each side of the column in the slab adjacent to the column face. These cracks opened and significant diagonal crushing on the slab surface occurred due to torsion in the 10th positive loading cycle.

Figure 3.31 shows the strain distributions in the No.10 slab bars, measured over the gauge lengths indicated, at different load stages during the test.

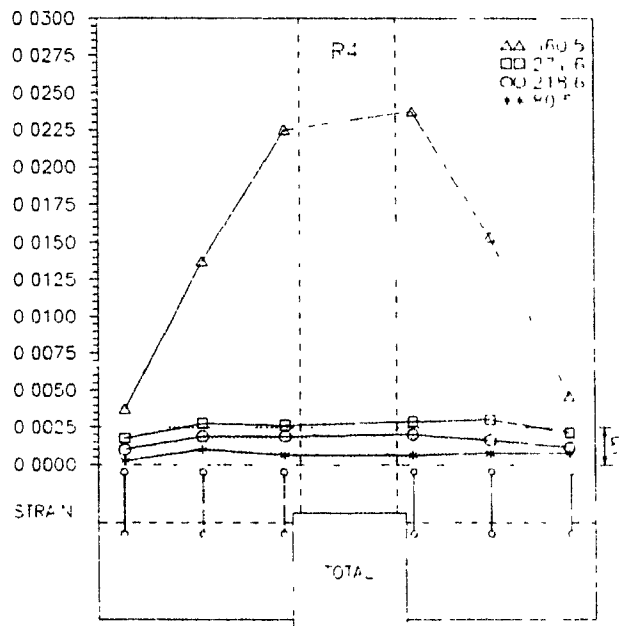


Figure 3.31: Strain distribution in slab bars for specimen R4

The yield strain for the bars of 0.0024 is indicated. At general yielding in the positive loading direction ($P = +271.6$ kN) the first two sets of top bars on either side of the beam yielded. This corresponds to a width of $4h_f$ on both sides of the main beam where the slab bars are assumed to be effective in providing bending moment resistance. In subsequent loading cycles, strains in the slab

bars varied nonlinearly, with higher strains near the beam and considerably smaller strains at the edges of the slab. At the maximum load level, all the slab bars across the width of the slab had yielded.

3.3.4 Spandrel beam behaviour

In the second positive loading cycle, a splitting crack had formed along the column interface over the entire depth of the spandrel on the west and east sides, with crack widths of 0.3 mm and 0.5 mm, respectively. One torsional crack had formed 100 mm from the column face on each side extending at 45 degrees away from the column over a distance of about 300 mm. The cracks widths were 0.25 mm and 0.05 mm at the level of the top reinforcement on the west and east sides, respectively

At general yielding in the positive loading direction, the 45 degree cracks extended further down into the spandrel and had crack widths of 0.5 mm and 0.4 mm respectively (see Fig. 3.32).

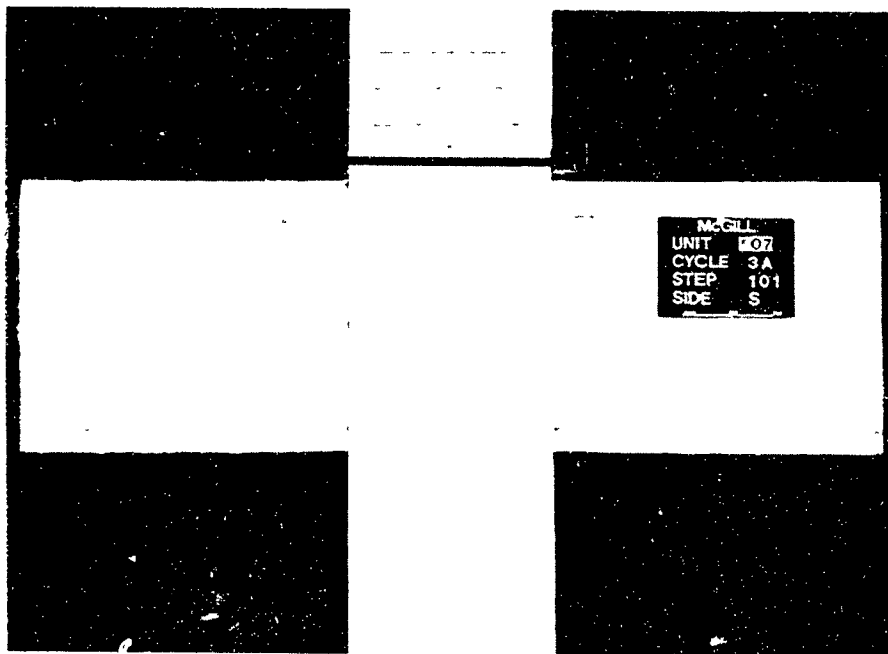


Figure 3.32 Photograph of spandrel beam of specimen R4 at general yielding

In the 4th positive loading cycle, the torsional cracks had propagated to the bottom of the spandrel and opened up to 1.4 mm and 0.9 mm respectively. On the interior face, separation between the spandrel and the slab had started and extended over the entire width by the 6th cycle. In the 6th downward loading cycle, several new torsional cracks formed. Crack widths at this point were 6.0 mm

and 4.0 mm, respectively and continued to open with signs of diagonal crushing and spalling of the concrete cover occurring in the 10th cycle (see Fig. 3.33)

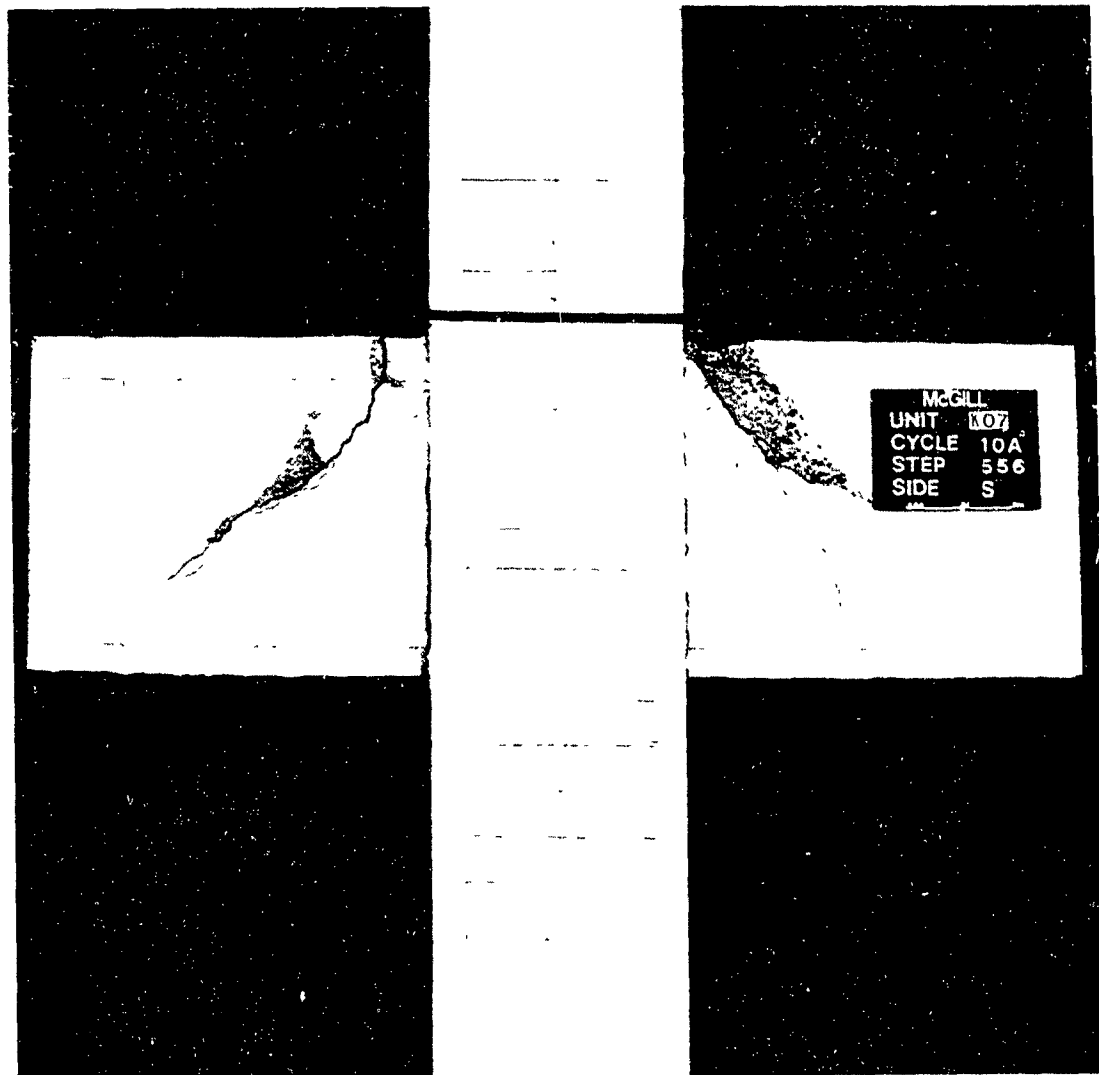


Figure 3.33. Exterior view of specimen R4 in the 10th loading cycle

3.3.5 Column behaviour

In the first two loading cycles, no cracking in the columns was observed. First cracking was noted at general yielding on the exterior face at the bottom of the spandrel beam with a crack width of 0.2 mm. In the 4th positive loading cycle, three flexural cracks were formed on the interior face above the slab at equal distances up to a height of 500 mm followed by a second crack on the exterior

face, 160 mm below the first crack. The crack widths increased slightly until the 8th positive loading cycle corresponding to the maximum moment transferred from the beam. At this stage the moment in the column was 331 kNm which is less than the predicted capacity of 375 kNm. Crushing and partial spalling of the column below the main beam occurred over a distance of 100 mm (see Fig 3.27c). Complete spalling did not occur until the 10th positive loading cycle (see Fig 3.34). On the exterior face of the upper column, a vertical splitting crack extending 150 mm above the slab signified the start of separation of the column cover from the confined core.



Figure 3.34: Photograph of joint region of specimen R4 in 10th loading cycle

3.3.6 Joint behaviour

The behaviour of the joint region for this specimen could not be readily observed since the entire side faces were covered by the spandrel beams. This confinement helped control the shear cracking in this region. As with the other two specimens, the joint hoop reinforcement was adequate.

Deformations in the joint region were monitored by a dial gauge located 85 mm from the column on the top of the slab. The readings from this dial gauge allowed the bond slip and joint shear deformation contribution to the beam tip deflection to be estimated. At the peak load of +292.8 kN at a ductility of 1.5Δ , this deformation was found to be 9.8 mm. At a displacement ductility of 4Δ , this deformation reached 38.1 mm.

Chapter 4

ANALYSIS AND COMPARISONS OF TEST RESULTS

4.1 Load-Deflection Response

Table 4.1 summarizes the overall behaviour and some of the key response parameters for the three test specimens. The specimens are listed in order of decreasing torsional resistance of the transverse spandrel beams. The displacement ductility of the specimens was computed from the ratio of the maximum recorded tip deflection Δ_u , to the displacement, Δ_y , recorded at general yielding. It must be noted that the testing was stopped due to displacement limitations on the loading apparatus and hence the specimens are capable of developing ductilities greater than that recorded in Table 4.1. The ability of the specimens to maintain load after general yielding is illustrated by the ratio of applied loads, P_u/P_y , where P_u is the load corresponding to Δ_u and P_y is the load corresponding to Δ_y . These ratios indicate that ability to maintain load decreased from specimen R4, to R4S, to R4T. Also given in Table 4.1 are the ratios of the stiffnesses. The terms k_y and k_u are the slopes obtained by joining the peak positive and negative load-displacement values for general yielding and the end of the test, respectively. As the spandrel beam is decreased in size this stiffness ratio decreases. Figures 4.1 to 4.6 shows the load versus tip deflection responses and photographs at the end of the test for specimens R4, R4S and R4T, respectively.

Table 4.1. Comparison of key response parameters for the three specimens

Specimen	Failure Mode	Ductility	P_u/P_y	k_u/k_y
R4	Beam flexural hinging	11.6	1.20	0.13
R4S	Beam flexural hinging	10.3	0.94	0.11
R4T	Beam flexural hinging and loss of shear transfer	10.0	0.67	0.10

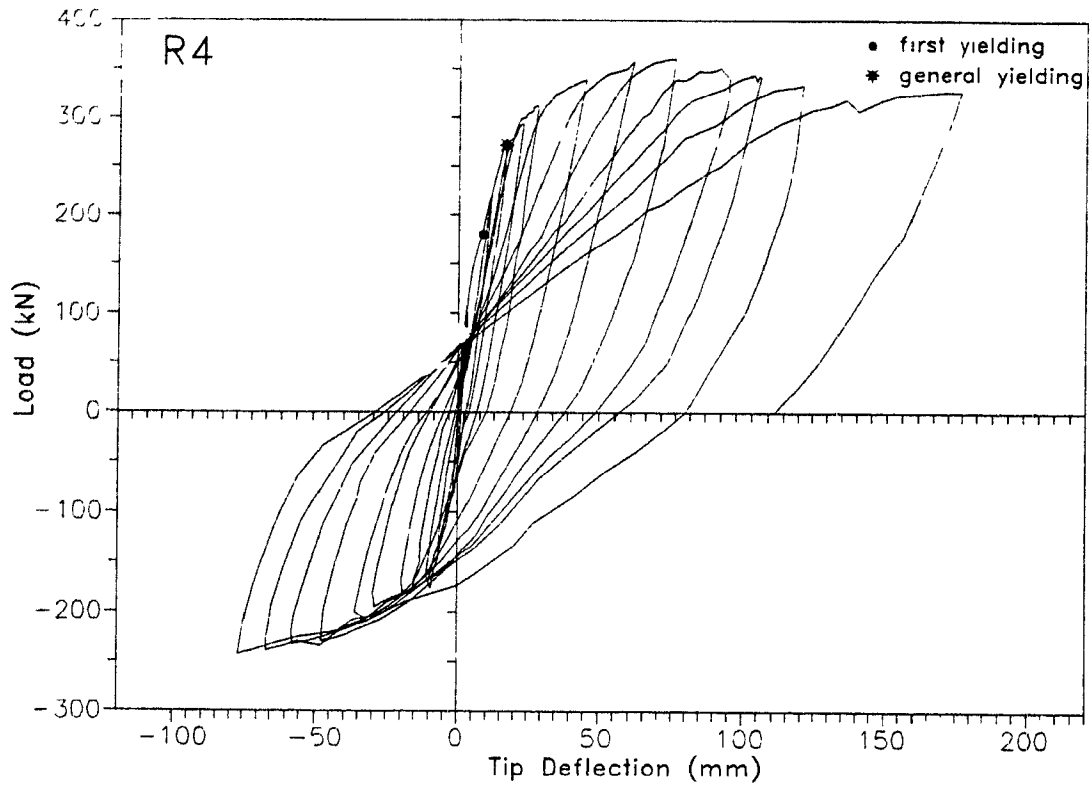


Figure 4.1: Load versus tip deflection response for specimen R4

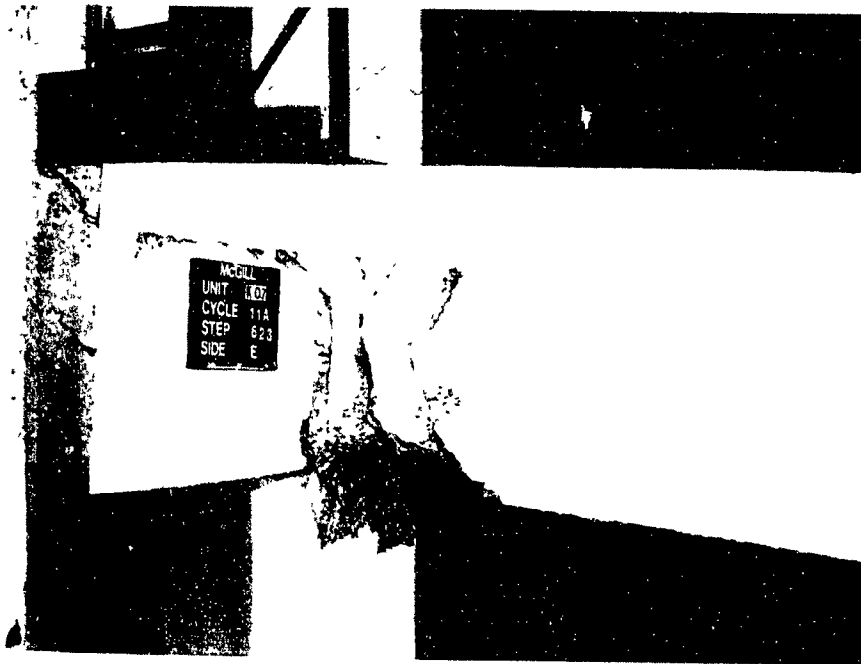


Figure 4.2 Photograph of damage to specimen R4 at the end of test

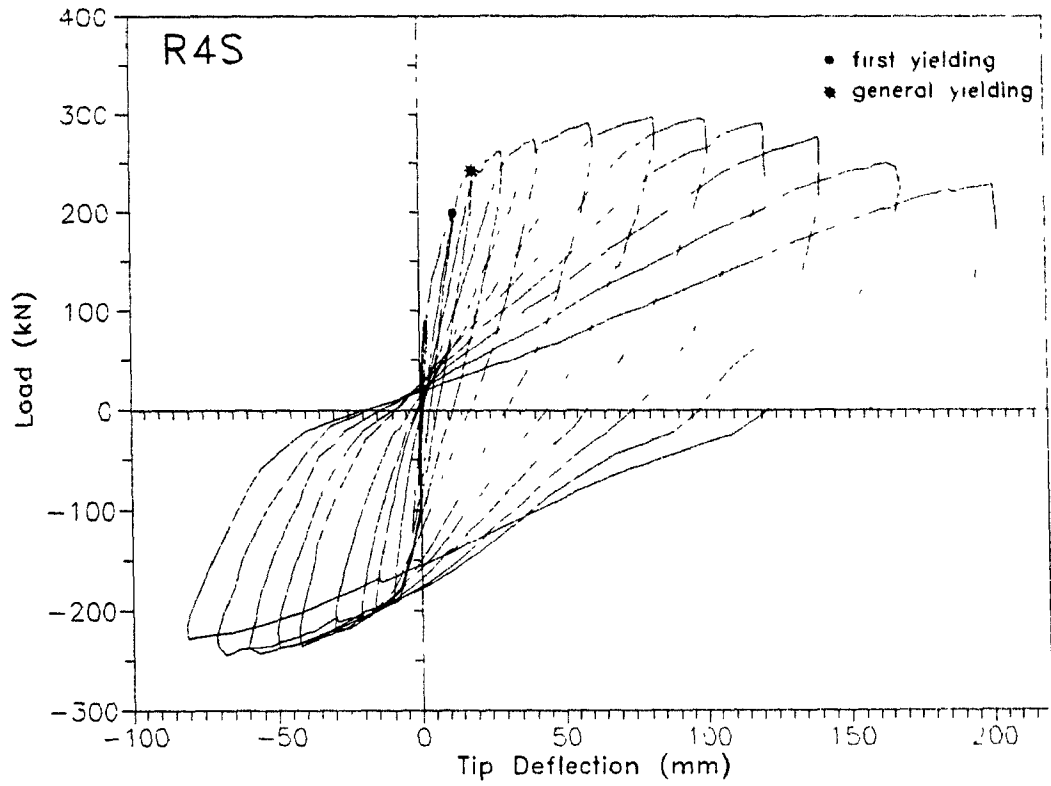


Figure 4.3: Load versus tip deflection response for specimen R4S

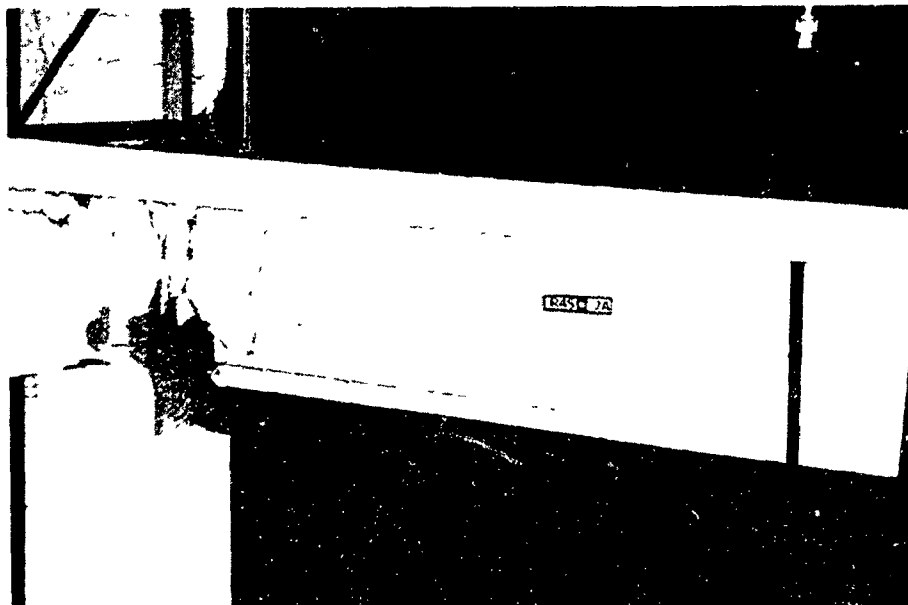


Figure 4.4 Photograph of damage to specimen R4S at the end of test

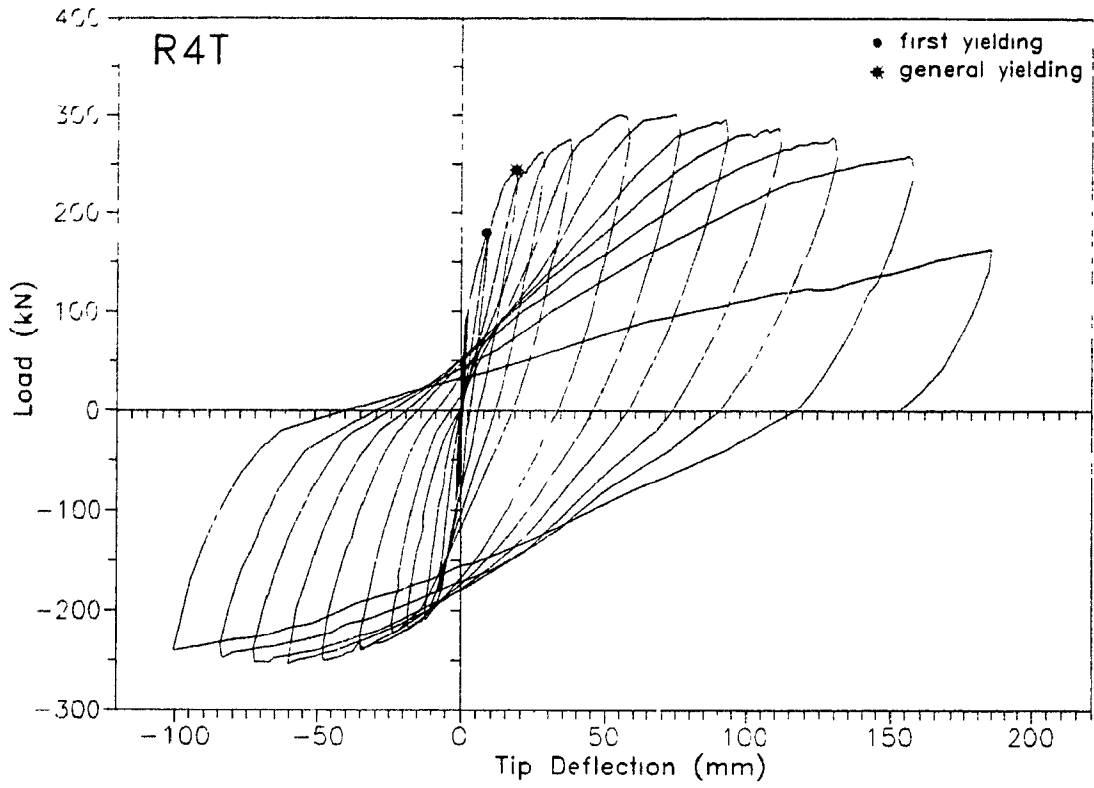


Figure 4.5: Load versus tip deflection response for specimen R4T

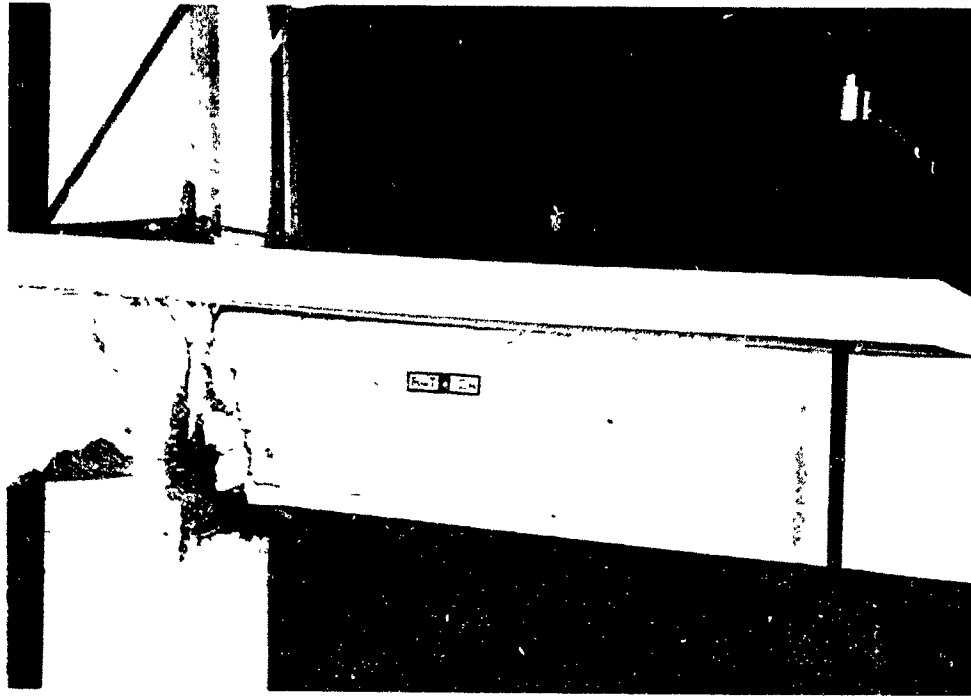


Figure 4.6. Photograph of damage to specimen R4T at the end of test

Specimen R4 maintained very stable hysteresis loops with peak loads higher than that of general yielding for the duration of the test. Specimens R4S and R4T behaved similarly to specimen R4 except the peak load was below that of general yielding in the final positive loading cycle. The flexural hinging in the beams is evident in each of the specimens due to the considerable amounts of spalling of the concrete in the regions close to the joint. Although the inclined shear cracking was well controlled the full-depth flexural cracking resulted in concentrated shear deformations along these vertical cracks. Specimen R4S and R4T experienced more significant torsional distress in the spandrel beams than specimen R4. The significant differences in the torsional distress are visible in Figs. 3.10, 3.23 and 3.33. Figure 4.2 shows that very little torsional distress occurred on the interior face of the spandrel of specimen R4. Figures 4.4 and 4.6 show increasingly more torsional cracking and concrete spalling on the interior faces of specimens R4S and R4T.

In each specimen, the 4 No 20 bottom longitudinal bars buckled between the closely spaced hoops near the column face in the 11th cycle, after loss of concrete cover had taken place.

Figure 4.7 compares the load-deflection response envelopes of the three specimens. Specimen R4, which had 400 x 600 mm spandrel beams, reached peak loads in the positive loading direction significantly higher than specimens R4S and R4T. Specimens R4S and R4T both had 250 x 600 mm spandrel beams, with R4T containing a smaller amount of torsional reinforcement than R4S. The peak loads in the negative loading direction were similar for the three tests since the size and strength of the spandrel beam plays a less significant role in positive bending. The small difference in the negative peak loads of the specimens can be attributed to the differences in the concrete compressive strengths. Specimens R4, R4S and R4T had concrete compressive strengths of 40.0, 34.3 and 46.6 MPa, respectively.

Specimen R4 displayed larger stiffness than the other two specimens in the positive loading cycles, before general yielding due to the larger torsional stiffness of the spandrel beam. Before significant torsional cracking occurred, specimen R4T displayed a larger initial stiffness than R4S due to the higher concrete strength in specimen R4T. In the last positive loading cycle of the three specimens, the following observations were made:

- (i) Specimen R4 showed signs that it could have continued to carry significant loads even after the end of the test.
- (ii) Specimen R4S showed a steady decrease in load carrying capacity due to significant loss of torsional stiffness and resistance and due to the buckling of the bottom beam bars.

- (iii) Specimen R4T showed a considerable drop in the peak load after a displacement of about 150 mm. Due to the smaller amount of torsional reinforcement this specimen displayed much more severe torsional distress in the spandrel beams (see Fig. 3.22)

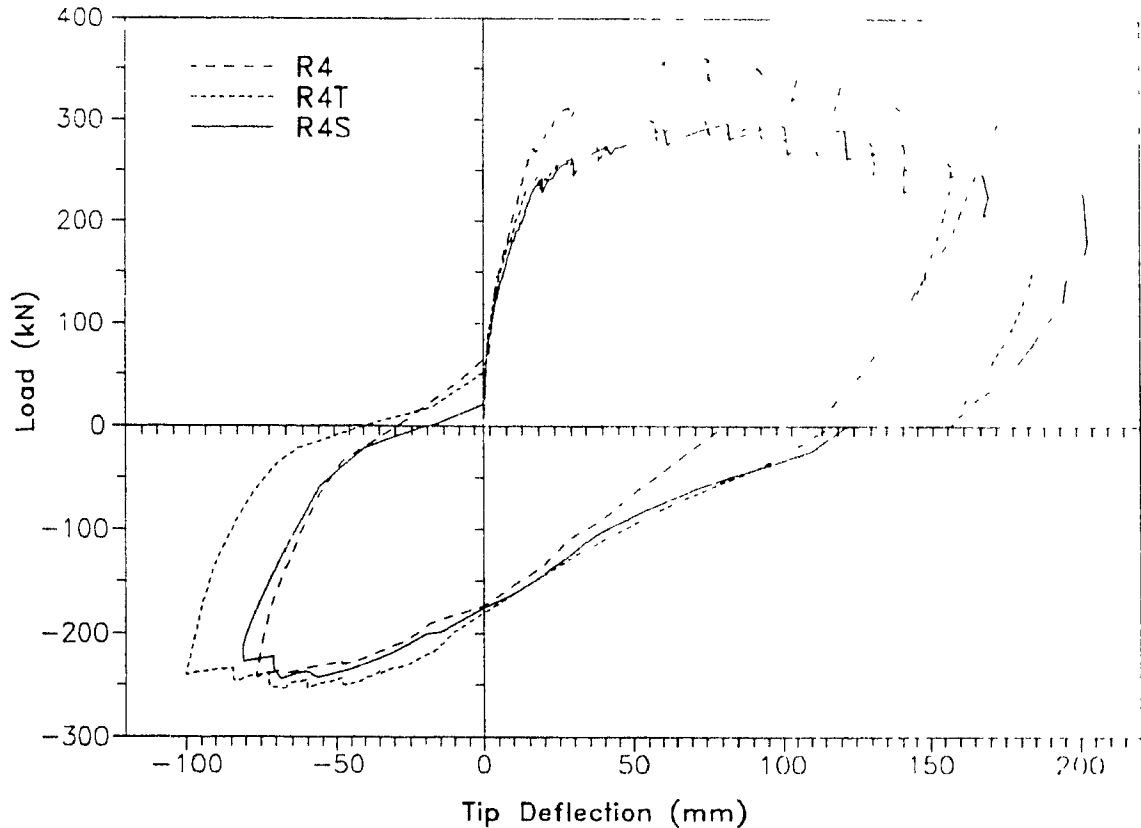


Figure 4.7: Load versus displacement envelopes for the three specimens

4.2 Tip Deflection Components

The tip deflection of the main beam is composed of the sum of the deformations in the beam plus the deformations of the joint. The contribution of the column due to rotation has been removed as discussed in Section 2.4.2.2. The beam displacement component consists of deflections due to flexural deformations plus shear deformations. The joint displacement consists of the shear distortion and the bond-slip of the reinforcing bars in the joint region. These components were estimated using the measurements taken from the test specimens.

The tip deflection is divided into three displacement components as follows

$$\Delta_{up} = \Delta_f + \Delta_s + \Delta_j \quad (\text{Eq 4.1})$$

where Δ_{up} is the estimated beam tip deflection,

Δ_f is the deflection component due to flexure

Δ_s is the deflection component due to shear

Δ_j is the deflection component due to joint shear distortion and bond-slip

The Δ_f component was calculated by applying the first moment-area theorem to the measured curvature distributions plotted in Figs. 3.4, 3.16, and 3.30 corresponding to specimens R4S, R4T, and R4, respectively, with the assumption that the joint is rigid. The equation used for this calculation is given in Fig. 4.8, where φ is the beam curvature and \bar{x} is the distance from the loading point to the centroid of a small element of area, φdx .

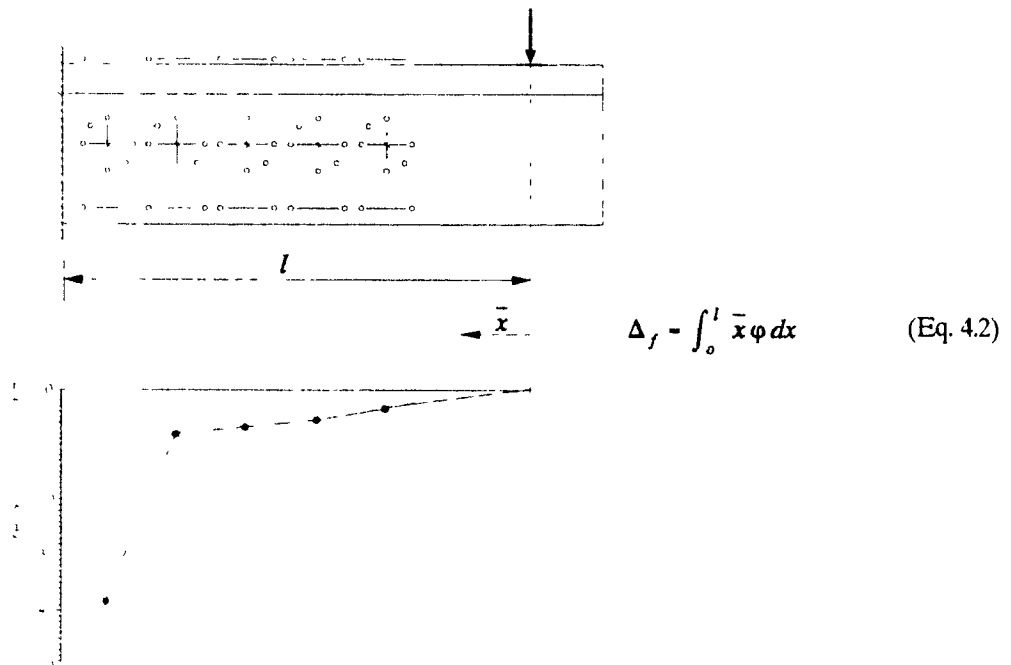


Figure 4.8 Equation for calculating Δ_f

The Δ_s component was calculated by integrating the measured shear strain distributions in the beam plotted in Figs. 3.4, 3.16, 3.30. The area under the curve can be found using the following equation (see Fig. 4.9).

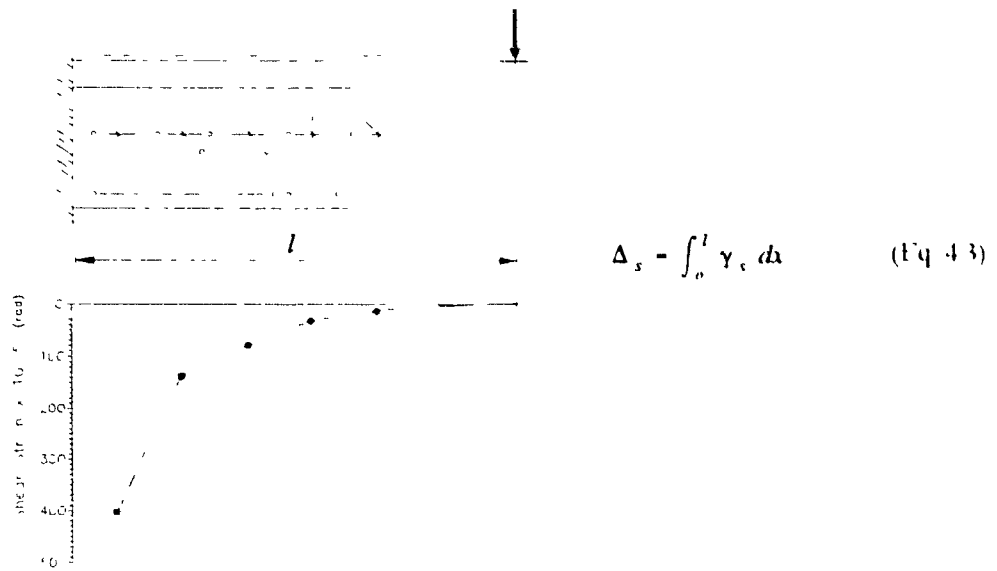


Figure 4.9. Equation for calculating Δ_s

The Δ_j component was estimated using the LVDT readings taken above the slab surface at the joint region as shown in Fig 4.10. The equations for this calculation are also given in Fig 4.10

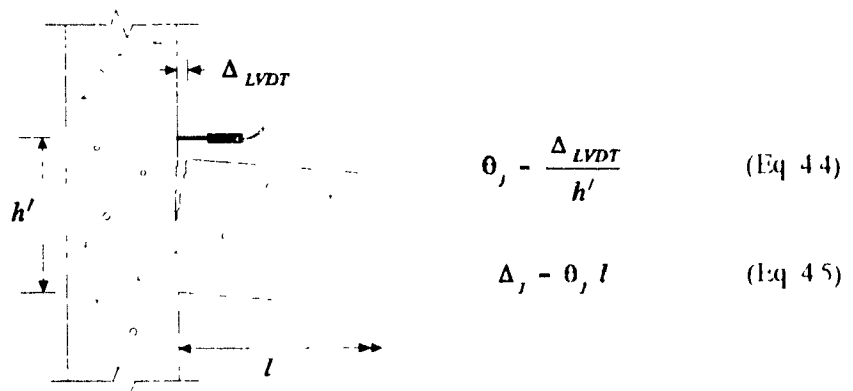


Figure 4.10 Equations for calculating Δ_j

Figures 4.11, 4.12, and 4.13 show the measured beam tip deflections which are compared with the experimentally determined deflection components for specimen R4, R4S, and R4T, respectively. As can be seen, the calculated tip deflection using the experimentally determined curvatures, shear strains and joint deformations, agree very well with the measured tip deflection. The small differences may be attributed to the very discrete nature of the crack pattern, with some cracks passing between the strain targets and others missing the strain targets.

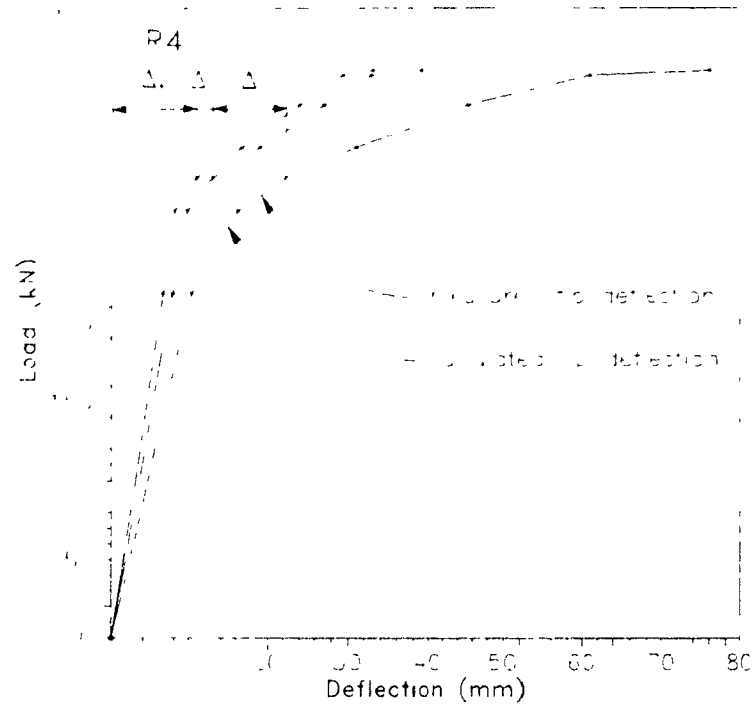


Figure 4.11 Beam tip deflection components for specimen R4

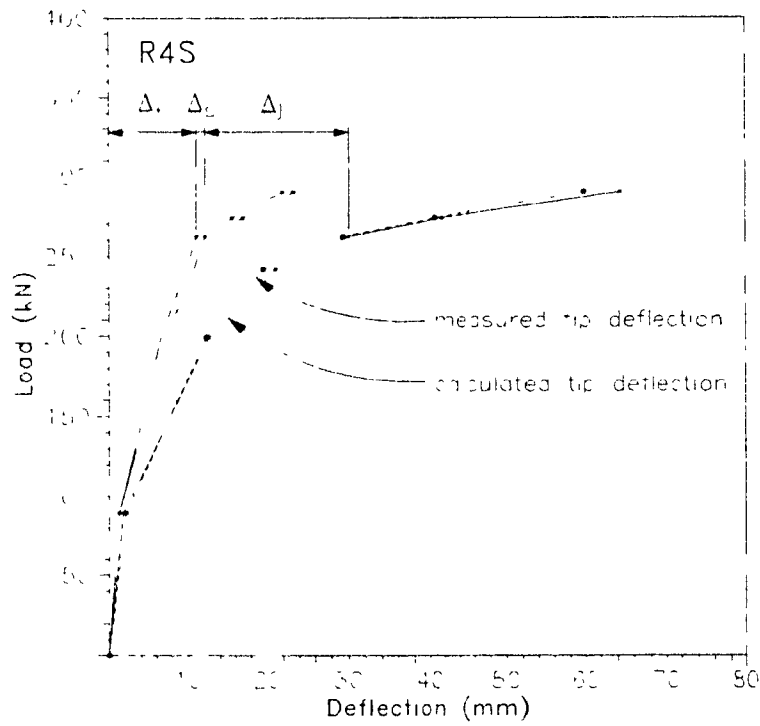


Figure 4.12 Beam tip deflection components for specimen R4S

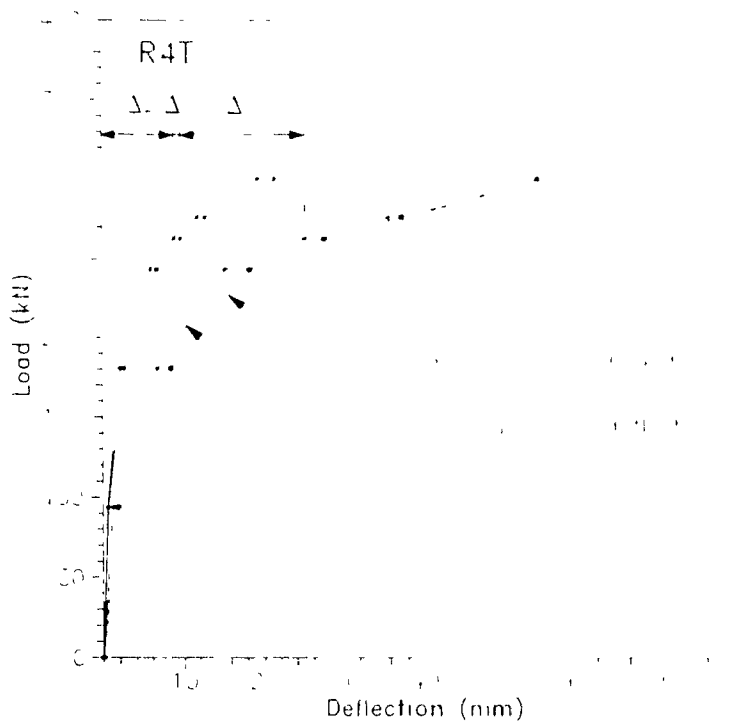


Figure 4.13 Beam tip deflection components for specimen R4T

Specimen R4 with the torsionally stronger spandrel showed signs of remaining very stiff until the 3rd loading cycle when general yielding occurred. Specimen R4S and R4T having the same smaller size spandrel started to curve in the 2nd loading cycle. R4T having the highest concrete compressive strength had the larger initial stiffness.

In all three specimens, the joint distortion and bond slip component contributed significantly. In the later loading cycles, this component was as large as the flexural component for specimens R4S and R4T. This indicated that bond deterioration and/or joint distortion had taken place after considerable yielding of the specimen. The shear component of deflection was quite small for all three tests. For specimen R4 this contribution was relatively larger than that of specimens R4S and R4T due to the higher applied shear.

4.3 Hysteretic Loading Behaviour

4.3.1 Energy Dissipation

The energy dissipating ability of the specimens can be obtained from the load versus deflection response loops. The area enclosed by the hysteresis loops in each loading cycle gives the energy dissipated in that cycle. Tables 4.2, 4.3, and 4.4 summarize the values for the energy dissipated in each half loading cycle for specimens R4, R4S and R4T respectively. The amount of energy increases with each cycle of loading since both the loads and the deflections increase.

Table 4.2 Energy dissipation at different ductility levels for specimen R4

Cycle	Load or Displacement	Δ_{peak}/Δ_y	Energy Dissipated (Nm)	P_{peak}/P_{yp} positive cycles
1A	1.2Mcr	0.19	101.5	----
1B		0.16	74.	
2A	1st yield	0.78	758.	----
2B		0.68	365.7	
3A	gen. yield Δ_y	1.00	1018.0	1.00
3B		1.00	635.8	
4A	1.5 Δ_y	1.48	1797.4	1.12
4B		1.58	1318.0	
5A	2 Δ_y	1.87	3155.6	1.19
5B		2.03	1886.8	
6A	3 Δ_y	3.01	6314.0	1.29
6B		3.09	4488.9	
7A	4 Δ_y	4.05	9225.6	1.36
7B		3.76	6415.5	
8A	5 Δ_y	5.04	12265.6	1.38
8B		5.00	9799.3	
9A	6 Δ_y	6.42	16130.1	1.34
9B		6.01	12093.1	
10A	7 Δ_y	7.02	18373.1	1.31
10B		6.92	14443.7	
11A	8 Δ_y	8.00	22225.9	1.27
11B		7.98	19520.2	
12A	maximum travel	11.64	32569.6	

Table 4.3 Energy dissipation at different ductility levels for specimen R4S

Cycle	Load or Displacement	Δ_{peak}/Δ_y	Energy Dissipated (Nm)	P_{peak}/P_{y1} positive cycles
1A	1.2Mr	0.10	100.2	
1B		0.08	57.9	
2A	1st yield	0.63	794.0	
2B		0.30	217.6	
3A	gen. yield Δ_y	1.00	1347.7	1.00
3B		1.00	802.7	
4A	1.5 Δ_y	1.51	2834.2	1.08
4B		1.58	2094.1	
5A	2 Δ_y	2.09	4179.9	1.13
5B		2.07	3129.2	
6A	3 Δ_y	3.08	7548.2	1.20
6B		2.97	6033.2	
7A	4 Δ_y	4.22	10710.1	1.23
7B		4.20	9644.7	
8A	5 Δ_y	5.10	13876.7	1.22
8B		4.96	12434.3	
9A	6 Δ_y	6.26	16752.3	1.20
9B		5.96	15958.1	
10A	7 Δ_y	7.24	19589.0	1.14
10B		7.01	19524.2	
11A	8.5 Δ_y	8.61	21052.3	1.03
11B		8.06	21318.9	
12A	10 Δ_y	10.34	23161.0	0.94

It should be noted that the amount of total energy dissipated is a function of the details of each specimen and the maximum tip deflection imposed. All the specimens have excellent energy dissipating characteristics.

4.3.2 Displacement Ductility

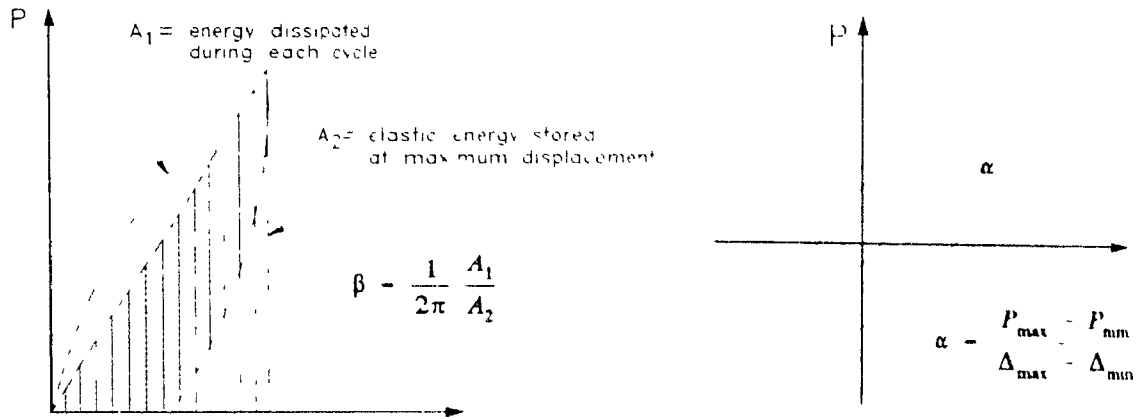
The displacement ductility of the test specimens defined as the ratio of the maximum deflection divided by the deflection at general yielding is a measure of the overall ductility of the structure. The specimens in this study reached displacement ductilities greater than 10 and showed excellent behaviour (see Tables 4.2, 4.3 and 4.4). Had the tests not been stopped due to lack of travel in the loading rams, higher ductilities could have been reached.

Table 4.4 Energy dissipation at different ductility levels for specimen R4T

Cycle	Load or Displacement	Δ_{peak}/Δ_y	Energy Dissipated (Nm)	P_{peak}/P_{vp} positive cycles
1A	1.2Mr	0.10	59.9	---
1B		0.11	36.6	
2A	1st yield	0.46	591.5	----
2B		0.59	490.0	
3A	gen. yield Δ_y	1.00	1584.2	1.00
3B		1.00	1178.7	
4A	1.5 Δ_y	1.49	2652.6	1.08
4B		1.50	2468.2	
5A	2 Δ_y	2.04	3957.5	1.13
5B		2.00	3795.2	
6A	3 Δ_y	2.98	7922.6	1.23
6B		2.87	8145.5	
7A	4 Δ_y	4.06	10999.6	1.24
7B		3.83	12033.9	
8A	5 Δ_y	5.02	13805.6	1.21
8B		5.06	15595.7	
9A	6 Δ_y	6.04	17388.3	1.18
9B		5.96	19527.6	
10A	7 Δ_y	7.03	20321.1	1.14
10B		7.00	22338.8	
11A	8.5 Δ_y	8.47	23495.7	1.06
11B		8.40	26329.2	
12A	10 Δ_y	9.99	17745.7	0.67

4.3.3 Damping and Stiffness

Two indicators for the damping characteristics of the test specimens are α , for the stiffness degradation and β , for the hysteretic damping. The β indicator, defined in Fig. 4.14a, is plotted in Fig. 4.15a for each test specimen. This value increases with loading and signifies greater damping. The α indicator, defined in Fig. 4.14b, is a measure of the decrease in the overall stiffness of the specimens as load is increased. Fig. 4.15b shows the change in stiffness of each specimen illustrating an initial rapid decrease in stiffness at the start of the test. Specimen R4, with the stiffest and strongest spandrel beam, displayed the largest stiffnesses.



a) Hysteretic damping coefficient, β

b) Stiffness degradation coefficient, α

Figure 4.14 Definition of damping coefficients α and β

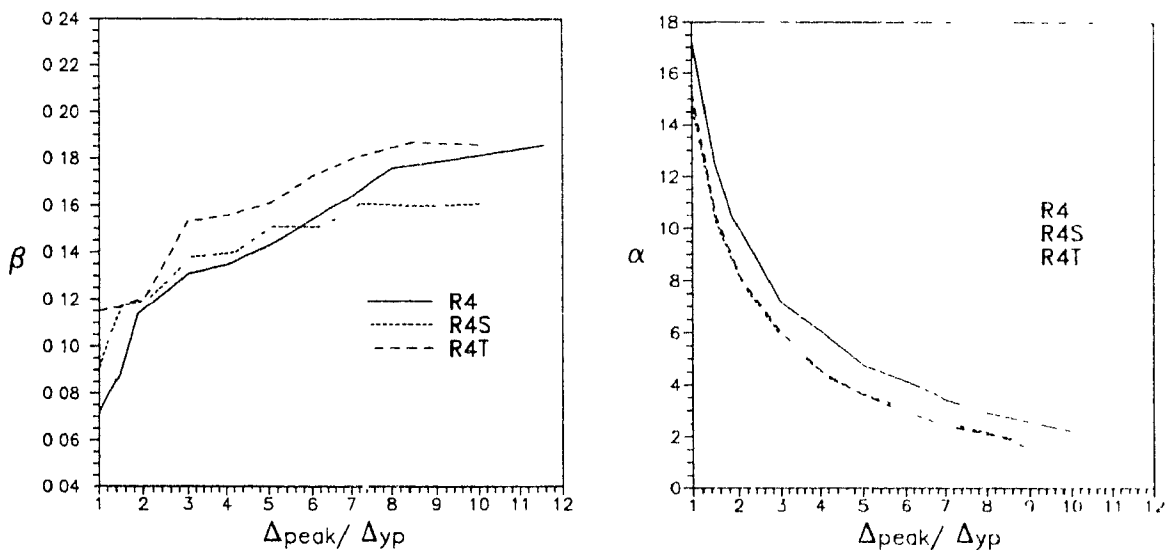


Figure 4.15 Hysteretic damping and stiffness degradation of the test specimen

4.4 Moment-Curvature Response and Predictions

In order to achieve a desired overall "structural" ductility, the ductility of individual members and hence the sectional or curvature ductility must be sufficient in regions expected to undergo plastic hinging. The "curvature" ductility is defined as φ_u / φ_y , where φ_y is the yield curvature and φ_u is taken as the maximum curvature attainable before significant drop in load carrying capacity. Table 4.5 summarizes the experimentally determined moments and curvatures in the main beam at the column face for each test specimen.

Table 4.5 Comparisons of maximum moments and curvature ductilities

Specimen	M_{max} (kNm)	ϕ_y (rad/m) $\times 10^3$	ϕ_u (rad/m) $\times 10^3$	ϕ_u / ϕ_y
R4	662.0	8.8	62.0	7.0
R4S	558.2	12.5	90.0	7.2
R4T	550.4	6.3*	90.2	14.3

* - this value is low because the cracks did not cross the gauge length

In order to assess the influence of the spandrel beam on the effective slab width, the moment-curvature responses of the main beam in negative bending will be predicted assuming varying effective slab widths. These predicted responses will then be compared with the experimentally determined moment-curvature responses of the test specimens. This comparison will enable an assessment of the effective slab width which best describes the actual response. A method of predicting the effective slab width is presented in Section 4.5.3. The predictions of the moment-curvature responses were made for the following cases:

- 1) A rectangular beam 400 x 600 mm without any slab flanges.
- 2) A T-beam including an effective slab width of $3h_f$ on each side of the beam. This resulted in an effective width, b_e of 1060 mm together with 4-No.10 slab bars.
- 3) A T-beam including an effective slab width of $4h_f$ on each side of the beam resulting in $b_e = 1280$ mm and 8-No.10 slab bars.
- 4) A T-beam including the entire slab width, $b_e = 1900$ mm, resulting in 12-No.10 slab bars being effective.
- 5) A T-beam including the entire slab width and assuming a non-linear strain distribution in the reinforcement across the slab.

Figure 4.16 shows the non-linear strain distribution measured in the slab for each test specimen near the end of testing (from Figs. 3.7, 3.19, and 3.31). Using the shaded distribution shown in Fig. 4.16 for the variations of the strains in the slab bars, moment-curvature predictions were made using program RESPONSE (Collins and Mitchell, 1991). These predicted moment-curvature responses are shown in Figs. 4.17, 4.18, and 4.19, along with the predictions of the other four cases listed above. These five predicted moment-curvature responses are compared with the experimentally determined responses of the test specimens. The varying strain distribution across the slab used in case (5) resulted in a "rounded" moment-curvature response curve due to the sequential yielding of the slab bars in the tension flange. The distribution of strain in the tension flange, is a function of the torsional stiffness and strength of the spandrel beam. In the case of an extremely stiff and strong

spandrel beam, the slab bar strains would tend to be uniform across the width of the slab, and hence, the bars would yield simultaneously giving a response similar to those of cases (1) through (4)

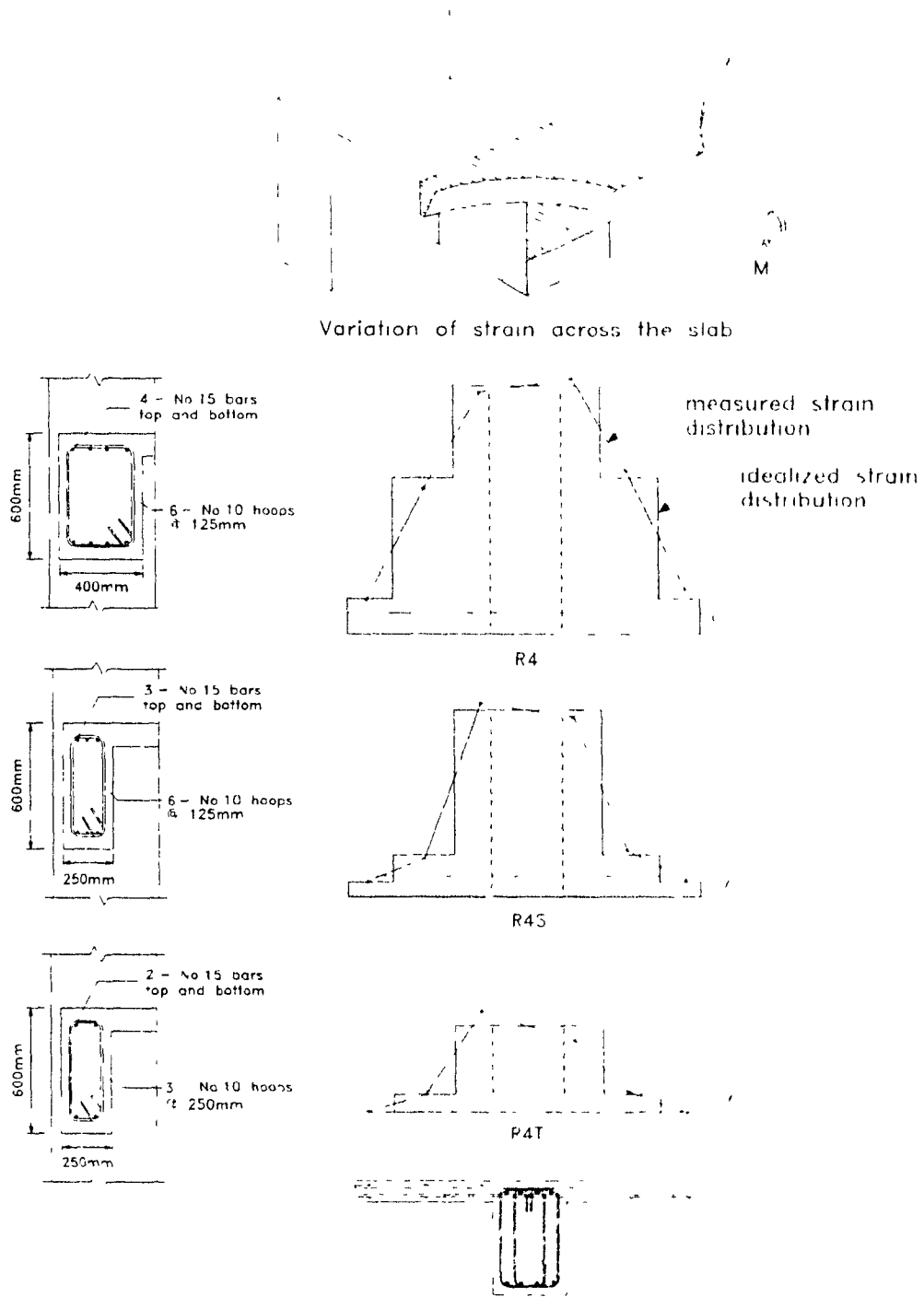


Figure 4.16: Non-linear strain distributions in the slab bars of the specimens

From these figures it is evident that the effective slab width computed using the Canadian Standard (CSA, 1984) of $3h_f$ is not appropriate in estimating the true contributions of the floor slabs for each of the three specimens

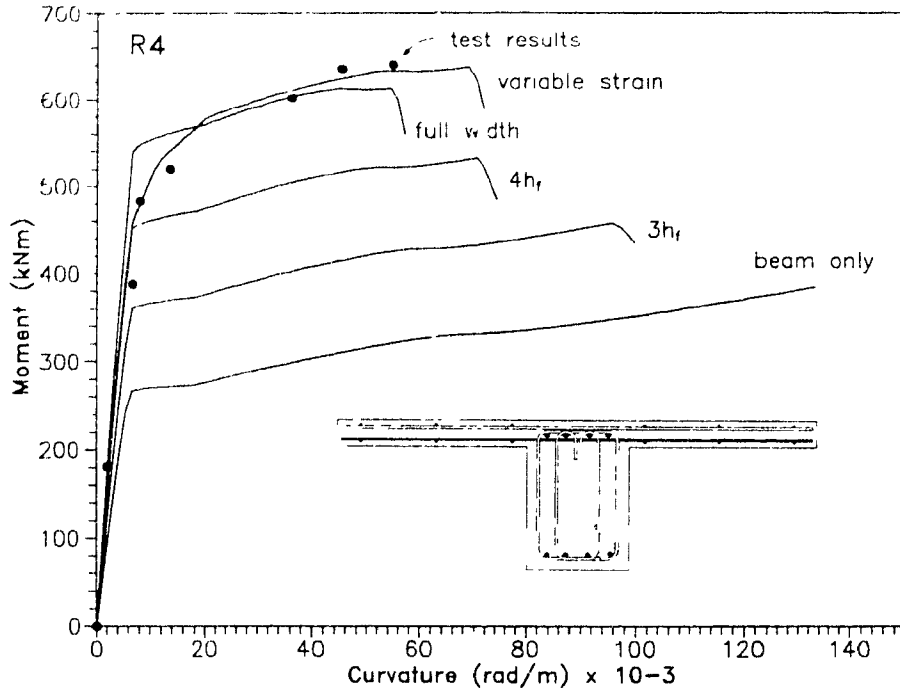


Figure 4.17 Predicted and experimental moment-curvature responses for specimen R4

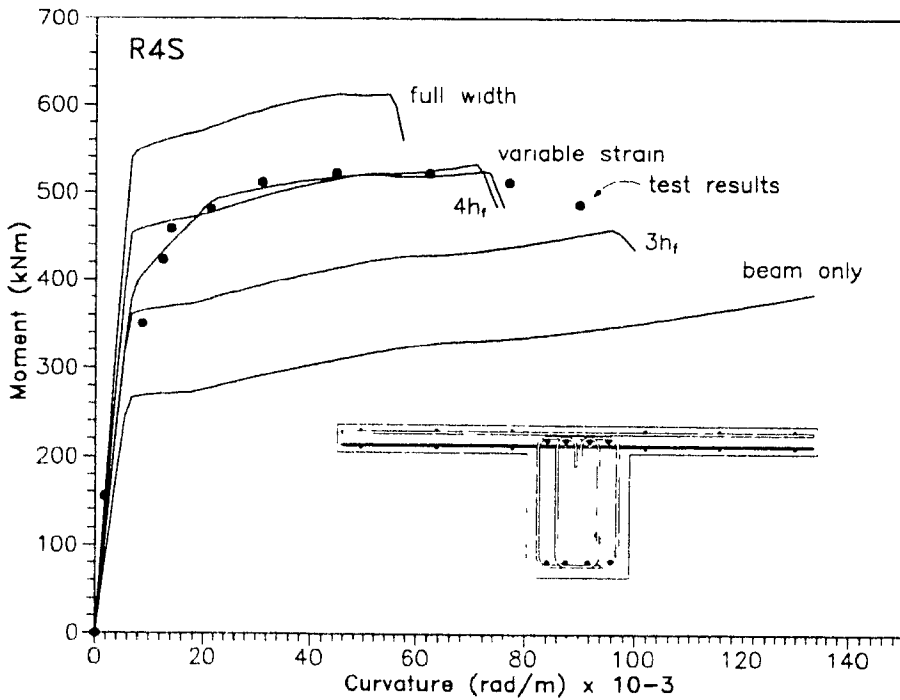


Figure 4.18 Predicted and experimental moment-curvature responses for specimen R4S

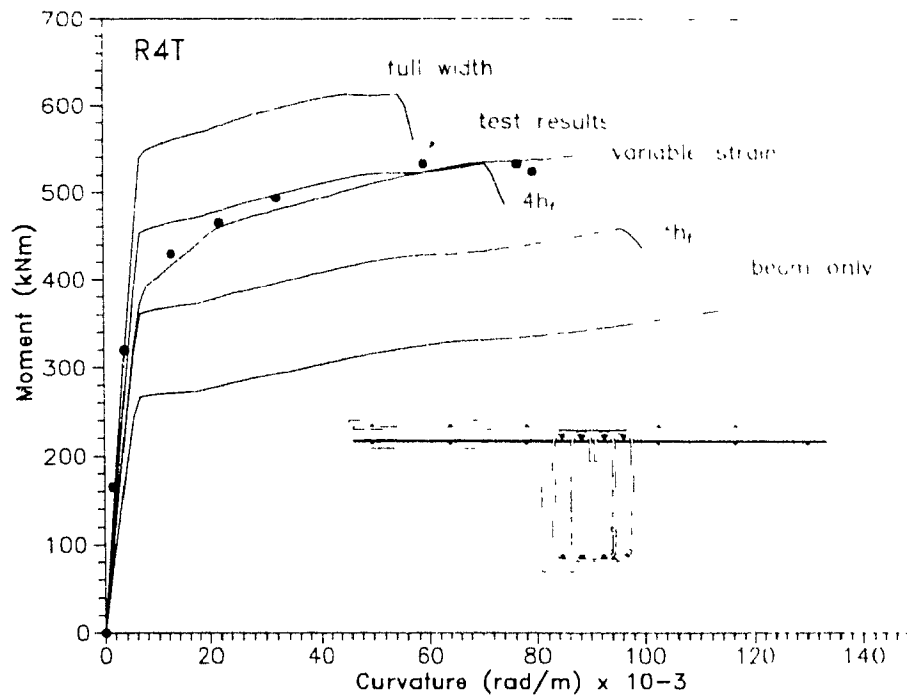


Figure 4.19: Predicted and experimental moment-curvature responses for specimen R4T

4.5 Role of Spandrel Beam and Slab

4.5.1 Effect of Torsion in Spandrel Beam

Figure 4.20 illustrates the free-body diagram of an exterior beam-column-slab connection showing the flow of forces from the main beam into the joint, and the flow of the forces from the slab bars into the spandrel beam. The torsion in the spandrel beam is caused by the eccentricity between the line of action of the forces in the slab bars and the centroid of the spandrel beam. As the negative moment in the main beam increases, the strains, and hence the forces in the slab bars also increase. When torsional cracks form in the spandrel beam, the torsional stiffness drops significantly. Upon further loading, the spandrel beam will reach torsional yielding which will limit the forces that can develop in the slab bars. The torsion in the spandrel beam builds up towards the column face and the side faces of the joint region are subjected to combined direct shear and torsional shear flow.

The torsional stiffness and torsional yielding moment of the spandrel beam will dictate the strain distribution in the slab bars. Therefore, the strain distribution in the slab bars would vary from uniform for an extremely stiff and torsionally strong spandrel beam, to a strain distribution which

decreases with distance from the column for more flexible, weaker spandrel beams (see Fig 4 16) Figure 4 21 shows the strain distributions in the slab bars at the slab-spandrel beam interface for the three specimens at maximum load level Specimen R4, which had the highest torsional stiffness and resistance, displayed yielding of all of the slab bars across the width of the slab, resulting in the yielding of 12 No 10 bars Specimen R4S and R4T had spandrel beams which were smaller than the spandrel beam in specimen R4 Therefore both of these specimens displayed strains in the slab bars which were less than those developed in specimen R4 Although specimen R4S and R4T had the same size of spandrel beam, specimen R4T had a smaller amount of torsional reinforcement As can be seen from Fig 4 21, specimen R4T had strains in the slab bars which were less than those in specimen R4S Only 4 No 10 slab bars reached their yield in specimen R4T This comparison provides strong evidence that both the size of the spandrel beam and the amount of torsional reinforcement in the spandrel beam have a significant effect on the strain distribution in the slab bars

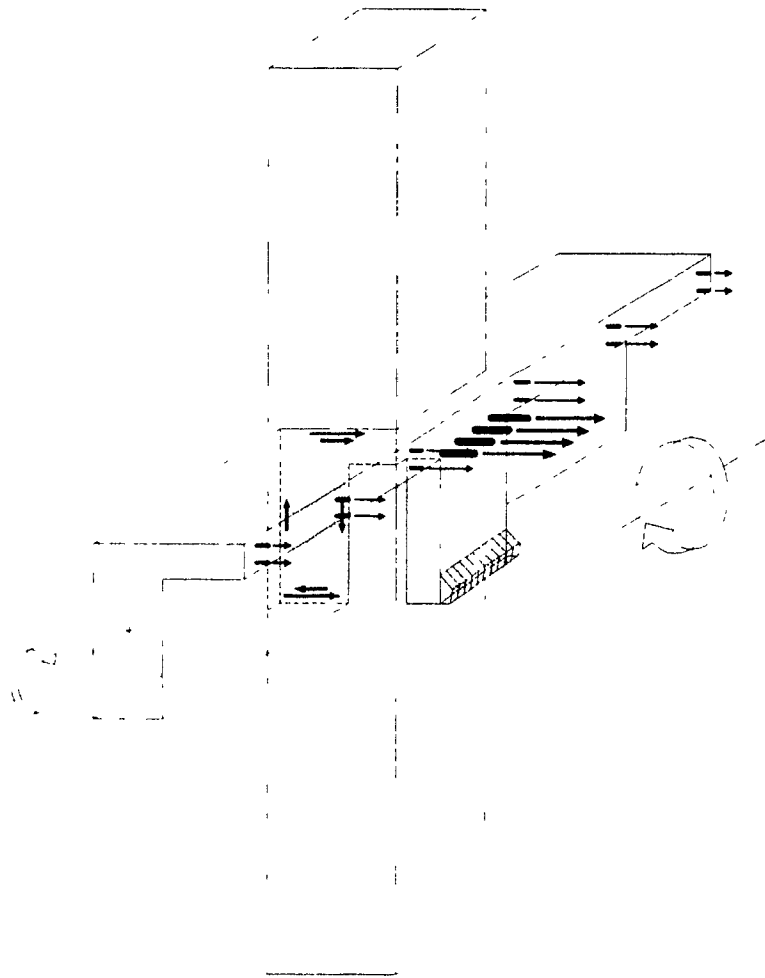


Figure 4.20 Role of the spandrel beam

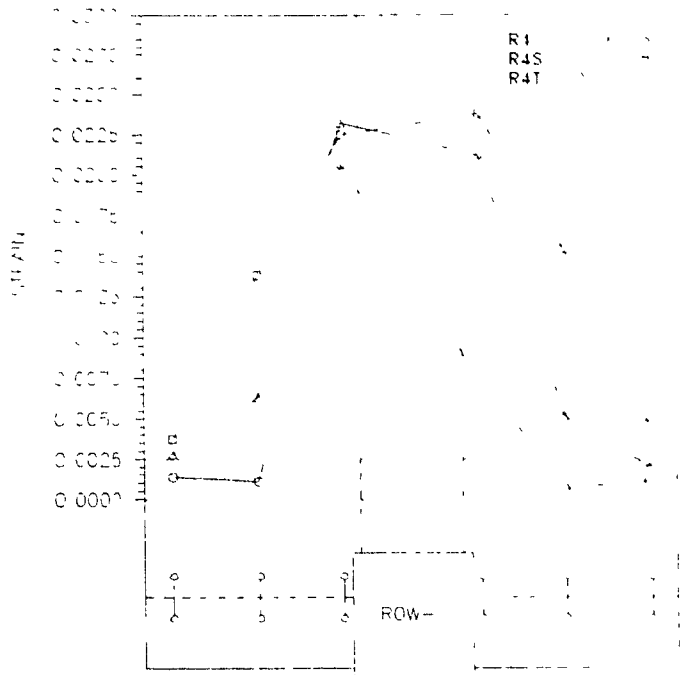


Figure 4.21: Measured strain distributions across the slabs at slab-spandrel interfaces

4.5.2 Strut and Tie Mechanism Transferring Forces from Slab Bars

Figure 4.22 shows a plan view of the specimen illustrating the approximate area of the "disturbed regions" around the column after significant yielding has occurred. At this stage, a different mechanism for the transferring of slab forces to the joint region develops. This mechanism can be visualized by a strut and tie model

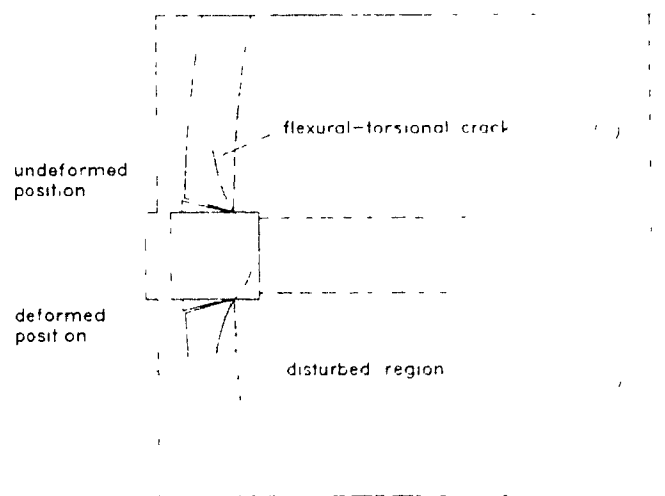


Figure 4.22. Disturbed regions of specimen after significant yielding

Figure 4.23 shows a plan view of the slab around the column region illustrating the flow of tensile and compressive forces idealized as a strut and tie model. It is assumed that the slab bars are anchored near the outer edge of the spandrel beam. The longitudinal bars in the spandrel beam form the tension chord in the idealized truss while the top horizontal legs of the closed hoops in the spandrel beam provide the tension members. This strut and tie mechanism forms in the top face of the spandrel beam and in the slab. In order to determine the tensions in the slab bars that can be resisted by the strut and tie mechanism, it is necessary to limit the forces in the tension ties to the yield forces in the bars which they represent. Hence, the forces in the slab bars which will cause yielding in the tension tie can be found knowing the geometry of the spandrel beam and the size, spacing and yield stress of the reinforcing bars.

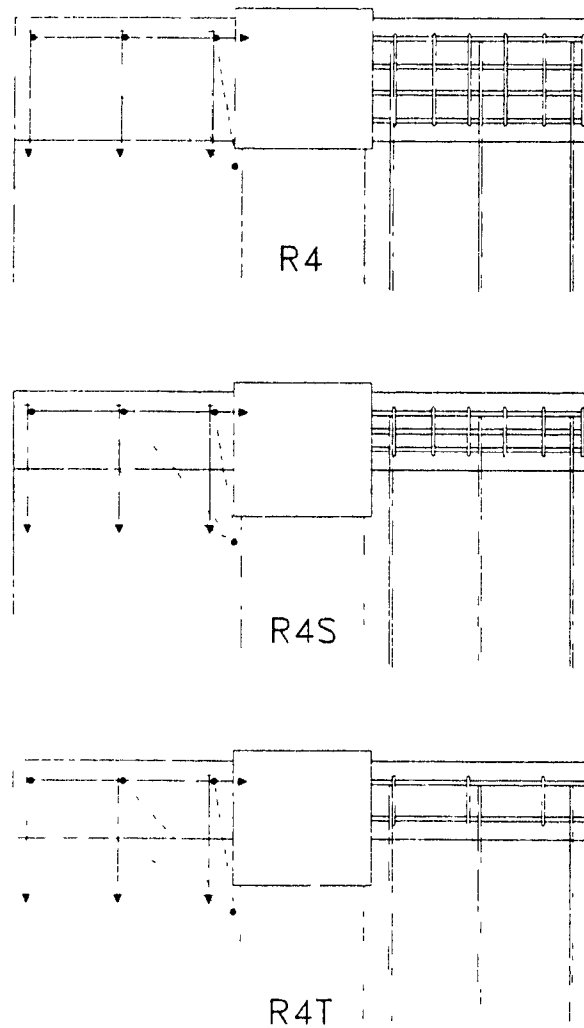


Figure 4.23 Flow of forces in the "disturbed regions" of the slab

Figure 4.24 shows an exploded view of the main cracked surfaces observed after the specimens were removed from the testing apparatus. The spiralling torsional cracks in the spandrel beam as well as the region of compressive stresses around the column on the top surface of the slab are apparent. A similar failure surface was observed by Durrani and Zerbe (1987).

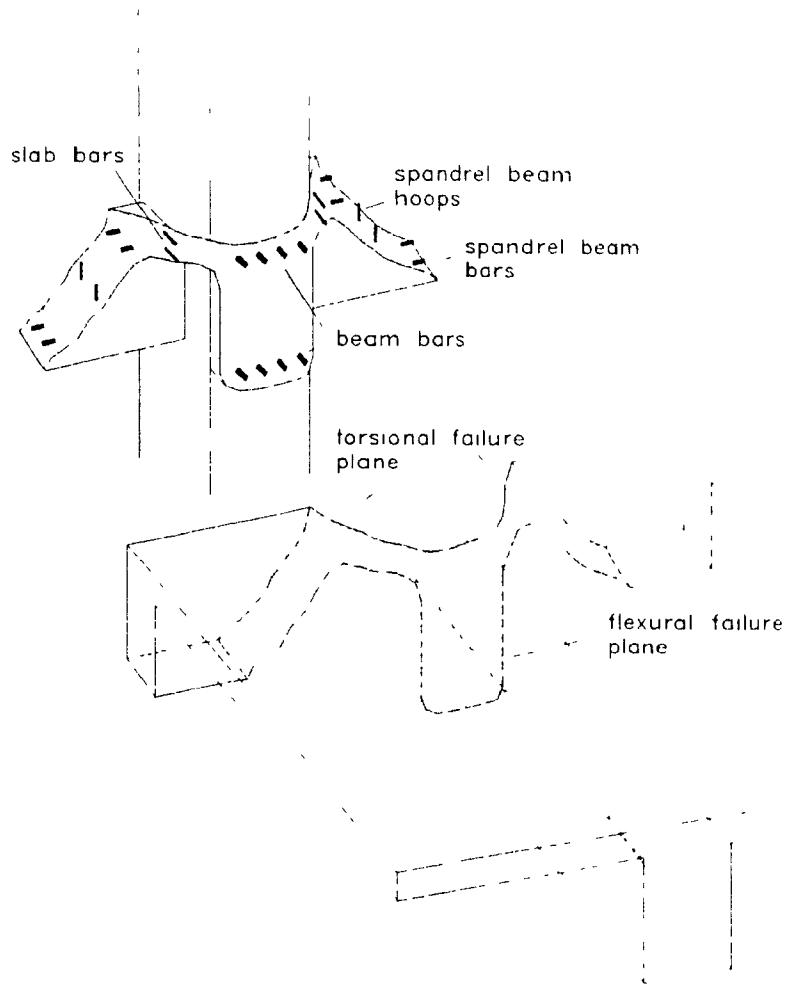


Figure 4.24: Failure surface in specimen R4T

4.5.3 Effective Slab Reinforcement (Effective Width)

The effective width of slab can be found by first determining the number of slab bars which can be resisted by the spandrel beam. Table 4.6 lists the effective slab widths recommended by the Canadian, New Zealand and U.S. codes for exterior joint connections. It is interesting to note that most tests that have been performed on exterior connections, resulted in the yielding of slab bars over a greater width than that recommended in current codes.

Table 4.6 Comparison of the "effective slab width" used in current design codes

Standard	"effective width" of slab in tension
CSA Standard (CSA, 1984)	$3h_f$
NZS Standard (NZS, 1981)	$2h_f$
ACI Code (ACI, 1989)	Chapter 21 does not specify an effective slab width. But in 8.10, the effective width of T-beam flanges must be less than $\frac{1}{4}$ of the span of the beam, and effective overhang flange must be less than (a) $8h_f$ (b) $\frac{1}{2}$ the clear span to next web

The "effective slab reinforcement" or "effective width" will be governed by either the torsional strength of the spandrel beam or by the capacity of the strut and tie mechanism in the top of the spandrel beam (see Sections 4.5.1 and 4.5.2).

The yielding torque of the spandrel beam can be estimated using the following expression (Mitchell and Collins, 1974 and Collins and Mitchell, 1991):

$$T = \frac{2 A_o A_t f_y}{s} \cot \theta \quad (\text{Eq. 4.6})$$

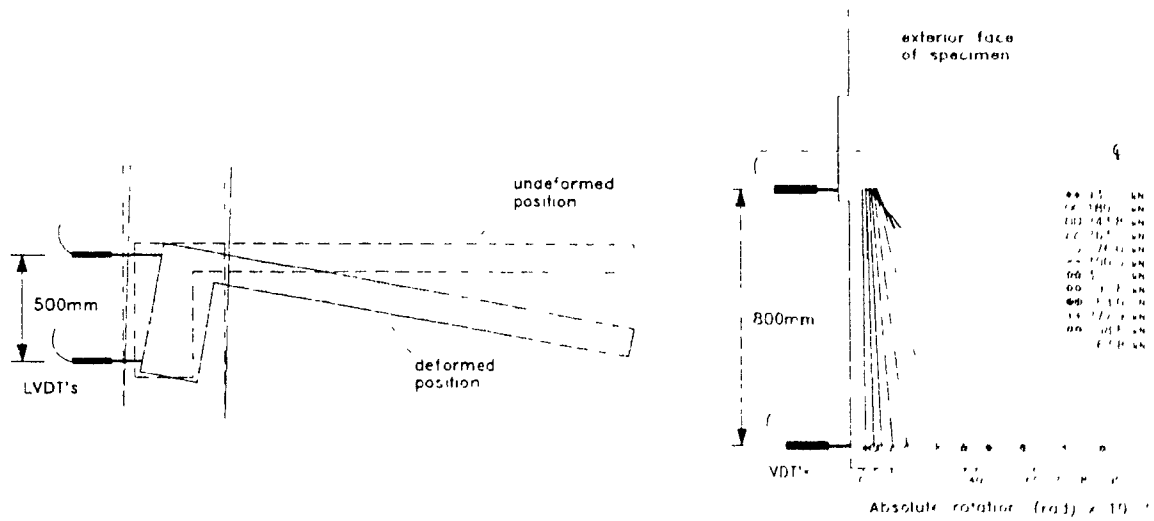
- where
- A_o area enclosed by the torsional shear flow path
 - A_t area of one leg of the closed hoop reinforcement
 - f_y yield stress of the hoop reinforcement
 - s spacing of the stirrups in the spandrel beam
 - θ angle of principal compression measured from the horizontal axis of the beam

4.5.4 Measured and Predicted Torsional Response of Spandrel Beams

Figure 4.25a shows the manner in which the twist of the spandrel beam of specimen R4T was measured. Pairs of LVDT's measured the rotation of the column and pairs of LVDT's measured the twist and rigid body rotation of the spandrel beam 800 mm away from the column (see Fig. 4.25b). These measurements enabled the twist of the spandrel beam to be determined at different load stages. As can be seen in Fig. 4.25b after yielding of the main beam and the spandrel beam the column does not experience increased rotations.

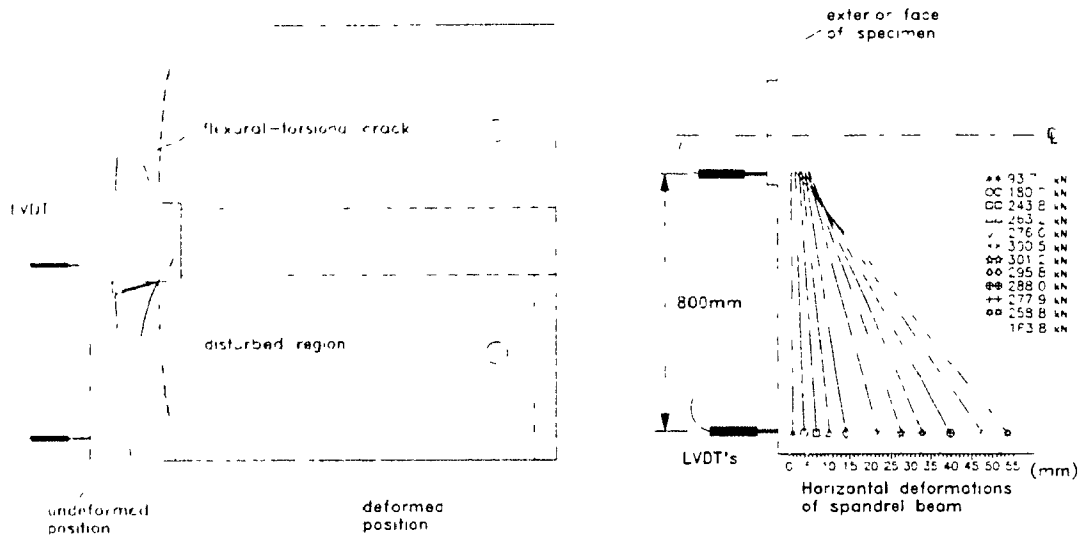
Along with the twisting, the spandrel beam also deflects inwards about its weak axis as shown in Fig. 4.26a. Figure 4.26b shows the displacements of a point located on the column and a point located 800 mm from the column. The horizontal movement at different loading stages were obtained by taking the average deflection reading from the top and bottom LVDT's (see Fig. 4.25a).

Figure 4.27 shows the torque versus twist response of the spandrel beam obtained from the experiment. The experimental torque was calculated from the forces in the slab bars. As can be seen from Fig. 4.27 the beam cracks at a relatively small torque and the beam develops a torque which greatly exceeds the predicted torsional strength. Hence, soon after cracking a different mechanism resists the load. This mechanism arises from the lateral bending of the spandrel beam in the form of a strut and tie mechanism (see Section 4.5.2).



a) Elevation view of deformed spandrel beam b) Plan view showing rotations of spandrel beam

Figure 4.25. Rotations of the column and the spandrel beam in specimen R4T



a) Plan view of deformed spandrel beam

b) Absolute rotations of spandrel beam

Figure 4.26 Bending deformations in the spandrel beams

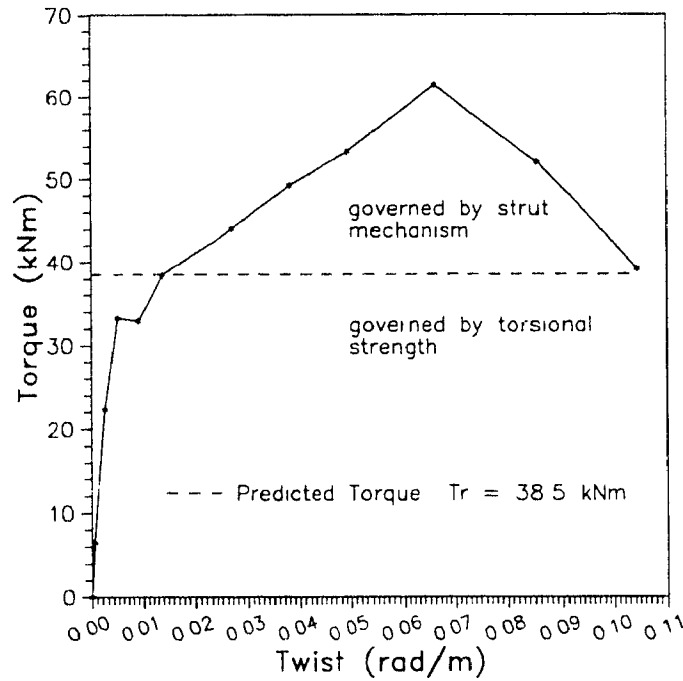


Figure 4.27 Torsional response of spandrel beam in specimen R4T

4.5.5 Determination of Effective Slab Reinforcement

Table 4.7 summarizes the number of bars effective in negative bending based on the measured slab strains along with the predicted effective number of bars based on both the torsional strength of the spandrel beam and on the capacity of the strut and tie model (see Appendix B)

Table 4.7 Comparison of predicted and experimentally determined number of bars yielding

Specimen and Researcher	Experimental values		Predicted from torsional strength		Predicted from strut and tie model	Lower limiting value predicted
	Torque (kNm)	Number of bars	Predicted Torque (kNm)	Number of bars	Number of bars	Number of bars
R4 Rattray (1986)	74.2*	60*	120.6	9.9	6.1	6.1
R4S this study	69.7	5.4	50.9	4.1	5.2	4.1
R4T this study	49.3	4.0	38.5	3.1	4.4	3.1
1S Ehsani (1982)	45.4	4.0	38.6	4.5	4.2	4.2
J4 Durrani (1987)	36.7	3.9	29.4	3.8	3.1	3.1
2D-E Cheung (1991)	56.8	9.0	56.8	10.0	10.4	10.0

* - the torsion was determined from the eccentricity of the slab bars and the forces in the slab bars corresponding to the measured strains

+ - these values were limited by the amount of slab reinforcement. If the slab were wider such that more slab bars were present, then it is predicted that 10 bars would have reached yield

Figure 4.28 shows the measured strain distributions in the slab bars at the maximum applied load. The experimental values for the number of slab bars yielding in Table 4.7 were determined from the strains shown in this figure

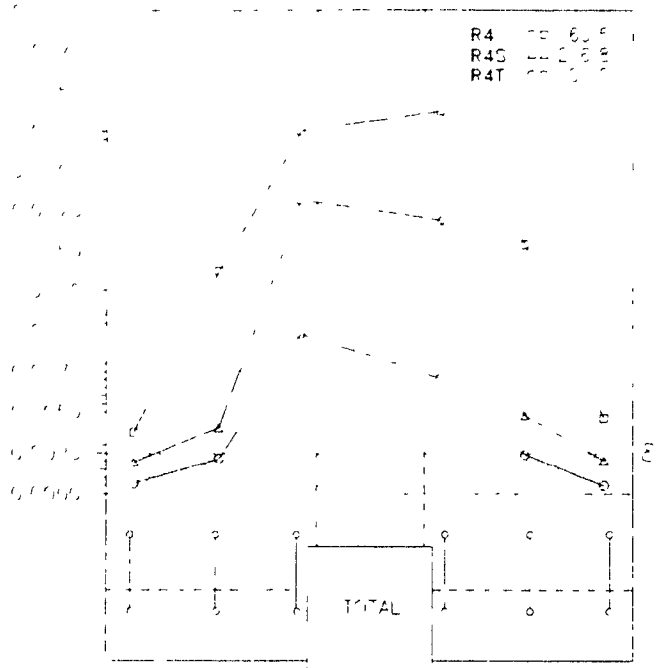


Figure 4.28. Measured strain distributions across the slab at maximum capacity

The method used to predict the number of bars corresponding to the predicted torsional capacity of the spandrel beam is discussed below. More detailed calculations for each of the specimens is given in Appendix B. For specimen R4S, the predicted torsional capacity is 50.9 kNm. This torque arises from tensions in the slab bars, which have an eccentricity of 254 mm from the centroid of the spandrel beam (see Fig 4.29). Hence, the force in the slab bars corresponding to torsional yielding is $F = T / e = 50900 \text{ kNm} / 254 \text{ mm} = 200.4 \text{ kN}$. Since the yield stress for the No 10 bars is 487 MPa, then the area of yielding slab bars can be calculated as $A_s = F / f_y = 200.4 * 1000 / 487 = 411 \text{ mm}^2$. This is equivalent to 4.1 No 10 bars.

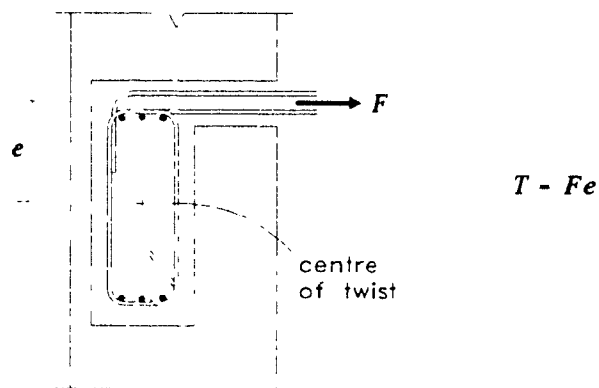


Figure 4.29 Loading of spandrel beam in torsion

The predicted number of effective slab bars using the strut and tie model were found from statics. The forces in the tension chords and diagonal compression struts are limited by the tensile strength of the reinforcement and the compressive strength of the concrete. Hence, these forces in turn limit the yielding of the slab bars. Figure 4.30 shows the strut and tie models with the maximum obtainable forces on the left side of the figure along with the configuration of the reinforcing steel in the spandrel beam on the right side. In constructing the model the following assumptions were made: (1) the stresses in the slab bars were taken as f_y since this steel had a small amount of strain hardening, (2) the ultimate stress in the spandrel beam reinforcement was taken as $1.25f_t$, (3) the node where the compressive forces collect was taken just past the interior corner of the column. This node is assumed to be located a distance equal to the column size, c , from the tension resultant (see Fig. 4.30). The tension resultant force in the top surface of the spandrel beam corresponds to 2.0, 1.5, and 1.0 bars for specimens R4, R4S, R4T, respectively. It was observed that all reinforcement in the outer half of the spandrel beam was effective. The strut and tie model using the configuration of specimen R4 allowed for all six slab bars to achieve their yield force. Specimen R4S with the

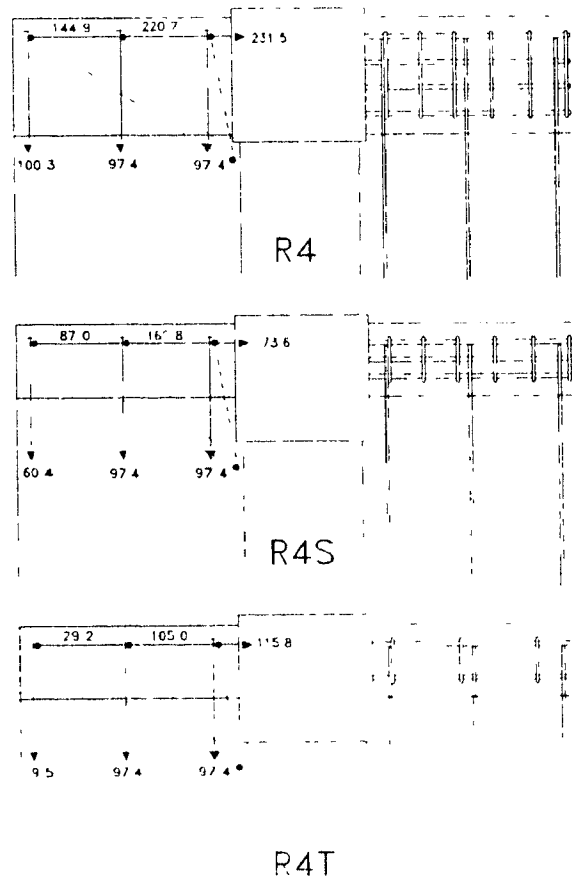


Figure 4.30. Strut and tie model showing yielding of slab bars

reduced spandrel beam dimension but the same closed hoop configuration was able to yield 5.2 slab bars. Specimen R4T, due to the decrease in the number of closed hoops in the spandrel beam was able to yield 4.4 slab bars.

4.5.6 Simplified Determination of Effective Slab Reinforcement

A simplification for the torsional strength using the equation developed by Collins and Mitchell (1974) and assuming that the angle of principle compression is acting at 45 degrees is:

$$T_r = \frac{2 A_o A_t f_v}{s} \quad (\text{Eq. 4.7})$$

which when equated to the induced torque from the slab bars gives:

$$T_r = \frac{2 b_o h_o A_t f_y}{s} = \frac{h_o}{2} n A_s f_y \quad (\text{Eq. 4.8})$$

where h_o is the eccentricity of the forces in the slab bars and n is the number of effective bars (see Fig. 4.31). Solving for n , the number of effective slab bars can be found from

$$n = \frac{4 b_o A_t}{s A_s} \quad (\text{Eq. 4.9})$$

In most cases, the same bar size is used for the slab reinforcement as for the closed hoops in the spandrel beam. Therefore, this equation can be further reduced to its simplest form as

$$n = 4 \frac{b_o}{s} \quad (\text{Eq. 4.10})$$

The values for the number of effective slab bars using this simplified equation are shown in Table 4.8.

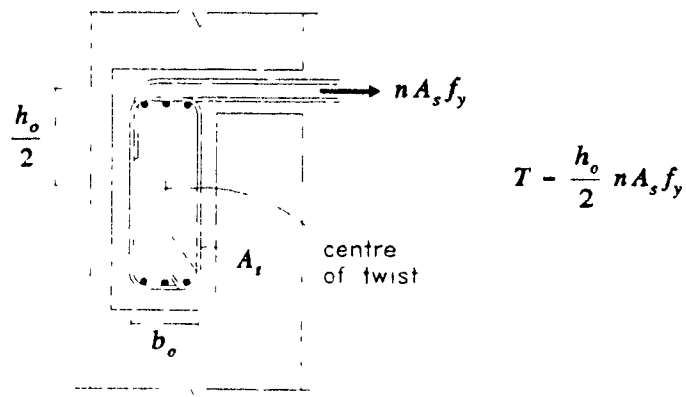


Figure 4.31: Induced torsion in spandrel beam

The method of estimating the number of effective bars by using a strut and tie model can be simplified somewhat by noting that the limiting parameter is the force in the longitudinal bars near the back face of the spandrel beam (see Fig. 4.32). In the strut and tie model, the resisting moment is provided by the force in the longitudinal bars multiplied by a lever arm to an assumed nodal point just past the corner of the column, where the compressive forces converge (see Fig. 4.32). For this simplified model, it is also assumed that the distance between the tension and compression resultants equals the column dimension, c . Taking moments about the nodal point shown in Fig. 4.32 gives

$$\frac{A_s^* f_y}{s_s} x \frac{x}{2} = A_{sl} f_y c \quad (\text{Eq. 4.11})$$

where A_s^* is the area of slab bars within a distance s_s

A_{sl} is the area of top longitudinal bars in the outer half of the spandrel beam

$\frac{x}{2}$ is the lever arm to the resultant of the slab bar forces

s_s is the spacing between the slab bars

Solving this equation for the effective width, x gives

$$x = \sqrt{\frac{2 A_{sl} c s_s}{A_s^*}} \quad (\text{Eq. 4.12})$$

Hence the number of slab bars expected to yield, n , is the total number of slab bars within the distance x . The values computed from this method are given in Table 4.8 (see Tables in Appendix B for the values used in the equations).

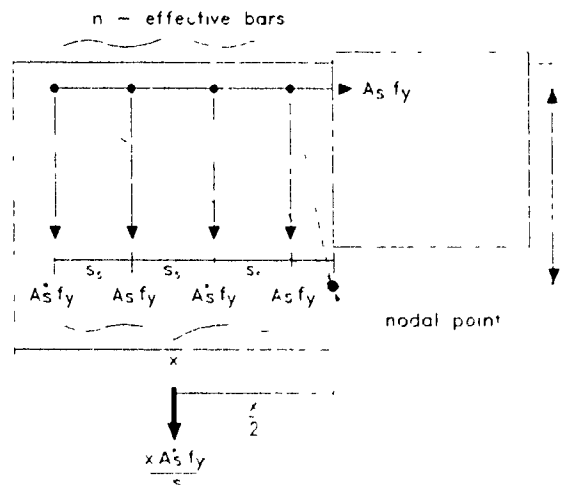


Figure 4.32 Simplified strut and tie model

Table 4.8 Simplified calculation of the number of effective slab bars

Specimen	$n = 4 \frac{b_o}{s}$	$x = \sqrt{\frac{2 A_{sl} c s}{A_s}}$ $n = \frac{x}{s_s} N$	Experimental Results
R4 - Rattray (1986)	99	49	6.0*
R4S - this study	51	42	5.4
R4T - this study	25	35	4.0
1S - Ehsani (1982)	42	36	4.0
J4 - Durrani (1987)	42	30	3.9
2D-E - Cheung (1991)	70	90	9.0

4.5.7 Flexural Strength Ratio

The flexural strength ratio between the columns and the main beam varies as a function of the effective slab reinforcement as can be seen from Table 4.9. As the contribution of the slab longitudinal reinforcement increases the flexural strength ratio decreases. The design flexural strength ratio for the three test specimens in this study was 1.68 calculated assuming that two sets of slab bars were effective. This ratio is above that of the Canadian Code (CSA, 1984) design recommendation of $M_R > 1.33$. The actual flexural strength ratios based on the recorded yield stresses of the reinforcement, compressive strengths of the concrete and the contributing slab reinforcement are given in Table 4.10. It can be noted that the actual ratios were less than the design value primarily due to the slab participation. It is therefore important to determine the number of contributing slab bars accurately to ensure an adequate hierarchy of yielding.

Table 4.9 M_R values for varying effective slab reinforcements

Case	Effective slab reinforcement	M_R
a)	the main beam alone, no slab bars effective	2.72
b)	1 set of slab bars on each side of beam, 4 slab bars effective	2.07
c)	2 sets of slab bars on each side of beam, 8 slab bars effective	1.68
d)	3 sets of slab bars on each side of beam, 12 slab bars effective	1.40

Table 4.10: Comparison of actual M_R values for the three specimens

Specimen	measured M_R
R4	1.15
R4S	1.35
R4T	1.41

Specimen R4T has a higher M_R than specimen R4S because it had a 35% increase in the concrete compressive strength over that of specimen R4S. This increase in strength resulted in an 8% increase in the flexural moment capacity. Had the specimens had identical concrete strengths, the moment capacity of specimen R4T would have been in the order of 8% lower than that of specimen R4S.

Table 4.11 summarizes the maximum measured negative moments in the main beams as well as the moments normalized to the concrete compressive strength of specimen R4. This allows a direct comparison of the effect of the reduced torsional strength of the spandrel beams. A considerable decrease in moment capacity is evident between the specimens. It must be noted that in the design of these specimens, the factored moment capacities were calculated to be equal. These results support the need to determine of the effective slab reinforcement more appropriately.

Table 4.11 Maximum recorded negative moments and normalized moments for each specimen

Specimen	M_{max} test (kNm)	f'_c (MPa)	M_{max} (f'_c of R4)
R4	662	40.0	662
R4S	550	34.3	566
R4T	558	46.6	536

Chapter 5

CONCLUSIONS AND RECOMMENDATIONS

5.1 Conclusions

This experimental programme investigated the response of two full-scale reinforced concrete beam-column-slab subassemblages subjected to reversed cyclic loading. The specimens were designed using the 1990 National Building Code of Canada (NBCC, 1990) and the 1984 CSA Standard (CSA, 1984) with a force reduction factor, R , of 4.0.

The main objective of these tests was to investigate the influence of different size spandrel beams and varying amounts of torsional reinforcement in these beams on the participation of the slab reinforcement in negative bending of the main beams. It was found that after torsional cracking and yielding of the spandrel beam a secondary force transfer mechanism develops in the slab which can be modelled by using a strut and tie approach. Tentative design equations are proposed for the determination of the effective slab reinforcement contributing in flexure. These equations consider both the torsional yield capacity of the spandrel beam and the resistance of the strut and tie mechanism to determine the effective slab reinforcement. The torsional yield capacity is dictated by the amount of torsional reinforcement in the spandrel beam. The resistance of the strut and tie mechanism is governed by the amount of longitudinal reinforcement in the top of the spandrel beam, the amount of slab reinforcement and the size of the column. These design proposals were applied to tests in this research programme as well as tests conducted by other researchers and resulted in good estimates of the amount of effective slab reinforcement. Furthermore, it was found that the presence of the spandrel beam increased the joint confinement before cracking and induced additional stresses on the joint region both through torsional shear flow from the spandrel beam and direct shear from the slab bars.

The current Standard (CSA 1984) does not explicitly account for the effect of the spandrel beams in the determination of the effective slab width. It was observed from the test results and an

analytical study that a better estimate of the effective slab reinforcement can be made by simple equations. The amount of effective slab reinforcement plays an important role in determining the hierarchy of yielding between the columns and the beams. A torsionally stiff and torsionally strong spandrel beam results in larger amounts of effective slab reinforcement and hence, stronger beams. Therefore, if the effect of the presence of a stiff, strong spandrel beam is not accounted for, then the "strong-column, weak-beam" design philosophy may not be achieved and hence, the failure mode of the structure may be altered.

The load versus deflection responses and energy dissipating capacities of the specimens, determined from the tests, indicated excellent ductility and energy absorbing characteristics. The excellent observed performances indicate that the design and detailing requirements of the CSA Standard (CSA, 1984), were adequate for these specimens designed with an R_n equal to 4.0.

5.2 Future Research Recommendations

The following aspects need further investigation:

- 1) the behaviour of a specimen consisting of a slab with no transverse spandrel beam to see if the same behavioural models developed in this research programme apply
- 2) the behaviour of multiple frame bays where the entire width of the slab on each side of the main beam is included. This would give more realistic boundary conditions at the ends of the spandrel beams.
- 3) the effect of varying torsional stiffnesses and resistances of transverse beams at interior joints connections.
- 4) the effect of longitudinal restraint on the torsional stiffness and strength of the spandrel beam.

REFERENCES

- ACI Committee 318, *Building Code Requirements for Reinforced Concrete (ACI 318-89)*, American Concrete Institute, Detroit, Michigan, 1989
- ACI-ASCE Committee 352, *Recommendations for Design of Beam-Column Joints in Monolithic Reinforced Concrete Structures*, ACI Journal, Vol 82, No 3, May-June 1985, pp 266-283
- Associate Committee on the National Building Code, National Building Code of Canada 1985 and Supplement to the National Building Code of Canada 1985, National Research Council of Canada, Ottawa, Ontario, 1985
- Associate Committee on the National Building Code, National Building Code of Canada 1990 and Supplement to the National Building Code of Canada 1990, National Research Council of Canada, Ottawa, Ontario, 1990.
- Bertero, V.V., and Popov, E P., *Seismic Behavior of Ductile Moment-Resisting Reinforced Concrete Frames - Reinforced Concrete Structures in Seismic Zones*, SP-53, American Concrete Institute, Detroit, Michigan, 1977, pp. 247-291
- Blume, J.A., Newmark, N M., and Corning, L.H., Design of Multi-Storey Reinforced Concrete Structure for Earthquake Motions, 4th edition, Portland Cement Association, Chicago, Illinois, 1961, 318 pp
- Canadian Standards Association, CSA Standard CAN3-A23 3-M84, Design of Concrete Structures for Buildings, Rexdale, Ontario, December 1984, 282 pp
- Castele, D.J , Effect of Column Strength on the Seismic Response of Concrete Frames, M.Eng. Thesis, Department of Civil Engineering and Applied Mechanics, McGill University, Montreal, July 1988, 96 pp
- Cheung, P C , Paulay, T, Park, R , *Seismic Design of Reinforced Concrete Beam-Column Joints with Floor Slab*, Research Report No 91-4, Department of Civil Engineering, University of Canterbury, Christchurch, New Zealand, October 1991.

- Collins, M P., and Mitchell, D , Prestressed Concrete Basics, Canadian Prestressed Concrete Institute, Ottawa, Ontario, 1987, 614 pp
- Collins, M P , and Mitchell, D , Prestressed Concrete Structures, Prentice Hall, Englewood Cliffs, New Jersey, 1991, 766 pp
- Durrani, A. J , and Zerbe, H E , *Seismic Resistance of R/C Exterior Connections with Floor Slab*, Journal of Structural Engineering, ASCE, Vol 113, No 8, August 1987, pp 1850-1864
- Eshani, M.R., and Wight, J K , *Behavior of External Reinforced Concrete Beam to Column Connections Subjected to Earthquake-Type Loading*, Report UMEE 82R5, Department of Civil Engineering, University of Michigan, Ann Arbor, Michigan, July 1982
- Eshani, M R., and Wight, J K., *Effect of Transverse Beams and Slab on Behavior of Reinforced Concrete Beam-to-Column Connections*, ACI Journal, Vol 82, No 2, March-April 1985, pp 188-195
- Eshani, M R , and Wight, J K , *Exterior Reinforced Concrete Beam to-Column Connections Subjected to Earthquake-Type Loading*, ACI Journal, Vol 82, No 4, July-August 1985, pp 492-499
- French, C W., and Boroojerdi, A., *Contribution of R/C Floor Slabs in Resisting Lateral Loads*, Journal of Structural Engineering, ASCE, Vol 115, No 1, January 1989, pp 1-18
- Gentry, T.R., and Wight, J K., *Reinforced Concrete Wide Beam-Column Connections Under Earthquake Type Loading*, Report UMCEE 92-12, Department of Civil Engineering, University of Michigan, Ann Arbor, June 1992, 203 pp
- Hanson, N W , and Connor, H W , *Seismic Resistance of Reinforced Concrete Beam Column Joints*, Journal of Structural Engineering, ASCE, Vol 93, No ST5, October 1967, pp 533-560
- Ma, S.M., Bertero, V V , and Popov, E P , *Experimental and Analytical Studies on the Hysteretic Behavior of Reinforced Concrete Rectangular and T-Beams*, EERC Report No 76.2 , Earthquake Engineering Research Center, University of California, Berkeley May 1976, 241 pp.
- Mitchell, D. and Collins, M P , *Diagonal Compression Field Theory - A Rational Model for Structural Concrete in Pure Torsion*, ACI Journal, Vol 71, No 8, August 1974, pp 396-408
- Mitchell, D., and Collins, M P , *Seismic Design - Chapter 11 of the Concrete Design Handbook*, CPC A Concrete Design Handbook, Canadian Portland Cement Association, Ottawa, Ontario, 1985, pp 11-1 to 11-31

- Mitchell, D , and Paultre, P , *Earthquake Resistant Design - Code Changes and Future Trends*, Canadian Journal of Civil Engineering, 1987, pp 245-262
- Paulay, T , *A Critique of the Special Provisions for Seismic Design of the Building Code Requirements for Reinforced Concrete (ACI 318-83)*, ACI Journal, Vol 83, No 2, March-April 1986, pp 274-283
- Paultre, P , and Mitchell, D , *Evaluation of Seismic Performance of Concrete Frame Structures in Canada*, Structural Engineering Series Report No 87-4, Department of Civil Engineering and Applied Mechanics, McGill University, Montreal, December 1987, 188 pp
- Paultre, P , Castele, D , Rattray, S and Mitchell, D , *Seismic Response of Reinforced Concrete Frame Subassemblages - A Canadian Perspective*, Canadian Journal of Civil Engineering, Vol. 16, No 5, October 1989, pp 627-649
- Rattray S , Reversed Cyclic Load Tests on Reinforced Concrete Frame Subassemblages, M.Eng Thesis, Department of Civil Engineering and Applied Mechanics, McGill University, May 1986, 143 pp
- Standards Association of New Zealand, NZS 3101:1982, Part 1: Code of Practice for the Design of Concrete Structures, 127 pp., and Part 2 Commentary on the Design of Concrete Structures, 156 pp., Wellington, New Zealand, 1982
- Yoshimura, M and Kurose, Y., *Inelastic Behavior of the Building, Earthquake Effects on Reinforced Concrete Structures US - Japan Research*, SP-84, American Concrete Institute, Detroit, 1985, pp 163-201

APPENDIX A

**Calculations for the Design and
Detailing of Test Specimens**

A.1 Beam Design

a) Design of Flexural Reinforcement

The factored negative design moment in the main beam at the face of the exterior column after 20% moment redistribution was found from a frame analysis to be $M_f = -299.8 \text{ kNm}$

- The diameter of bars passing through the joint is limited to $d_b \leq l_j / 24$ which is equal to $450 / 24 = 19 \text{ mm}$. Clause 21.6.5.6

Hence use No. 20 bars

- Assuming a flexural lever arm of $0.75h = 0.75 \times 600 = 450 \text{ mm}$, we can get a preliminary area of steel using $A_s = \frac{M_f}{\phi_s f_y J_d}$

$$A_s = 299.8 \times 1000 / (0.450 \times 0.85 \times 400) = 2000 \text{ mm}^2$$

- If slab bars are effective within a distance $3h_f$ which is equal to $3 \times 110 = 330 \text{ mm}$ on each side of the beam, the number of slab bars to be included in flexure is 4 - No. 10's Clause 21.4.2.2

- Since the second set of slab bars are fairly close to this cut-off, and are judged to contribute, they will be included in the design. Hence assume 8 - No. 10 bars

- Therefore area of No. 20 bars needed is $2000 - 800 = 1200 \text{ mm}^2$.

- Since there will be a reversal of moment at this section due to seismic loads, compression steel will enhance moment capacity. Clause 21.3.2.2

- Try 4 - No. 20 bars on top giving us area of 1200 mm^2 .

- Since the positive moment capacity must be one-half that of the negative moment, try 4 - No. 20 bottom bars. Figure A.1 shows the arrangement of longitudinal reinforcement

- For this configuration the negative moment capacity assuming that the compression steel yields and that the concrete compressive

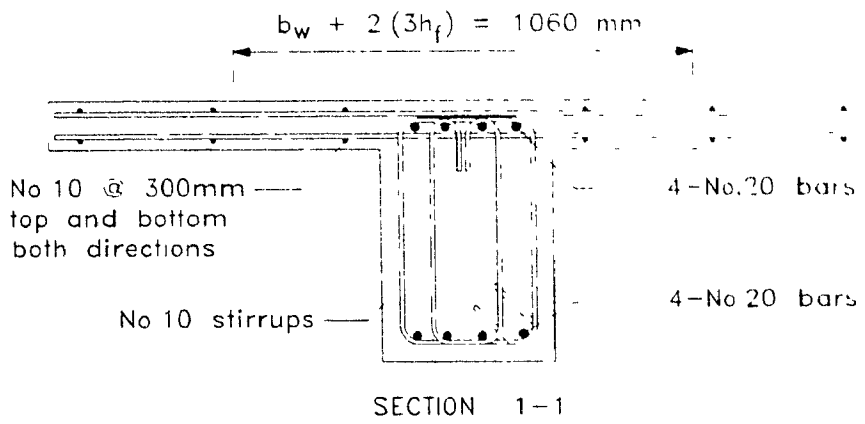


Figure A.1: Arrangement of longitudinal reinforcement

block is within the slab thickness is found from

$$f'_c = 30 \text{ MPa}$$

$$f_y = 400 \text{ MPa}$$

$$M_r^- = A_{s1} \phi_s f_y \left(d - \frac{a}{2} \right) + A_{s'} \left(\phi_s f_y - 0.85 \phi_c f'_c \right) \left(d - d' \right)$$

The resulting factored negative moment capacity was found to be $M_r^- = -339 \text{ kNm}$. This value of M_r^- is greater than M_r , therefore the design is satisfactory

The positive moment capacity was found to be $M_r^+ = 229 \text{ kNm}$. This value is greater than $\frac{1}{2} M_r = -170 \text{ kNm}$ OK

- Check minimum reinforcement (top and bottom)

$$\rho_{\min} = \frac{1.4 b_w d}{f_y} = 1.4 \times 400 \times 540 / 400 = 756 \text{ mm}^2 \quad \text{Clause 21.3.2.1}$$

756 < 1200 provided on the bottom OK.

- Check maximum reinforcement permitted

$$\rho_{\min} = 0.025 b_w d = 0.025 \times 400 \times 540 = 5400 \text{ mm}^2 \quad \text{Clause 21.3.2.1}$$

5400 > 1600 provided on the top OK

b) **Design of Transverse Reinforcement in Beam**

The transverse reinforcement in the beam is designed based on the shear corresponding to the probable moment capacity of the beam. The probable negative moment capacity was found to be $M_{pr} = 1.47 \times -339 = -498.3 \text{ kNm}$. Therefore, the design shear is $V = 498.3 / 1.775 = 280.8 \text{ kN}$.

1) Design Shear, $V = 280.8 \text{ kN}$

- Assuming the concrete shear resistance to be negligible we get

$$V_c = 0$$

- Therefore, $V_r = V_c + V_s = 280.8 \text{ kN}$

Clause 21.7.3.1

- Try 4 legs of No 10 transverse reinforcement near the column face

- The spacing is found from $V_r = \phi_s A_v f_y d / s$

$$V_r = \frac{\phi_s A_v f_y d}{s}$$

- Hence, $s = 0.85 \times 4 \times 100 \times 400 \times 540 / 280.8 \times 1000 = 261.6 \text{ mm}$

2) Check maximum V_s

- Maximum $V_s = 0.8 \phi_c \sqrt{f_c} b_w d$

$$= 0.8 \times 0.6 \times 5.48 \times 400 \times 540 / 1000$$

$$= 567.88 > 277.85 \text{ kN}$$

OK

Clause 11.3.6.6

3) Minimum shear reinforcement requirements

- $s < A_v f_y / 0.35 b_w = 4 \times 100 \times 400 / 0.35 \times 400$

$$s < 1140 \text{ mm}$$

Clause 11.2.5.4

- Spacing Limits

if $V_s > 0.4 \lambda \phi_c \sqrt{f_c} b_w d$

$$= 0.4 \times 0.6 \times 5.48 \times 400 \times 540$$

$$= 284 \text{ kN}$$

then $s_{max} = d/4 = 135 \text{ mm}$

Clause 11.3.8.3

if $V_s < 284 \text{ kN}$

then $s_{max} = d/2 = 270 \text{ mm}$

Clause 11.3.8.1

- Therefore $s_{max} = 270 \text{ mm}$

4) "Anti-buckling" and confinement requirements

Hoops must be provided over a length $2d$ from the face of the column and the spacing shall not exceed

Clause 21.3.3.2

a) $d/4 = 540 / 4 = 135 \text{ mm}$

b) $8d_p = 8 \times 19.5 = 156 \text{ mm}$

Clause 21.3.3.3

c) $24d_p \text{ (hoop)} = 24 \times 11.3 = 271 \text{ mm}$

d) 300 mm

- Therefore the confinement requirements control
Provide hoops spaced at 130 mm over length 1080 mm .
Outside this region, 2 legged stirrups may be used

- Spacing for shear $s = 0.85 \times 2 \times 100 \times 540 \times 400 / (280.8 \times 1000)$

$$s = 132 \text{ mm}$$

- Hence use constant spacing over the entire beam of 130 mm (see Figure A2 for details)

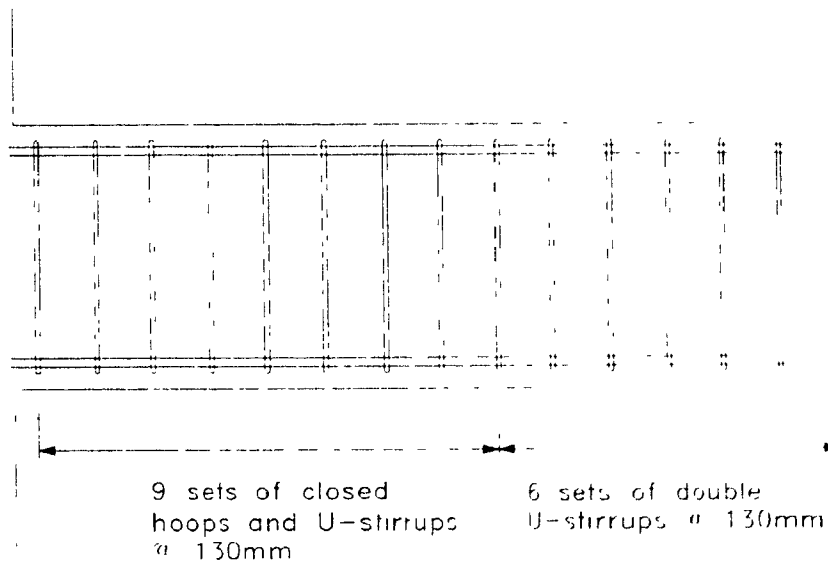


Figure A.2 Details of beam shear reinforcement

A.2 Column Design

The design axial load for the test is $P_f = 1076 \text{ kN}$

This axial load corresponds to 90% of the structure dead load on a second story exterior column. Try the following column details.

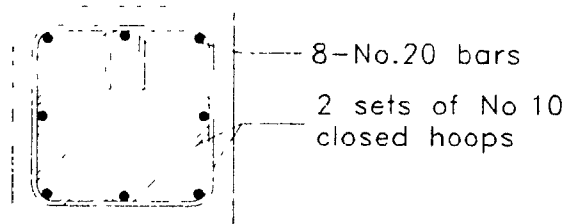


Figure A.3 Trial column reinforcement configuration

a) Design of longitudinal reinforcement

1) Check if Clause 21.4 applies

$$A_g \Gamma_c / 10 = (0.450 \times 0.450) \times 30 / 10 \\ = 607.5 \text{ kN}$$

Clause 21.4.1

- Since $P_f > 607.5$, then requirements of Clause 21.4 apply.

2) Check strength requirements

$$P_{r(max)} = 0.8 (0.85 \phi_c \Gamma_c (A_g - A_{st}) + \phi_s f_s A_{st})$$

$$P_{r(max)} = 3102 \text{ kN} > P_f \quad \text{OK}$$

From program RESPONSE (Collins and Mitchell, 1991) for an axial load of $P = 1076 \text{ kN}$, the factored moment resistance of the column, $M_{r_c} = 340 \text{ kNm}$

3) Check strength hierarchy

$$\Sigma M_{rc} > 1.1 M_{nb}$$

Clause 21.4.2.2

$$\Sigma M_{rc} = 340 + 340 = 680 \text{ kNm}$$

$$M_{nb} = 1.2 \times M_r = 1.2 \times 339 = 406.8 \text{ kNm}$$

$$1.1 M_{nb} = 1.1 \times 406.8 = 447.5 \text{ kNm}$$

Since $680 > 447.5$ the requirement is satisfied OK

b) Design of transverse reinforcement

The design shear force is determined considering the development of the probable moment capacity in the beam

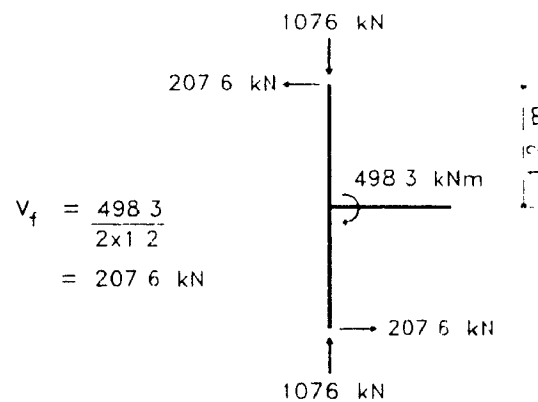


Figure A.4 Determination of design shear force in column

1) Determine stirrup spacing

$$V_c = 0.2 \lambda \phi_c \sqrt{f_c} \left(1 + \frac{3N_f}{A_g f_c} \right) b_w d$$

Clause 11.3.4.3

$$= 0.2 \times 0.6 \times 5.48 \times \left(1 + \frac{3 \times 1076 \times 1000}{450 \times 400 \times 30} \right) \times 450 \times 390$$

$$V_c = 176.2 \text{ kN}$$

$$V_s = 2076 - 1762 = 314$$

$$s = 0.85 \times 341.4 \times 400 \times 390 / (31.4 \times 1000)$$

$$s = 1442 \text{ mm}$$

- provide minimum requirements

spacing shall not exceed

$$a) 16 d_b (19.5) = 320 \text{ mm}$$

Clause 7.6.5.2

$$b) 48 d_b (11.3) = 542.4 \text{ mm}$$

c) smallest dimension of column, 450 mm

- minimum spacing for shear = $d / 2$

$$s = 194.5 \text{ mm}$$

Clause 11.3.8.1

- Use a spacing of 190 mm in central regions of the column with 4 legged hoops configuration as in Fig A4.

2) Check minimum area of reinforcement required

$$A_s f_y / b_w s = 341.42 \times 400 / 450 \times 190 = 1.6 > 0.35$$

OK

Clause 11.2.5.4

3) Check confinement requirements

- Confining hoops must be provided in end regions

$$A_{sh} = 0.3 \frac{s h_c f'_c}{f_{yh}} \left(\frac{A_g}{A_{ch}} - 1 \right)$$

$$= 0.3 (s \times 370 \times 30 / 400) (450 \times 450 / (370 \times 370) - 1)$$

Clause 21.4.4.2

$$= 3.99 s$$

but not less than

$$A_{sh} = 0.12 \left(\frac{s h_c f'_c}{f_{yh}} \right)$$

$$= 0.12 (s \times 370 \times 30 / 400)$$

$$= 3.33 s$$

Area of hoops = $200 + 200 \cos 45^\circ = 341.4 \text{ mm}^2$

$s = 341.4 / 3.99 = 85.6$

However, the spacing shall not exceed

Clause 21.4.4.3

a) $h/4 = 450/4 = 112.5$

b) 100 mm

c) $6 d_b \text{ (long. bar)} = 6 \times 19.5 = 117 \text{ mm}$

d) $48 d_b \text{ (transv. bar)} = 48 \times 11.3 = 547.4 \text{ mm}$

Therefore use No. 10 hoops as shown at 80 mm

Length, l_o , over which this spacing is provided

$l_o > \text{a) } h = 450 \text{ mm}$

b) $l_o / 6 = 306 / 6 = 508 \text{ mm}$

c) 450 mm

Clause 21.4.4.5

confinement required over length of 508 mm

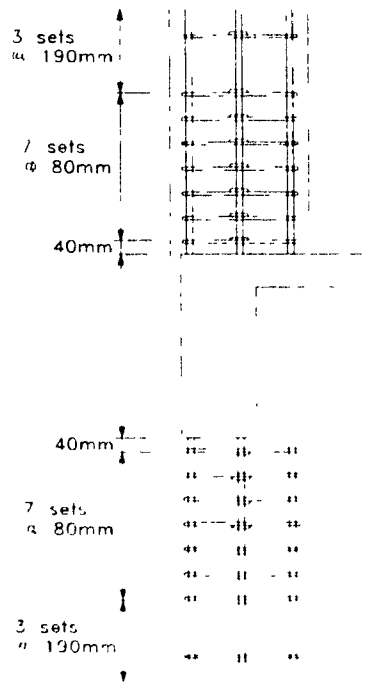


Figure A.5 Details of column reinforcement

A.3 Joint Design

1) Capacity Design

$$\begin{aligned}\text{Probable steel force is found using } 1.25 A_s f_s &= 1.25 \times 2000 \times 400 \\ &= 1000 \text{ kN}\end{aligned}$$

$$V_{s,d} \text{ corresponding to } M_{pr} \text{ in beam} = 205.5 \text{ kN}$$

$$V_{s,d} = 1000 - 205.5 \text{ kN}$$

$$V_s = 794.5 \text{ kN}$$

$$V_c = 0.2 \lambda \phi_c \sqrt{f_c} (1 + 3N_f/A_g f_c) b_w d$$

$$= 0.2 \times 0.6 \times 5.48 \times (1 + \frac{3 \times 1076 \times 1000}{450 \times 400 \times 30}) \times 450 \times 390$$

$$V_c = 176.2 \text{ kN}$$

$$V_s = 794.5 - 176.2 \text{ kN}$$

$$V_s = 618.3 \text{ kN}$$

$$V_s = \phi A_s f_s d / s$$

$$s = 0.85 \times 341.4 \times 400 \times 390 / 618.3$$

$$s = 73 \text{ mm}$$

Therefore use a spacing of 70 mm in joint region.

This corresponds to 6 sets of square and diamond closed hoops

2) Check maximum allowable joint shear

$$\begin{aligned}\text{Resistance of joint} &= 1.8 \lambda \phi_c \sqrt{f_c} A_g && \text{Clause 21.6.4.2} \\ &= 1.8 \times 0.6 \times 5.48 \times 450 \times 450 \\ &= 1198 \text{ kN} > V_j && \text{OK}\end{aligned}$$

3) Check confinement requirements

Transverse hoop reinforcement as specified in Clause 21.4.4 shall be provided within the joint region and must be < 80 mm. OK

4) Anchorage of beam reinforcement

Both top and bottom steel must be anchored in tension according to Clause 21.6.5

Development length for bar with standard 90° hooks

$$l_{db} > a) 8 d_b = 8 \times 19.5 = 156 \text{ mm}$$

$$b) 150 \text{ mm}$$

$$c) f_y d_b / 5.4 \sqrt{f'_c} = 264 \text{ mm}$$

But reinforcement must be extended to far face of column

Clause 21.6.1.3

l_{db} provided for the top steel is 400 mm

l_{db} provided for the bottom steel is 380 mm

Extension of free end $12 d_b = 12 \times 19.5 = 263 \text{ mm}$

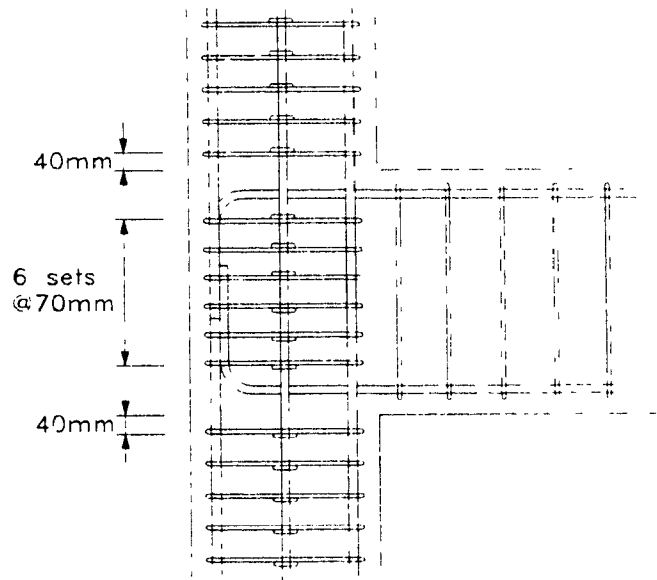


Figure A.6: Details of joint region

APPENDIX B

Calculations for the Amount of Effective Slab Reinforcement

B.1 : Specimen R4 Rattray (1986)

B.1.1 : Table of spandrel beam and slab parameters

spandrel section	properties	useful values
Specimen R4 Rattray (1986) h = 600 mm b = 400 mm hf = 110 mm	fc = 40 MPa	
	cover = 40 mm	
	slab bar = No 10	ho = 509 mm
	fy = 480 MPa	bo = 309 mm
	As = 100 mm ²	e = 254 mm
	N = 2	ph = 1796 mm *
	As* = 200 mm ²	
	s s = 300 mm	
	s beam bar = No 15	Ac = 240000 mm ²
	fy = 463 MPa	pc = 2000 mm
	At = 100 mm ²	Aoh = 160047 mm ²
	Al = 1600 mm ²	Ao = 136040 mm ²
	Asl = 400 mm ²	
	s = 125 mm	
bar = 11.3 mm		
column c = 450 mm		

B.1.2 : Effective slab reinforcement using torsional strength method (see Section 4.5.5)

Estimated α = 40.9 degrees = 0.714 rad	Choose α until $f_2 = f_2^{max}$												
$T_r = 2 A_o A_t f_y / s / \tan \alpha = 120.6 \text{ kNm}$													
$f_2 = 17.1 \text{ MPa}$													
vs													
$f_2^{max} = 17.2 \text{ MPa}$													
ao = 27 mm													
Ao = 135627 mm ²													
po = 1687 mm													
Nv = 864 kN													
es = 0.0027 mm/mm													
e1 = 0.0090 mm/mm													
	<table border="1"> <tbody> <tr> <td>Torsional Resistance</td> <td>T_r</td> <td>120.6 kNm</td> </tr> <tr> <td>Max Tensile Force in Slab Bars</td> <td>=</td> <td>474 kN</td> </tr> <tr> <td>Corresponding area of steel</td> <td>=</td> <td>988 mm² of</td> </tr> <tr> <td></td> <td>Therefore</td> <td>9.9 bars yield</td> </tr> </tbody> </table>	Torsional Resistance	T_r	120.6 kNm	Max Tensile Force in Slab Bars	=	474 kN	Corresponding area of steel	=	988 mm ² of		Therefore	9.9 bars yield
Torsional Resistance	T_r	120.6 kNm											
Max Tensile Force in Slab Bars	=	474 kN											
Corresponding area of steel	=	988 mm ² of											
	Therefore	9.9 bars yield											

B.1.3 : Effective slab reinforcement using strut and tie model method (see Section 4.5.5)

Taking moments about the nodal point in Fig B.1 we obtain																							
$F_1 \times d_1 + F_2 \times d_2 + F_3 \times d_3 = F_s \times c$ where																							
$F_{max} = N A_s f_y = 2 \times 100 \times 487 = 97.4 \text{ kN}$																							
$F_s = 1.25 A_s l f_y = 1.25 \times 400 \times 463 = 231.5 \text{ kN}$																							
Assuming that the first two rows of bars yield (i.e. 4 bars) we can solve for F3 to find the remaining number of yielding slab bars																							
LHS =	<table border="1"> <thead> <tr> <th></th> <th>kN</th> <th>x</th> <th>mm</th> <th>kNm</th> </tr> </thead> <tbody> <tr> <td>F1 x d1</td> <td>97.4</td> <td>x</td> <td>50</td> <td>4870</td> </tr> <tr> <td>F2 x d2</td> <td>97.4</td> <td>x</td> <td>350</td> <td>34090</td> </tr> <tr> <td>F3 x d3</td> <td>F3</td> <td>x</td> <td>650</td> <td>650 x F3</td> </tr> </tbody> </table>		kN	x	mm	kNm	F1 x d1	97.4	x	50	4870	F2 x d2	97.4	x	350	34090	F3 x d3	F3	x	650	650 x F3		
	kN	x	mm	kNm																			
F1 x d1	97.4	x	50	4870																			
F2 x d2	97.4	x	350	34090																			
F3 x d3	F3	x	650	650 x F3																			
RHS =	$F_s \times c$	231.5	x	450 = 104175																			
LHS = RHS	Therefore	F3	=	100.3 kN																			
	Since one bar has a yield force of	48.7	kN																				
	Then the number corresponding																						
	yield bars is	2.1	bars																				
	Hence n =	4 + 2.06	6.1 bars	(see Table 4.7)																			

B 2 Specimen R4S

B 2.1 Table of spandrel beam and slab parameters

spandrel section		properties	useful values
Specimen	R4S	$f_c' = 34.3$ MPa	
		cover = 40 mm	
		slab bar = No 10	$h_o = 509$ mm
		$f_y = 487$ MPa	$b_o = 159$ mm
this study		$A_s = 100$ mm ²	$e = 254$ mm
		$N = 2$	$ph = 1796$ mm *
		$A_s^* = 200$ mm ²	
		$s_s = 300$ mm	
$h = 600$ mm		s beam bar = No 15	$A_c = 150000$ mm ²
$b = 250$ mm		$f_y = 463$ MPa	$p_c = 1700$ mm
$h_f = 110$ mm		$A_t = 100$ mm ²	$A_{oh} = 92547$ mm ²
		$A_l = 1200$ mm ²	$A_o = 78665$ mm ²
		$A_{sl} = 300$ mm ²	
		$s = 125$ mm	
		bar = 11.3 mm	
		column c = 450 mm	

B.2.2 Effective slab reinforcement using torsional strength method (see Section 4.5.5)

Estimated $\theta = 50.3$ degrees =	0.878 rad	Choose θ until $f_2 = f_2max$
$T_r = 2 A_o A_t f_y / s / \tan \theta =$	50.9 kNm	
$f_2 = 21.7$ MPa		
vs		
$f_2max = 21.7$ MPa		
$a_o = 23$ mm		
$A_o = 71623$ mm ²		
$p_o = 1703$ mm		
$N_v = 457$ kN		
$e_s = 0.0019$ mm/mm		
$e_l = 0.0046$ mm/mm		

Torsional Resistance	$T_r = 50.9$ kNm
Max Tensile Force in Slab Bars	$= 200$ kN
Corresponding area of steel	$= 411$ mm ² or
Therefore	4.1 bars yield

B.2.3 Effective slab reinforcement using strut and tie model method (see Section 4.5.5)

Taking moments about the nodal point in Fig B 1 we obtain

$$F_1 \times d_1 + F_2 \times d_2 + F_3 \times d_3 = F_s \times c \quad \text{where}$$

$$F_{max} = N A_s f_y = 2 \times 100 \times 487 = 97.4 \text{ kN}$$

$$F_s = 1.25 A_{sl} f_y = 1.25 \times 300 \times 463 = 173.6 \text{ kN}$$

Assuming that the first two rows of bars yield (i.e. 4 bars), we can solve for F_3 to find the remaining number of yielding slab bars

		kN		mm	kNm
LHS =	$F_1 \times d_1$	97.4	x	50	4870
	$F_2 \times d_2$	97.4	x	350	34090
	$F_3 \times d_3$	F_3	x	650	$650 \times F_3$
RHS =	$F_s \times c$	173.625	x	450	= 78131
LHS = RHS	Therefore	F_3	=	60.26	kN
	Since one bar has a yield force of	48.7	kN		
	Then the number corresponding				
	yield bars is	1.2	bars		
	Hence $n =$	$4 + 1.24 = 5.2$	bars		(see Table 4.7)

B.3: Specimen R4T

B.3.1: Table of spandrel beam and slab parameters

spandrel section		properties	useful values
Specimen R4T this study		$f_c = 46.6 \text{ MPa}$ cover = 40 mm slab bar = No 10 $f_y = 487 \text{ MPa}$ $A_s = 100 \text{ mm}^2$ $N = 2$ $A_s^* = 200 \text{ mm}^2$ $s = 300 \text{ mm}$	$h_o = 509 \text{ mm}$ $b_o = 159 \text{ mm}$ $e = 254 \text{ mm}$ $ph = 1796 \text{ mm}^2$
	$h = 600 \text{ mm}$ $b = 250 \text{ mm}$ $hf = 110 \text{ mm}$	s beam bar = No 15 $f_y = 163 \text{ MPa}$ $A_t = 100 \text{ mm}^2$ $A_l = 800 \text{ mm}^2$ $A_{sl} = 200 \text{ mm}^2$ $s = 250 \text{ mm}$ bar = 11.3 mm column c = 450 mm	$A_c = 150000 \text{ mm}^2$ $p_c = 1700 \text{ mm}$ $A_{oh} = 92547 \text{ mm}^2$ $A_o = 78665 \text{ mm}^2$

B.3.2: Effective slab reinforcement using torsional strength method (see Section 4.5.5)

Estimated $\alpha = 38.5 \text{ degrees} = 0.67 \text{ rad}$	Choose α until $f_2 = f_{2max}$
$T_r = 2 A_o A_t^* f_y / s / \tan \alpha = 38.5 \text{ kNm}$	
$f_2 = 16.6 \text{ MPa}$	
vs	
$f_{2max} = 16.6 \text{ MPa}$	
$a_o = 13 \text{ mm}$	
$A_o = 80784 \text{ mm}^2$	
$p_o = 1744 \text{ mm}$	
$N_v = 537 \text{ kN}$	
$e_s = 0.0034 \text{ mm/mm}$	
$e_1 = 0.0118 \text{ mm/mm}$	

Torsional Resistance	$T_r = 38.5 \text{ kNm}$
Max Tensile Force in Slab Bars	151 kN
Corresponding area of steel	311 mm^2 or
Therefore	3.1 bars yield

B.3.3 Effective slab reinforcement using strut and tie model method (see Section 4.5.5)

Taking moments about the nodal point in Fig B.1 we obtain

$$F_1 \times d_1 + F_2 \times d_2 + F_3 \times d_3 = F_s \quad \text{where}$$

$$F_{max} = N A_s f_y = 2 \times 100 \times 487 = 97.4 \text{ kN}$$

$$F_s = 1.25 A_{sl} f_y = 1.25 \times 200 \times 463 = 115.8 \text{ kN}$$

Assuming that the first two rows of bars yield (i.e. 4 bars) we can solve for F_3 to find the remaining number of yielding slab bars

		kN	x	mm	kNm
LHS =	$F_1 \times d_1$	97.4	x	50	4870
	$F_2 \times d_2$	97.4	x	350	34090
	$F_3 \times d_3$	F_3	x	650	$650 \times F_3$
RHS =	$F_s \times c$	115.75	x	450	52088
LHS = RHS	Therefore	F_3	=	20.2	kN

Since one bar has a yield force of 48.7 kN
Then the number corresponding yield bars is 0.4 bars

Hence $n = 4 + 0.4 = 4.4 \text{ bars}$ (see Table 4.7)

B 4 . Specimen 1S Ehsani (1982)

B 4.1 Table of spandrel and slab parameters

spandrel section		properties	useful values
Specimen	1S	$f_c = 42.6 \text{ MPa}$	
		cover = 40 mm	
		slab bar = #4	$h_o = 387 \text{ mm}$
		$f_y = 345 \text{ MPa}$	$b_o = 157 \text{ mm}$
		$A_s = 129 \text{ mm}^2$	$e = 194 \text{ mm}$
		$N = 1$	$ph = 1542 \text{ mm}^*$
		$A_s^* = 200 \text{ mm}^2$	
		$s = 150 \text{ mm}$	
$h = 480 \text{ mm}$		s beam bar = #6	$A_c = 120000 \text{ mm}^2$
$b = 250 \text{ mm}$		$f_y = 345 \text{ MPa}$	$p_c = 1460 \text{ mm}$
$h_f = 100 \text{ mm}$		$A_t = 129 \text{ mm}^2$	$A_{oh} = 70440 \text{ mm}^2$
		$A_l = 1704 \text{ mm}^2$	$A_o = 59874 \text{ mm}^2$
		$A_{sl} = 426 \text{ mm}^2$	
		$s = 150 \text{ mm}$	
		bar = 12.8 mm	
		column c = 300 mm	

B 4.2 Effective slab reinforcement using torsional strength method (see Section 4.5.5)

Estimated $f_1 = 42.6 \text{ degrees} = 0.744 \text{ rad}$	Choose α until $f_2 = f_{2max}$
$T_r = 2 A_o A_t f_y / s \tan \alpha = 38.6 \text{ kNm}$	
$f_2 = 24.1 \text{ MPa}$	
vs	
$f_{2max} = 24.2 \text{ MPa}$	
$a_o = 18 \text{ mm}$	
$A_o = 56212 \text{ mm}^2$	
$p_o = 1468 \text{ mm}$	
$N_v = 515 \text{ kN}$	
$e_s = 0.0015 \text{ mm/mm}$	
$e_1 = 0.0057 \text{ mm/mm}$	

Torsional Resistance	$T_r = 38.6 \text{ kNm}$
Max Tensile Force in Slab Bars	$= 200 \text{ kN}$
Corresponding area of steel	$= 578 \text{ mm}^2$ or
Therefore	4.5 bars yield

B.4.3 Effective slab reinforcement using strut and tie model method (see Section 4.5.5)

Taking moments about the nodal point in Fig B 1 we obtain

$$F_1 \times d_1 + F_2 \times d_2 + F_3 \times d_3 + F_4 \times d_4 = F_s \times c \quad \text{where}$$

$$F_{max} = N A_s f_y = 1 \times 129 \times 345 = 44605 \text{ kN}$$

$$F_s = 1.25 A_{sl} f_y = 1.25 \times 426 \times 345 = 183712.5 \text{ kN}$$

Assuming that the first three rows of bars yield (i.e. 3 bars) we can solve for F_4 to find the remaining number of yielding slab bars

	kN	mm	kNmm
LHS = $F_1 \times d_1$	45.4	50	2270
$F_2 \times d_2$	45.4	200	9082
$F_3 \times d_3$	45.4	350	15893
$F_4 \times d_4$	F_4	500	$500 \times F_4$
RHS = $F_s \times c$	183.7	300	55114

LHS = RHS Therefore $F_3 = 55.7 \text{ kN}$

Since one bar has a yield force of 45.4 kN
Then the number corresponding yield bars is 1.2 bars

Hence $n = 3 + 1.2 = 4.2 \text{ bars}$ (see Table 4.7)

B.5 Specimen J4 Durrani (1987)

B.5.1 : Table of spandrel beam and slab parameters

spandrel section	properties	useful values
Specimen J4 Durrani (1987)	$f_c = 41 \text{ MPa}$ cover = 40 mm slab bar = #4 $f_y = 414 \text{ MPa}$ $A_s = 129 \text{ mm}^2$ $N = 1$ $A_s^* = 200 \text{ mm}^2$ $s_s = 150 \text{ mm}$ s beam bar = #6 $f_y = 414 \text{ MPa}$ $A_t = 129 \text{ mm}^2$ $A_l = 1136 \text{ mm}^2$ $A_{sl} = 284 \text{ mm}^2$ $s = 150 \text{ mm}$ bar = 12.8 mm column c = 300 mm	$h_o = 287 \text{ mm}$ $b_o = 157 \text{ mm}$ $e = 143 \text{ mm}$ $ph = 1.312 \text{ mm}^2$ $A_c = 95000 \text{ mm}^2$ $p_c = 1260 \text{ mm}$ $A_{oh} = 54720 \text{ mm}^2$ $A_o = 46512 \text{ mm}^2$
$h = 380 \text{ mm}$ $b = 250 \text{ mm}$ $h_f = 100 \text{ mm}$		

B.5.2 Effective slab reinforcement using torsional strength method (see Section 4 5 5)

Estimated $\theta = 48.4 \text{ degrees} = 0.845 \text{ rad}$	Choose θ until $f_2 = f_{2max}$
$T_r = 2 A_o A_t f_y / s / \tan \theta = 29.4 \text{ kNm}$	
$f_2 = 26.5 \text{ MPa}$	
vs	
$f_{2max} = 26.6 \text{ MPa}$	
$a_o = 19 \text{ mm}$	
$A_o = 42071 \text{ mm}^2$	
$p_o = 1266 \text{ mm}$	
$N_v = 355 \text{ kN}$	
$e_s = 0.0016 \text{ mm/mm}$	
$e_1 = 0.0044 \text{ mm/mm}$	

Torsional Resistance	$T_r = 29.4 \text{ kNm}$
Max Tensile Force in Slab Bars	205 kN
Corresponding area of steel	= 495 mm ² or
Therefore	3.8 bars yield

B.5.3 Effective slab reinforcement using strut and tie model method (see Section 4 5 5)

Taking moments about nodal point in Fig B 1 we obtain

$$F_1 \times d_1 + F_2 \times d_2 + F_3 \times d_3 + F_4 \times d_4 = F_s \times c \quad \text{where}$$

$$F_{max} = N A_s f_y = 1 \times 129 \times 531 = 68.5 \text{ kN}$$

$$F_s = 1.25 A_{sl} f_y = 1.25 \times 284 \times 414 = 147.0 \text{ kN}$$

Assuming that the first three rows of bars yield (i.e. 3 bars) we can solve for F_4 to find the remaining number of yielding slab bars

	kN	mm	kNmm
LHS = $F_1 \times d_1$	68.5	50	3425
$F_2 \times d_2$	68.5	200	13700
$F_3 \times d_3$	68.5	350	23975
$F_4 \times d_4$	F_4	500	$500 \times F_4$
RHS = $F_s \times c$	147.0	300	44091
LHS = RHS	Therefore F_3		6.0 kN
	Since one bar has a yield force of		68.5 kN
	Then the number corresponding		
	yield bars is		0.1 bars
Hence $n =$	$3 + 0.1$		3.1 bars (see Table 4.7)

B 6 : Specimen 2D-E Cheung (1991)

B 6.1 Table of spandrel beam and slab parameters

spandrel section		properties	useful values
Specimen 2D-E Cheung (1991)		$f_c = 38$ MPa cover = 40 mm slab bar = D10 $f_y = 300$ MPa $A_s = 78$ mm ² $N = 2$ $A_{s^*} = 200$ mm ² $s_s = 260$ mm s beam bar = D20 $f_y = 300$ MPa $A_t = 78$ mm ² $A_l = 3000$ mm ² $A_{s_l} = 750$ mm ² $s = 120$ mm bar = 10 mm column c = 550 mm	$h_o = 485$ mm $b_o = 210$ mm $e = 243$ mm $ph = 1770$ mm * $A_c = 172500$ mm ² $pc = 1750$ mm $A_{oh} = 113850$ mm ² $A_o = 96773$ mm ²
h	575 mm		
b	300 mm		
hf	130 mm		

B 6 2 Effective slab reinforcement using torsional strength method (see Section 4.5.5)

Estimated $\theta = 33.6$ degrees =	0.586 rad	Choose θ until $f_2 = f_{2max}$
$T_r = 2 A_o A_t f_y / s / \tan \theta =$	56.8 kNm	
$f_2 = 16.8$ MPa	vs	
$f_{2max} = 16.8$ MPa		
$a_o = 20$ mm		
$A_o = 95843$ mm ²		
$p_o = 1689$ mm		
$N_v = 746$ kN		
$e_s = 0.0012$ mm/mm		
$e_l = 0.0086$ mm/mm		

Torsional Resistance	$T_r = 56.8$ kNm
Max Tensile Force in Slab Bars	= 234 kN
Corresponding area of steel	= 781 mm ² or
Therefore	10.0 bars yield

B 6.3 : Effective slab reinforcement using strut and tie model method (see Section 4.5.5)

Taking moments about the nodal point in Fig B 1 we obtain

$$F_1 \times d_1 + F_2 \times d_2 + F_3 \times d_3 + F_4 \times d_4 + F_5 \times d_5 = F_s \times c \quad \text{where}$$

$$F_{max} = N A_s f_y = 2 \times 78 \times 326 = 50.9 \text{ kN}$$

$$F_s = 1.25 A_{s_l} f_y = 1.25 \times 750 \times 300 = 281.3 \text{ kN}$$

Assuming that the first four rows of bars yield (i.e. 8 bars), we can solve for F_5 to find the remaining number of yielding slab bars

	kN	mm	kNm
F1 x d1	50.9	50	2543
F2 x d2	50.9	300	15257
F3 x d3	50.9	550	27971
F4 x d4	50.9	800	40685
F5 x d5	F5	1050	500 x F5
RHS - F _s x c	281.3	550	154688

LHS = RHS Therefore $F_5 = 65.0$ kN

Since one bar has a yield force of 25.4 kN
Then the number corresponding yield bars is 2.6 bars

Hence $n = 8 + 2.6 = 10.6$ bars (see Table 4.7)

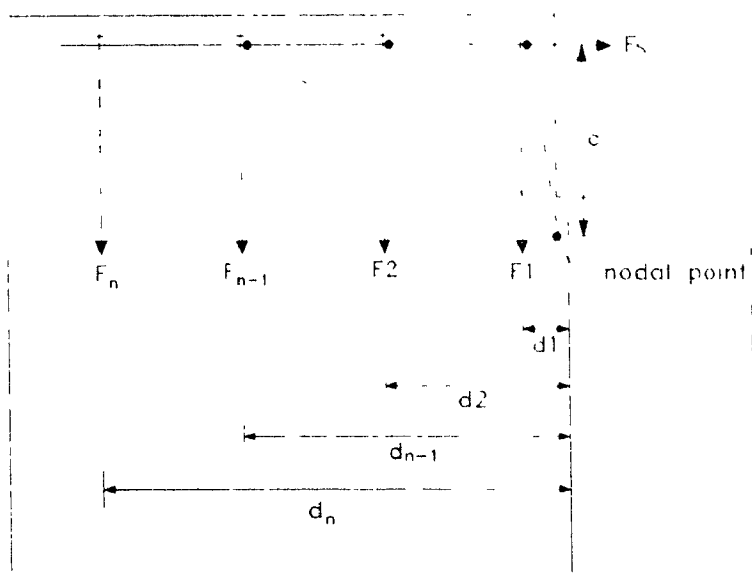


Figure B.1: Strut and tie model to determine the effective slab reinforcement